---

**Article:**
Aad, G. orcid.org/0000-0002-6665-4934, Aakvaag, E. orcid.org/0000-0001-7616-1554, Abbott, B. orcid.org/0000-0002-5888-2734 et al. (2871 more authors) (2025) Cross-section measurements for the production of a W-boson in association with high-transverse-momentum jets in pp collisions at √s = 13 TeV with the ATLAS detector. The European Physical Journal C, 85 (7). 738. ISSN 1434-6044

https://doi.org/10.1140/epjc/s10052-025-14078-0

---

Eur. Phys. J. C (2025) 85:738
https://doi.org/10.1140/epjc/s10052-025-14078-0

THE EUROPEAN PHYSICAL JOURNAL C

Regular Article - Experimental Physics

# Cross-section measurements for the production of a $W$-boson in association with high-transverse-momentum jets in $pp$ collisions at $\sqrt{s} = 13$ TeV with the ATLAS detector

**ATLAS Collaboration**[⋆]

CERN, 1211 Geneva 23, Switzerland

Received: 17 December 2024 / Accepted: 14 March 2025


**Abstract** A set of measurements for the production of a $W$-boson in association with high-transverse-momentum jets is presented using 140 fb$^{-1}$ of proton–proton collision data at a centre-of-mass energy of $\sqrt{s} = 13$ TeV collected by the ATLAS detector at the LHC. The measurements are performed in final states in which the $W$-boson decays into an electron or muon plus a neutrino and is produced in association with jets with $p_{\mathrm{T}} > 30$ GeV, where the leading jet has $p_{\mathrm{T}} > 500$ GeV. The angular separation between the lepton and the closest jet with $p_{\mathrm{T}} > 100$ GeV is measured and used to define a collinear phase space, wherein measurements of kinematic properties of the $W$-boson and the associated jet are performed. The collinear phase space is populated by dijet events radiating a $W$-boson and events with a $W$-boson produced in association with several jets and it serves as an excellent data sample to probe higher-order theoretical predictions. Measured differential distributions are compared with predictions from state-of-the-art next-to-leading order multi-leg merged Monte Carlo event generators and a fixed-order calculation of the $W + 1$-jet process computed at next-to-next-to-leading order in the strong coupling constant.

## Contents



⋆ e-mail: atlas.publications@cern.ch

## 1 Introduction

Measurements of electroweak (EW) bosons in the electron or muon decay modes provide a clean experimental signature to test the EW sector of the Standard Model (SM) and perturbative quantum chromodynamics (QCD) in high jet-multiplicity final states. The large production cross-section for a single $W$-boson provides a very large data sample with which to explore the modelling of kinematic variables in the high-momentum phase space. Moreover, the $W+$ jets process represents a significant irreducible background to a wide range of analyses within the Large Hadron Collider (LHC) physics programme, such as Higgs boson [1–4] and top quark measurements [5–8], and searches for new physics phenomena beyond the Standard Model (BSM) [9–14]. Therefore, an accurate description of this process across a large energy range is critical to the success of the LHC physics programme.

At next-to-leading order (NLO) in $\alpha_{\mathrm{s}}$, new partonic scattering topologies emerge that can contribute very large enhancements to the overall production rate (Fig. 1b). Of particular importance are diagrams where dijet production is accompanied by the emission of a real $W$-boson from the incoming or outgoing quarks, as shown in Fig. 1. These contributions lead to large enhancements in the production rate that are proportional to $\alpha_{\mathrm{s}} \ln^2 p_{\mathrm{T}}^{\text{closest jet}}/m_W$, where $p_{\mathrm{T}}^{\text{closest jet}}$ is the transverse momentum of the closest jet, and $m_W$ is the $W$-boson mass. This results in an overall cross-section enhancement at small values in the distribution of the angular separation between the $W$-boson and the closest jet in events with high-$p_{\mathrm{T}}$ jets, referred to as *collinear enhancement*. The collinear region also contains contributions where the $W$-boson is produced in association with larger numbers of jets. An accurate description of $W$-bosons produced in association with many jets demands theoretical predictions computed at the highest possible order in both the strong and electroweak couplings.

Published online: 04 July 2025

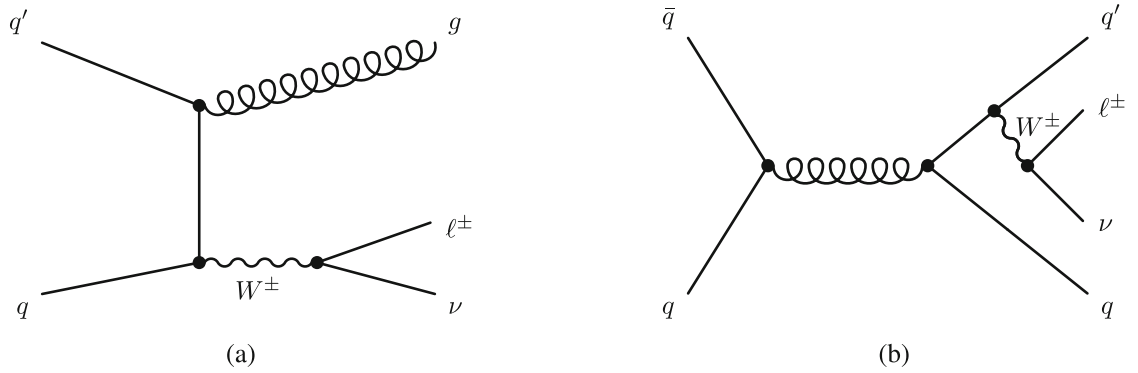


**Fig. 1** Representative Feynman diagrams for the production of a $W$-boson in association with jets. The $t$-channel diagram shown in **a** typically leads to large angular separation between the recoiling jet and the lepton, while the $s$-channel diagram shown in **b** can lead to small angular separations between the lepton and the outgoing quark

Measurements of $W$-bosons emitted from high-momentum partons in the muon channel only were reported in proton–proton collisions at a centre-of-mass energy of 8 TeV by the ATLAS Collaboration using a data sample with 20.3 fb$^{-1}$ [15] of integrated luminosity, and a more inclusive measurement by the CMS Collaboration using a data sample with 19.6 fb$^{-1}$ [16]. CMS performed an initial measurement of $W$+ jets events in a high-momentum region using 2.2 fb$^{-1}$ of proton–proton collision data at a centre of mass energy of 13 TeV in the muon decay channel [17]. This paper presents an extension of those measurements using the full Run 2 data sample corresponding to 140 fb$^{-1}$ of proton–proton collision data at a centre-of-mass energy of 13 TeV, via a combination of the cross-section measurements from the electron and muon channels. The large data sample allows the measurement of kinematic variables typically probed in searches for new phenomena beyond the 1 TeV energy scale. ATLAS also performed a measurement of $Z$ + jets events in the high-momentum region with the full Run 2 data sample [18]. The measurement presented here is complementary to the $Z$ + jets measurement, and is able to probe higher energy regimes due to the nearly ten times larger production cross-section.

This paper presents inclusive and differential cross-section measurements of a $W$-boson produced in association with high-$p_{\mathrm{T}}$ jets. It targets events where the $W$-boson decays into a lepton (electron or muon) in association with jets with $p_{\mathrm{T}} > 30$ GeV and $|\eta| < 2.5$, where the leading jet has $p_{\mathrm{T}} > 500$ GeV. This phase space is referred to as the *inclusive* region, and measurements of the differential cross-section for observables sensitive to collinear enhancement in the production rate are performed:

- $\Delta R_{\mathrm{min}}(\ell, \mathrm{jet}_i^{100})$: angular separation[1] between the lepton and closest jet with transverse momentum greater than 100 GeV. Events with $\Delta R_{\mathrm{min}}(\ell, \mathrm{jet}_i^{100}) > 2.6$ (for each jet $i$ in the event) are expected to be dominated by leading-order $W + 1$-jet production and referred to as the *back-to-back* region. The opposing selection $\Delta R_{\mathrm{min}}(\ell, \mathrm{jet}_i^{100}) < 2.6$, expected to be dominated by $W+\geq$ 2-jet processes, is referred to as the *collinear* region.
- $p_{\mathrm{T}}^{\ell\nu}/p_{\mathrm{T}}^{\text{closest jet}}$: the ratio of the transverse momentum of the lepton–neutrino system ($p_{\mathrm{T}}^{\ell\nu}$) to the transverse momentum of the jet that is closest to the lepton. Values around one represent events where the $W$-boson and closest jet have similar momentum, and therefore are expected to be dominated by leading-order $W$ + 1-jet production. Values away from one are expected to be dominated by $W+\geq$ 2-jets production.
- $m_{\mathrm{jj}}$: the invariant mass of the highest momentum pair of jets. This observable is measured in the *inclusive 2-jet* region where at least two jets are required. This is an observable often explored in EW induced measurements [19] or BSM searches [20–22], but is difficult to model in the multi-TeV kinematic range.

In addition, differential measurements are performed of observables sensitive to $W$-boson production in association with many jets in the *collinear* region. These observables are:

[1] ATLAS uses a right-handed coordinate system with its origin at the nominal interaction point (IP) in the centre of the detector and the $z$-axis along the beam pipe. The $x$-axis points from the IP to the centre of the LHC ring, and the $y$-axis points upwards. Polar coordinates $(r, \phi)$ are used in the transverse plane, $\phi$ being the azimuthal angle around the $z$-axis. The pseudorapidity is defined in terms of the polar angle $\theta$ as $\eta = -\ln\tan(\theta/2)$ and is equal to the rapidity $y = \frac{1}{2}\ln\left(\frac{E+p_z}{E-p_z}\right)$ in the relativistic limit. Angular distance is measured in units of $\Delta R \equiv \sqrt{(\Delta y)^2 + (\Delta\phi)^2}$.

- the transverse momentum of the leading jet,
- the transverse momentum of the lepton–neutrino system ($p_{\mathrm{T}}^{\ell\nu}$),
- the jet multiplicity for jets with $p_{\mathrm{T}} > 30$ GeV, and
- the total scalar sum of the transverse momentum of all jets ($S_{\mathrm{T}}$).

State-of-the-art event generator programs that are multi-leg matrix element accurate to NLO in $\alpha_{\mathrm{s}}$ merged with parton-shower models to emulate the higher missing orders are compared with the measured data. In addition, fixed-order predictions for $W$ + 1-jet production computed at next-to-next-to-leading order (NNLO) in $\alpha_{\mathrm{s}}$ using the MCFM program [23], are compared with the measured data. The data from this publication will be publicly provided through both HEPDATA [24] and RIVET [25] and can be used to improve the theoretical description of these high-energy events.

The paper is organised as follows. The ATLAS detector is described in Sect. 2. Section 3 presents the data sample and simulated samples used in the measurement, while Sect. 4 details the reconstruction of leptons, jets, and the missing transverse momentum. The event selection is described in Sect. 5, and the estimation of background processes to the measurement are explained in Sect. 6. The unfolding of detector effects is described in Sect. 7, and systematic uncertainties in Sect. 8. The final results are presented in Sect. 9, with concluding remarks in Sect. 10.

## 2 ATLAS detector

The ATLAS detector [26] at the LHC covers nearly the entire solid angle around the collision point. It consists of an inner tracking detector surrounded by a thin superconducting solenoid, electromagnetic and hadronic calorimeters, and a muon spectrometer incorporating three large superconducting air-core toroidal magnets.

The inner-detector system (ID) is immersed in a 2T axial magnetic field and provides charged-particle tracking in the range $|\eta| < 2.5$. The high-granularity silicon pixel detector covers the vertex region and typically provides four measurements per track, the first hit generally being in the insertable B-layer (IBL) installed before Run 2 [27,28]. It is followed by the SemiConductor Tracker (SCT), which usually provides eight measurements per track. These silicon detectors are complemented by the transition radiation tracker (TRT), which enables radially extended track reconstruction up to $|\eta| = 2.0$. The TRT also provides electron identification information based on the fraction of hits (typically 30 in total) above a higher energy-deposit threshold corresponding to transition radiation.

The calorimeter system covers the pseudorapidity range $|\eta| < 4.9$. Within the region $|\eta| < 3.2$, electromagnetic calorimetry is provided by barrel and endcap high-granularity lead/liquid-argon (LAr) calorimeters, with an additional thin LAr presampler covering $|\eta| < 1.8$ to correct for energy loss in material upstream of the calorimeters. Hadronic calorimetry is provided by the steel/scintillator-tile calorimeter, segmented into three barrel structures within $|\eta| < 1.7$, and two copper/LAr hadronic endcap calorimeters. The solid angle coverage is completed with forward copper/LAr and tungsten/LAr calorimeter modules optimised for electromagnetic and hadronic energy measurements respectively.

The muon spectrometer (MS) comprises separate trigger and high-precision tracking chambers measuring the deflection of muons in a magnetic field generated by the superconducting air-core toroidal magnets. The field integral of the toroids ranges between 2.0 and 6.0 T m across most of the detector. Three layers of precision chambers, each consisting of layers of monitored drift tubes, cover the region $|\eta| < 2.7$, complemented by cathode-strip chambers in the forward region, where the background is highest. The muon trigger system covers the range $|\eta| < 2.4$ with resistive-plate chambers in the barrel, and thin-gap chambers in the endcap regions.

The luminosity is measured mainly by the LUCID–2 [29] detector that records Cherenkov light produced in the quartz windows of photomultipliers located close to the beampipe.

Events are selected by the first-level trigger system implemented in custom hardware, followed by selections made by algorithms implemented in software in the high-level trigger [30]. The first-level trigger accepts events from the 40 MHz bunch crossings at a rate below 100 kHz, which the high-level trigger further reduces in order to record complete events to disk at about 1 kHz.

A software suite [31] is used in data simulation, in the reconstruction and analysis of real and simulated data, in detector operations, and in the trigger and data acquisition systems of the experiment.

## 3 Data and simulated event samples

The data used in this analysis were recorded with the ATLAS detector from 2015 to 2018 in proton–proton collisions at $\sqrt{s} = 13$ TeV and correspond to a total integrated luminosity of 140 fb$^{-1}$. The uncertainty in the combined 2015–2018 integrated luminosity is 0.83% [32], obtained using the LUCID-2 detector for the primary luminosity measurements, complemented by measurements using the inner detector and calorimeters. The mean number of proton–proton interactions per bunch crossing, including hard scattering events and other interactions in the same and neighbouring bunch crossings (pile-up), was $\langle\mu\rangle = 34$.

Monte Carlo (MC) simulated samples are used to estimate various background processes, to unfold the data to particle

**Table 1** Overview of Monte Carlo simulated samples used to model signal and background processes. The perturbative accuracy of the QCD calculation in the matrix element is given in the last column

| Process | Matrix element<br>Parton shower | Ref. | PDF set<br>Tune | Ref. | pQCD |
|---|---|---|---|---|---|
| $W$+jets | Sherpa 2.2.11 | [41, 43, 69]<br>[46, 70] | NNPDF30NNLO<br>Sherpa default | [45] | 0-2j@NLO+3-5j@LO |
| $W$+jets | MadGraph v2.6.5<br>Pythia 8.240 | [49]<br>[50] | NNPDF3.1luxQED<br>A14+FxFx | [53] | 0-3j@NLO |
| $Z/\gamma^*$ + jets | Sherpa 2.2.11 | [41, 43, 69]<br>[46, 70] | NNPDF30NNLO<br>Sherpa default | [45] | 0-2j@NLO+3-5j@LO |
| Diboson | Powheg v2<br>Pythia 8.210 | [56–58, 63]<br>[50] | NLO CT10<br>AZNLO | [65]<br>[64] | 0j@NLO |
| $t\bar{t}$+jets | Sherpa 2.2.12 | [41, 43, 69]<br>[46, 70] | NNPDF30NNLO<br>Sherpa default | [45] | 0-1j@NLO+2-3j@LO |
| $t$ ($s$-channel) | Powheg v2<br>Pythia 8.230 | [56–58, 71]<br>[50] | NLO CT10<br>Perugia2012 | [65]<br>[72] | 0j@NLO |
| $t$ ($t$-channel) | Powheg v2<br>Pythia 8.230 | [56–58, 71]<br>[50] | NLO CT10f4<br>Perugia2012 | [65]<br>[72] | 0j@NLO |
| $t+W$ | Powheg v2<br>Pythia 8.230 | [55–58]<br>[50] | NLO CT10<br>Perugia2012 | [65]<br>[72] | 0j@NLO |
| EW $W$+jj | Sherpa 2.2.11 | [41, 43, 69]<br>[46, 70] | NNPDF30NNLO<br>Sherpa default | [45] | 2j@LO |
| Multijet | Pythia 8.230 | [50] | NNPDF2.3lo<br>A14 | [37] | 2j@LO |

level, to estimate systematic uncertainties and for the comparison with the unfolded data distributions. Generated events were processed using a full detector simulation [33] based on Geant4 [34] for the detector response to final-state particles. Simulated events were processed and then reconstructed with the same reconstruction algorithms as used for the data. To account for pile-up, multiple overlaid inelastic $pp$ collisions were simulated with Pythia 8.186 [35] using the A3 set of tuned parameters (tune) [36] and the NNPDF2.3lo set of parton distribution functions (PDFs) [37]. The simulated events are reweighted so that the mean number of proton–proton interactions in simulation matches that observed in each of the data-taking periods. A summary of the simulated samples is provided in Table 1. All simulated samples are normalised to the cross-section predicted by the generator unless otherwise specified.

The nominal modelling for the $W$+ jets signal process uses the Sherpa 2.2.11 event generator [38–40]. Matrix elements accurate to NLO in both the strong and EW couplings (virtual corrections only, denoted NLO $\mathrm{EW_{virt}}$) for up to two jets were computed by OpenLoops [41,42], while LO-accurate matrix elements for up to five jets were calculated with the Comix [43] library. The matrix elements were merged with the Sherpa parton shower following the MEPS@NLO prescription [44] and used the tune developed by the Sherpa authors. The NNPDF3.0nnlo set of PDFs [45] was used. The default Sherpa parton shower [46] based on Catani–Seymour dipoles and the cluster hadronisation model [47] was used. The phase space was statistically enhanced using the $\max(S_{\mathrm{T}}, p_{\mathrm{T}}^{V})$ variable using an analytic enhancement technique, where $S_{\mathrm{T}}$ is the scalar sum of the transverse momenta of all outgoing particles and $p_{\mathrm{T}}^{V}$ is the transverse momentum of the vector boson. The NLO $\mathrm{EW_{virt}}$ corrections are available as alternative generator weights in three different schemes for the combination with the QCD matrix elements: additive, multiplicative and exponentiated [40]. Nominal predictions were obtained without the NLO $\mathrm{EW_{virt}}$ corrections, but results are also presented with these corrections using the multiplicative scheme as default and an uncertainty computed from the envelope of all other combination schemes. Scale and PDF uncertainties were evaluated on-the-fly [48] using 7-point variations of the factorisation and renormalisation scales in the matrix elements and parton shower and using the Hessian PDF eigenvector variations for the NNPDF3.0nnlo set of PDFs. The scales were varied coherently in the matrix element and parton shower by factors of 0.5 and 2 relative to the nominal scale, but avoiding combinations where renormalisation and factorisation scales are varied in opposite directions.

A second multijet merged configuration with NLO accuracy in $\alpha_{\mathrm{s}}$ was provided using MadGraph5_aMC@NLO interfaced with Pythia8. Samples were produced using the MadGraph5_aMC@NLO v2.6.5 [49] program to generate matrix elements for vector-boson production with up

to three additional jets in the final state to NLO accuracy in $\alpha_s$. The showering and subsequent hadronisation were performed using PYTHIA 8.240 [50] with the A14 tune [51], using the NNPDF2.3LO PDF set with $\alpha_s = 0.130$. The different jet multiplicities were merged using the FxFx prescription [52]. The PDF set used for event generation was NNPDF3.1LUXQED [53] computed at NNLO with $\alpha_s = 0.118$. The samples were generated with additional weights for the PDF eigenvector variations as well as variations of the renormalisation and the factorisation scales [54].

Electroweak production of $W$+jj (with $W \to \ell\nu$) and $Z$+jj (with $Z \to \ell\ell$ or $\nu\nu$) final states was simulated with SHERPA 2.2.11 using LO matrix elements with up to two additional parton emissions. The matrix elements were merged with the SHERPA parton shower following the MEPS@LO prescription [44] and used the tune developed by the SHERPA authors. The NNPDF3.0NNLO set of PDFs was employed. The samples were produced using the VBF approximation, which avoids overlap with semileptonic diboson topologies by requiring a $t$-channel colour-singlet exchange. The EW production of $\ell\nu$jj is treated as a background and is subtracted from the data before unfolding. Interference between EW and QCD induced vector-boson processes was neglected.

The production of $t\bar{t}$+jets events was modelled using the SHERPA 2.2.12 event generator. In the SHERPA 2.2.12 samples NLO-accurate matrix elements, for up to one additional jet and LO-accurate matrix elements, for up to four additional jets, were calculated with the COMIX and OPENLOOPS libraries. Aside from this, the same general configuration as the signal $W$+ jets described above was used. Single-top quark production (single-top) included $s$- and $t$-channel diagrams and the associated production of a single top quark with a $W$-boson ($tW$). All single-top processes were modelled using the POWHEG BOX v2 [55–58] generator that provides matrix elements at NLO in $\alpha_s$. The NNPDF3.0NLO PDF set was used in the matrix element and events were interfaced with PYTHIA 8.230 using the A14 tune and the NNPDF2.3LO set of PDFs. The inclusive cross-section for single-top was normalised to the theory prediction calculated at NNLO in QCD with next-to-leading logarithmic (NNLL) soft-gluon corrections [59–62].

The POWHEG BOX v2 [56–58] generator was used to simulate diboson ($WW$, $WZ$ and $ZZ$) production at NLO accuracy in $\alpha_s$ [63]. The effect of singly resonant amplitudes and interference effects due to $Z/\gamma^*$ and same-flavour lepton combinations in the final state were included, where appropriate. Events were interfaced with PYTHIA 8.210 for the modelling of the parton shower, hadronisation, and underlying event, with parameters set according to the AZNLO tune [64]. The CT10 PDF set [65] was used for the hard-scattering processes, whereas the CTEQ6L1 PDF set [66] was used for the parton shower. The EVTGEN 1.2.0 program [67] was used to decay bottom and charm hadrons. The factorisation and renormalisation scales were set to the invariant mass of the boson pair. An invariant mass of $m_{\ell\ell} > 4$ GeV was required at matrix element level for any pair of same-flavour charged leptons.

Multijet production was simulated using PYTHIA 8.230 with LO matrix elements matched to the parton shower. The renormalisation and factorisation scales were set to the geometric mean of the squared transverse masses of the two outgoing particles in the matrix element. The NNPDF2.3LO PDF set was used in the matrix element generation, the parton shower, and the simulation of the multi-parton interactions. The A14 set of tuned parameters was used. Perturbative uncertainties were estimated through event weights [68] that encompass variations of the scales at which $\alpha_s$ is evaluated in the initial- and final-state shower as well as the PDF uncertainty in the shower and the non-singular part of the splitting functions.

All simulated event samples are corrected to compensate for small efficiency differences between data and simulation. These include correction factors relating to the efficiency of $b$-tagging for $b$-, $c$- and light-jets, lepton trigger, reconstruction, identification, and isolation, and the efficiency for jet-to-vertex association requirements. Further details on the event reconstruction can be found in Sect. 4.

## 4 Event reconstruction

Events are required to satisfy a set of quality requirements that ensures the detector was in good operating condition [73]. In addition, events are required to have a reconstructed primary vertex with two or more associated tracks, where the primary vertex is chosen as the vertex with the highest scalar sum of the $p_T^2$ of associated tracks [74]. The data sample was collected using either a single-electron or single-muon trigger with different transverse momentum, isolation and identification criteria, which depended on the data-taking periods, each characterised by a different instantaneous luminosity [75–77].

Baseline electrons are reconstructed by algorithms that combine ID tracks and clusters of energy deposits in the electromagnetic calorimeter. The track associated to the electron candidate is required to have a longitudinal impact parameter ($|z_0 \sin\theta|$) less than 0.5 mm and the significance of the transverse impact parameter ($|d_0/\sigma_{d_0}|$) is required to be less then 5.0 to ensure the electron candidate originates from the primary vertex. Baseline electron candidates are required to have $p_T > 10$ GeV and $|\eta| < 2.47$. Additionally, electrons reconstructed in the transition region between the calorimeter barrel and endcap regions, which contains a relatively large amount of inactive material, are removed by excluding electrons with $1.37 < |\eta| < 1.52$. Baseline

electron candidates are identified using the electromagnetic shower shape, calorimeter energy to tracker momentum ratio, and other discriminating variables that are combined into likelihood-based parameters; they are selected if they satisfy the *TightLLH* quality criterium [78]. The signal electron candidates must additionally satisfy the *Tight_VarRad* isolation requirement [78], which uses the calorimeter isolation and track-based isolation cones around the electron candidate. Unlike muon candidates defined below, the isolation cones for electrons are variable-radius. The electron energy scale and resolution is determined using electrons from $Z$-boson decays in data and applied to simulation [79].

Baseline muon candidates are reconstructed by combining tracks from the ID and MS sub-detectors via a global refit. Baseline muons are required to be of at least *Medium* quality [80] with transverse momentum greater than 10 GeV and $|\eta| < 2.4$. To ensure signal muon candidates are well isolated from other tracks, they are required to satisfy a combination of calorimeter and track-based isolation criteria implemented into the *Loose_FixedRad* isolation working point [80]. The associated ID track is required to satisfy $|z_0 \sin\theta| < 0.5$ mm and $|d_0/\sigma_{d_0}| < 3.0$ to be consistent with the primary vertex. The muon energy scale and resolution is determined using muons from $Z$-boson decays in data and applied to simulation [81].

Jets are clustered using the anti-$k_t$ algorithm [82] implemented in the FastJet package [83] with a radius parameter of $R = 0.4$. The jets are clustered from particle flow objects [84], which are charged-particle tracks matched to the hard-scatter vertex and calorimeter energy clusters following an energy subtraction algorithm that removes the calorimeter deposits associated with good-quality tracks from any vertex. Different MC-based calibration steps are applied to the reconstructed jets [85], including an area-based correction to account for energy contributions from pile-up interactions, a $p_{\mathrm{T}}$- and $\eta$-dependent calibration to match the generator-level energy scale of the jets, and the 'global sequential calibration' to minimize energy calibration differences between quark- and gluon-initiated jets. Finally, an in situ calibration is applied to jets in data to match the energy scale in simulation. All calibrated jets are required to have $p_{\mathrm{T}} > 30$ GeV and $|y| < 2.5$. Jets with $p_{\mathrm{T}} < 60$ GeV and $|y| < 2.4$ must also satisfy a requirement based on the output of the multivariate 'jet vertex tagger' (JVT) algorithm, which is used to identify and reject jets from pile-up vertices [86]. The *Tight* (default) working point is used and jets failing to satisfy the JVT requirements are discarded. These remaining jets are categorised as baseline jets.

Baseline jets originating from $b$-quarks need to be rejected to suppress background contributions from processes involving top quarks. Jets containing a $b$-hadron ($b$-jets) are identified using the DL1r $b$-tagging procedure [87], a deep learning multivariate algorithm trained using information on tracks and secondary vertices. Jets are rejected if they satisfy the DL1r working points tuned to have a 60% efficiency on average for jets associated with generated $b$-hadrons in simulated $t\bar{t}$ events. This working point is chosen to improve the purity of the $t\bar{t}$ control region described in Sect. 6. At the chosen working point, the light-jet (charm-jet) rejection measured in $t\bar{t}$ MC simulation is about a factor of 1155 (29) on average.

The missing transverse momentum (with magnitude $E_{\mathrm{T}}^{\mathrm{miss}}$) is estimated as the negative vector sum of the transverse momentum of all identified electrons, photons, jets and muons [88]. All electrons, muons and jets described above are used as input to the reconstruction. Tracks not associated with any such object are included in the so-called soft term.

An overlap-removal procedure is applied to uniquely identify signal lepton candidates and signal jet candidates in an event. Baseline electrons are removed if they share an ID track with a baseline muon. Baseline jets within $\Delta R < 0.2$ of a baseline electron are removed, then any remaining baseline electrons with $0.2 < \Delta R < 0.4$ of a baseline jet are removed. Finally, baseline muons closer than $\Delta R = 0.4$ to any remaining baseline jets are removed.

## 5 Event selection

Events are required to contain a single electron or muon satisfying the criteria described in Sect. 4 and summarised in the first section of Table 2. The leading (highest $p_{\mathrm{T}}$) lepton is required to be matched to the single lepton that triggered the event and have transverse momentum $p_{\mathrm{T}} >$ 30 GeV. In addition, the angular separation between the lepton and any selected jet is required to be $\Delta R(\ell, \mathrm{jet}) > 0.4$. To enrich the selected data sample in events where the $W$-boson is produced in association with many jets, events are required to contain at least one jet with transverse momentum $p_{\mathrm{T}} >$ 500 GeV. Contributions from $Z$ + jets and dileptonic $t\bar{t}$ processes are suppressed by imposing a veto on any additional leptons in the event. To further suppress the contribution of top-quark backgrounds to the measurement region, a $b$-jet veto is applied. The event selection is summarised in the second section of Table 2.

The selection described above forms the *inclusive* region. Three additional regions that are subsets of the inclusive selection are defined. The first is the *inclusive-2 jets* region, where a requirement of at least two jets is applied. The second region is the *collinear region*, where the angular separation between the lepton and the closest jet with $p_{\mathrm{T}} > 100$ GeV is required to be $\Delta R_{\mathrm{min}}(\ell, \mathrm{jet}_i^{100}) < 2.6$. The final region is the *back-to-back region*, where the angular separation requirement is inverted relative to the collinear region and so that $\Delta R_{\mathrm{min}}(\ell, \mathrm{jet}_i^{100}) > 2.6$. A summary of the region selection criteria can be found at the bottom section of Table 2.

**Table 2** Detector-level selections used to define the signal regions at reconstruction level (see text for details)

| | |
|---|---|
| **Object selection** | |
| Lepton momentum | $p_{\mathrm{T}}^{\ell} > 10$ GeV |
| Electron pseudorapidity | $\lvert\eta\rvert < 1.37,\ 1.52 < \lvert\eta\rvert < 2.47$ |
| Muon pseudorapidity | $\lvert\eta\rvert < 2.4$ |
| Jet transverse momentum | $p_{\mathrm{T}}^{\mathrm{jet}} > 30$ GeV |
| Jet rapidity | $\lvert y\rvert < 2.5$ |
| **Event selection** | |
| Leading lepton | $p_{\mathrm{T}}^{\ell} > 30$ GeV, trigger matched |
| Number of leptons | $n_{\ell} = 1$ |
| Angular separation of leptons and jets | $\Delta R(\ell, \mathrm{jet}) > 0.4$ |
| Number of jets | $n_{\mathrm{jet}} \geq 1$ |
| Leading jet transverse momentum | $p_{\mathrm{T}}^{\mathrm{jet}} > 500$ GeV |
| $b$-jet veto | $n_{b\text{-jet}} = 0$ |
| **Signal regions** | |
| Inclusive | All requirements above |
| Inclusive 2-jet | Inclusive plus $n_{\mathrm{jet}} \geq 2$ |
| Collinear | Inclusive plus $\Delta R_{\mathrm{min}}(\ell, \mathrm{jet}_i^{100}) < 2.6$ |
| Back-to-back | Inclusive plus $\Delta R_{\mathrm{min}}(\ell, \mathrm{jet}_i^{100}) > 2.6$ |

## 6 Background estimation

Several SM processes can give rise to a signature similar to the $W+$ jets signal process. These background processes need to be estimated and subtracted from data before performing the unfolding procedure. The dominant prompt-lepton backgrounds arise from processes involving the decay of an EW boson to final states with leptons, and are therefore primarily associated with $t\bar{t}$ and $Z$ + jets processes. The $t\bar{t}$ and $Z$ + jets backgrounds contribute up to 8% of the total expected event yield across the four regions. They contribute equally to both the electron and muon channels. Backgrounds can also arise from multijet events for which the leptons are either non-prompt (i.e. arising from heavy-quark decays), or jets misidentified as leptons, collectively referred to as 'fake leptons'. The latter contribution represents a significant background in the back-to-back region of the electron selection (up to 20%), while the contribution of fake leptons in the muon channel is a sub-dominant background. Multijet backgrounds in all other regions contribute up to 8% (3%) for electrons (muons), respectively. The single-top-quark and diboson processes represent sub-dominant backgrounds. Their contributions are estimated directly from simulation, and are expected to account for up to 2% (3%) for electrons (muons). The EW production of $V+$jj contributes up to 10% of the total expected event yield for large invariant jet mass in the inclusive-2 jets region.

The dominant backgrounds, namely $t\bar{t}$, $Z$ + jets, and multijet are estimated by using a semi-data-driven technique separately for each background. The normalisation of these background contributions is extracted from data in dedicated control regions enriched in their respective processes. The goal of this method is to extract normalisation factors for each of the backgrounds without introducing a bias from the contributions of other backgrounds that are known to be mismodelled in the high momentum region of phase space. The control regions are constructed such that they are kinematically similar to the inclusive measurement region, except for a few selections that allow the control region to be enriched in the targeted background process. These factors are statistically compatible with normalisation factors derived within each individual signal region. Since the perturbative accuracy of the $t\bar{t}$ and $Z$ + jets samples varies with additional QCD emissions, the normalisation factors are parameterised as a function of the number of jets ($n_{\mathrm{jet}}$). The multijet normalisation factor is parameterised as a function of lepton $p_{\mathrm{T}}$ and $|\eta|$ to capture the variations of the fake-lepton composition as a function of detector geometry and momentum of the fake leptons. The $t\bar{t}$ and $Z$ + jets normalisation factors are determined first using the MC predictions for multijets, and then applied to the multijets control region where the multijet normalisation factor is subsequently derived. This approach is valid because of the small contribution of the multijets process in the $t\bar{t}$ and $Z$ + jets control regions.

The $t\bar{t}$ control region is defined in the same way as the inclusive region, except the $b$-jet veto is replaced with the requirement of at least two $b$-tagged jets. The purity of this region in terms of $t\bar{t}$ events is more than 80%, with small contributions from single-top and $W$+ jets processes. In both the electron and muon channels, the extracted normalisation factors are $0.8 \pm 0.1$ for the 2-jet and 3-jet bins and close to unity for the higher jet multiplicities. The background contribution to the 1-jet bin is less than 1% of the total expected event yield for all samples. Good agreement between the background model with the normalisation factors applied and data is observed as a function of all observables measured. The only exception is the $m_{\mathrm{jj}}$ distribution, where the expected event yield is $1\sigma$ higher than the data for $m_{\mathrm{jj}} > 1$ TeV, where $\sigma$ is the total uncertainty. An additional $m_{\mathrm{jj}}$ modelling uncertainty is applied to account for this mis-modelling as described in Sect. 8.

Most of the $Z$ + jets contribution in the signal region consists of events where one of the two leptons fails the kinematic or geometric requirements, resulting in a single-lepton event. The remaining $Z$ + jets contributions arise from one of the leptons being mis-identified as a jet. The $Z$ + jets control region is defined in the same way as the inclusive region, except the single-lepton requirement is replaced by requiring exactly two same-flavour opposite-sign leptons with an invariant mass between $60 < m_{\ell\ell} < 120$ GeV. In the $Z$ + jets control region, the purity of the $Z$ + jets process is approximately 90% with the remaining contributions arising primarily from diboson production. The average normalisation factor for $Z$ + jets events with up to three jets is $1.05 \pm 0.05$ and decreases to $0.80 \pm 0.05$ for events with greater than five jets. Mis-identified jets that are matched to generator-level electrons from the $Z$-boson decay are excluded from the jet-multiplicity-dependent normalisation factor in the signal region to match the jet counting in the control region, where both electrons are reconstructed. The corrected background model provides an excellent description of the data in the control region as a function of all measurement observables, except for $m_{\mathrm{jj}}$. As for the $t\bar{t}$ process, an additional modelling uncertainty is applied to the $Z$ + jets of the $m_{\mathrm{jj}}$ distribution in the signal region.

The multijet control region is defined in the same phase space as each of the signal regions, but the lepton is instead required to fail to satisfy the impact parameter or the isolation lepton criteria. The purity of this region in terms of multijet events is more than 80%, with small contributions from top and $W$+ jets processes. The normalisation factor is roughly independent of lepton $p_{\mathrm{T}}$ for the electron and muon channels, but ranges from $0.3 \pm 0.1$ to $0.8 \pm 0.1$ for high to low electron $|\eta|$. After the application of the lepton $p_{\mathrm{T}}$ and $|\eta|$ correction factors to the multijet MC sample, an excellent description of the data is observed for all observables measured. The modelling of the multijet estimate is additionally checked in a region where the lepton signal criteria are satisfied, but the missing transverse momentum is below 100 GeV. This validation region has a small 8% overlap with the measurement signal region while the multijet background accounts for more than half of the total event yield. Good agreement is found between the simulated events and observed data in the validation region for the full set of measured observables; therefore, no additional uncertainties are assigned to the multijet normalisation factors.

The event yields in each measured signal region, after the corrections extracted from the control regions as described above, are summarised in Table 3 with signal theory uncertainties included. The $W$+ jets signal prediction is obtained from the SHERPA 2.2.11 simulation. The large $p_{\mathrm{T}}$ requirement on the leading jet selects high jet multiplicity events, so the total uncertainty in the number of $W$+ jets is dominated by LO matrix elements for SHERPA 2.2.11. Overall, the total signal-plus-background predictions are in good agreement with the observed data across all regions for both the electron and muon channels. Differential distributions in the electron and muon channels are shown in Fig. 2 for $\Delta R_{\mathrm{min}}(\ell, \mathrm{jet}_i^{100})$, $p_{\mathrm{T}}^{\ell\nu}/p_{\mathrm{T}}^{\text{closest jet}}$, $p_{\mathrm{T}}^{\ell\nu}$, and leading jet $p_{\mathrm{T}}$. The combined signal plus background predictions are in good agreement with the observed data for the full set of observables, except for the $m_{\mathrm{jj}}$ distribution where the combined signal plus background prediction is about 1–$2\sigma$ higher than the data including all signal and all background uncertainties, similar to that observed in the $t\bar{t}$ and $Z$ + jets control regions.

## 7 Unfolding

The cross-section are unfolded to particle level using an iterative Bayesian unfolding technique [89] to account for object and selection inefficiencies, small acceptance corrections, and resolution effects. The data are unfolded to particle-level regions that closely match the reconstruction-level object and phase-space selections shown in Table 2. Final-state photons radiated from the leptons are added to the lepton four-momentum within a cone of $\Delta R = 0.1$. These leptons are referred to as 'dressed leptons'. The anti-$k_t$ jet clustering algorithm is used to cluster all final state particles with a lifetime greater than 30 ps into jets, excluding the neutrino and the electron or muon from the $W$-boson decay and any photon included in the dressed lepton. The missing transverse momentum is computed from the final-state neutrino from the $W$-boson decay. Events are then selected to contain at least one particle-level jet with transverse momentum greater than 500 GeV and exactly one dressed lepton with transverse momentum greater than 30 GeV and $|\eta| < 2.5$. The lepton $\eta$ requirements are harmonised between the electron and muon channels to unfold to a common fiducial region. All other

**Table 3** Event yields in the electron and muon channels for the different signal regions after the application of the background normalisation factors. The uncertainties in the predictions include statistical and systematic uncertainties added in quadrature. The nominal SHERPA 2.2.11 signal prediction is used to compare with the data. Theoretical uncertainties are also included for signal

| Process | Inclusive | Collinear | Inclusive 2-jet | Back-to-back |
|---|---|---|---|---|
| | | **Electron channel** | | |
| $t\bar{t}$ | 7 200 ± 1 700 | 5 800 ± 1 200 | 7 100 ± 1 600 | 1 400 ± 400 |
| Multijet | 14 600 ± 1 900 | 6 300 ± 1 300 | 11 600 ± 1 700 | 8 300 ± 700 |
| Single top | 2 100 ± 600 | 1 600 ± 500 | 2 100 ± 600 | 540 ± 140 |
| EW $V$+jj | 4 200 ± 800 | 3 000 ± 600 | 3 700 ± 700 | 1 150 ± 220 |
| $Z$+jets | 6 350 ± 210 | 5 110 ± 200 | 5 990 ± 200 | 1 241 ± 68 |
| $W(\rightarrow \tau\nu)$+jets | 6 500 ± 1 000 | 4 000 ± 500 | 5 600 ± 800 | 2 500 ± 400 |
| Diboson | 3 440 ± 340 | 2 220 ± 240 | 3 070 ± 320 | 1 220 ± 110 |
| $W$+jets | 77 000 ± 25 000 | 54 000 ± 21 000 | 68 000 ± 24 000 | 23 000 ± 4 000 |
| SM Total | 122 000 ± 25 000 | 82 000 ± 21 000 | 108 000 ± 25 000 | 40 000 ± 4 000 |
| Data | 119 880 | 79 890 | 105 740 | 39 990 |
| | | **Muon channel** | | |
| $t\bar{t}$ | 5 500 ± 1 200 | 4 800 ± 1 000 | 5 500 ± 1 200 | 690 ± 200 |
| Multijet | 3 640 ± 150 | 2 460 ± 130 | 3 250 ± 160 | 1 176 ± 56 |
| Single top | 1 700 ± 500 | 1 400 ± 400 | 1 700 ± 500 | 373 ± 89 |
| EW $V$+jj | 3 600 ± 700 | 2 600 ± 500 | 3 200 ± 600 | 940 ± 180 |
| $Z$+jets | 4 330 ± 150 | 3 590 ± 140 | 4 150 ± 140 | 743 ± 44 |
| $W(\rightarrow \tau\nu)$+jets | 5 100 ± 800 | 3 300 ± 500 | 4 500 ± 700 | 1 780 ± 320 |
| Diboson | 2 880 ± 300 | 1 930 ± 210 | 2 590 ± 280 | 953 ± 90 |
| $W$+jets | 72 000 ± 24 000 | 52 000 ± 20 000 | 65 000 ± 23 000 | 20 000 ± 3 500 |
| SM Total | 99 000 ± 24 000 | 72 000 ± 20 000 | 90 000 ± 23 000 | 27 000 ± 3 500 |
| Data | 94 230 | 67 970 | 85 130 | 26 260 |

requirements are applied that define the regions in Table 2, except for the $b$-jet veto requirement to keep the particle-level measurement inclusive in jet flavour. The unfolding algorithm implemented in the ROOUNFOLD toolkit [90] is used with two iterations. The electron and muon channels are unfolded separately and then combined as discussed in Sect. 9.

The signal event yields are determined by subtracting the estimated background contributions from the data satisfying the detector-level selection. The resulting distributions are corrected for detector-level effects to the fiducial phase space at particle level. The SHERPA 2.2.11 generator is used as the nominal signal prediction in the unfolding procedure. Simulated signal events, satisfying both the detector-level and particle-level selections, are used to generate a response matrix for each distribution and the particle-level distribution is used as the initial prior to determine the first estimate of the unfolded data distribution. For the second iteration, the new estimate of unfolded data is obtained using the background-subtracted data and an unfolding matrix, which is derived using Bayes' theorem, from the response matrix and the current prior. Before entering the iterative unfolding, the background-subtracted data are corrected for the expected fraction of events that satisfy the detector-level selection, but not the particle-level one (unmatched-events). For each bin of each differential distribution, the unfolded event yields are divided by the integrated luminosity of the data sample and by the bin width, to obtain the measured cross-section.

A $\Delta R$-matching procedure is applied to fill the matrices and the unmatched-events fraction is defined accordingly. The lepton and highest $p_{\mathrm{T}}$ jet at reconstruction and generator level are required to be matched within an angular cone of $\Delta R = 0.4$. Moreover the reconstructed jet that is found to be closest to the lepton is required to be matched to the closest particle-level jet within an angular cone of $\Delta R = 0.4$. In the case of the inclusive-2 jets region, the sub-leading jet at reconstruction level is also required to be matched to the sub-leading jet at particle level. If the matching criteria fail, the corresponding event does not enter the response matrix calculation and is considered as an unmatched fake object that is subtracted from the data alongside other backgrounds before unfolding.

Jets that satisfy the generator-level selection on the leading jet of $p_{\mathrm{T}} > 500$ GeV may fail this requirement at reconstruction level due to the finite jet energy resolution. To account for these migration effects, an additional underflow bin is added for all observables, where the selection on the reconstruction level leading jet transverse momentum is relaxed to $400 < p_{\mathrm{T}} < 500$ GeV. These migrations account for less than 10% of the total events in the fiducial region.

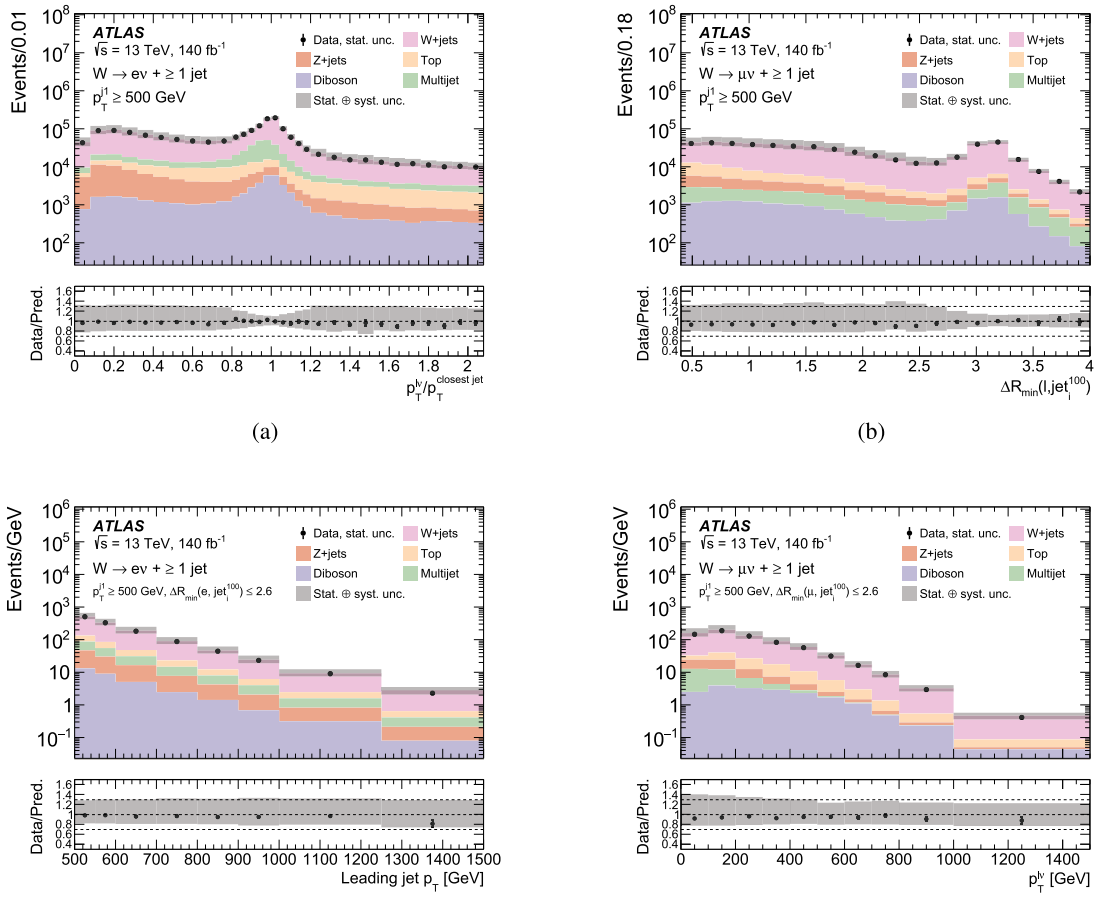


**Fig. 2** Differential distributions at reconstruction level in the **a**, **c** electron or **b**, **d** muon channel for **a**, **b** inclusive and **c**, **d** collinear signal regions after the application of the background normalisation factors. The signal process is stacked above all background predictions. The bottom panel shows the ratio of the data to the total signal plus background prediction. The shaded band includes statistical and systematic uncertainties from signal and background processes added in quadrature

## 8 Systematic uncertainties

Several sources of experimental and theoretical uncertainties are considered during the unfolding process. Systematic uncertainties are derived for each observable by propagating changes from each systematic source through the MC unfolding inputs and the subtracted background in the unfolded data. For all sources of uncertainty that affect the background model, the background estimate is recalculated with the modified background model and propagated to the subtracted background before unfolding. For experimental uncertainties affecting the reconstructed signal and background in a similar way, the unfolding response matrices, reconstruction efficiencies and the unmatched events corrections are adjusted alongside the subtracted background in the unfolded data. Uncertainties are assessed separately for the electron and muon channels, with correlations taken into account as necessary.

Systematic uncertainties relating to the lepton triggering, reconstruction, identification, and isolation are included [78, 80, 91]. Muon reconstruction uncertainties include variations in muon momentum scale, the ID and MS resolution, and the sagitta-bias corrections [81]. Variations of the electron energy scale and resolution are included and arise from material interactions, in situ calibrations, shower shapes, and pile-up modelling [92]. Electron and muon identification uncertainties account for variations of the efficiency scale factors by varying the statistical and systematic components of the scale factors.

The jet energy scale (JES) and resolution (JER) uncertainties are derived as a function of the jet transverse momentum, rapidity, and flavour [85]. A reduction scheme is applied resulting in 29 nuisance parameters for the JES and 13 nui-

sance parameters for the JER. Aspects of the JES/JER uncertainty that rely on the relative fraction of quark- to gluon-initiated jets are estimated as a function of the jet momentum and rapidity from simulation. The uncertainty in the efficiency corrections for the JVT requirement that is used to mitigate the impact of pile-up jets is evaluated by shifting the scale factors by the corresponding uncertainties. Uncertainties in the correction factors for the $b$-tagging efficiency are applied to the MC samples using dedicated flavour-enriched samples in data and an additional term is included to extrapolate the measured uncertainties to the very high-$p_{\mathrm{T}}$ phase space using MC-based uncertainties [93–95].

Variations in the energy scale and resolution of all physics objects are also propagated to the reconstruction of the missing transverse momentum.

Sources of uncertainty relating to the background estimation include statistical uncertainties in the background normalisation factors, theoretical uncertainties including variations of the renormalisation and factorisation scales and PDF eigenvector variations for each background. Additional uncertainties are applied to the $m_{\mathrm{jj}}$ background model for $t\bar{t}$ and $Z$ + jets processes. Residual mis-modelling of the $m_{\mathrm{jj}}$ distribution in the control regions persists at the 1–2$\sigma$ level for $m_{\mathrm{jj}} > 1$ TeV. No additional uncertainties are added to the multijet process as described in Sect. 6 given the good modelling observed in the corresponding multijet validation region. The difference between the nominal prediction and the data is symmetrised and taken as a conservative uncertainty. Due to the small contributions of these backgrounds in the $m_{\mathrm{jj}} > 1$ TeV measurement regions, this uncertainty has a very small impact on the final results.

The uncertainty in the combined 2015–2018 integrated luminosity is 0.83% [32]. The uncertainty in pile-up effects is assessed by varying the average number of pile-up interactions.

Several additional sources of uncertainties are assigned to the unfolding procedure, which account for possible simulation or theoretical biases:

- *Prior-related unfolding bias*: These assess the sensitivity of the unfolded data to the choice of the initial prior from the nominal SHERPA 2.2.11 signal model. The SHERPA 2.2.11 sample is reweighted at generator level such that it matches the background-subtracted data at reconstruction level for each measured observable. This pseudo-data sample is unfolded with the nominal response matrix, and the basic unfolding bias uncertainty is obtained from the difference between the unfolded distribution and the reweighted generator-level distribution.
- *Uncertainty in migrations, efficiencies and fakes modelling*: The alternative MADGRAPH5_AMC@NLO +PYTHIA8 sample is used to assess the uncertainty due to the mis-modelling of the migrations, the reconstruction efficiency and the fake corrections. In this procedure, first the alternative signal sample is reweighted to match the nominal SHERPA 2.2.11 sample at generator level to avoid double-counting with the prior-related uncertainty. Then the reweighted sample is used to unfold the data and the difference between that and the nominal unfolding result is taken as the systematic error.
- *Signal modelling uncertainty*: An uncertainty in the measured cross-section is assessed from signal theory uncertainties. The scale and PDF variations in the nominal SHERPA 2.2.11 prediction are varied in the unfolding MC inputs, and the unfolded data are compared with the nominal unfolded cross-section in data to derive an uncertainty. This uncertainty is negligible compared to the two other uncertainties.

The statistical uncertainty in the unfolded measurement and its bin-by-bin correlations are assessed using the *bootstrap method* [96] with an ensemble of 10,000 replicas of the original data sample for each measured observable.

Measurements in the electron and muon channels are combined and an average value is reported, as described in Sect. 9. During the combination, common sources of uncertainties are correlated across the channels, while those uniquely affecting the electron or muon channel are treated as uncorrelated. The statistical and systematic uncertainties in the unfolded inclusive cross-sections after the combination are shown in Table 4. Uncertainties in the inclusive cross-sections across all regions are approximately 3%–4% and dominated by systematic uncertainties, while statistical uncertainties constitute less than 0.5% of the uncertainty in the measured cross-section. The dominant sources of systematic uncertainty arise from the background modelling driven by the statistical uncertainty in the normalisation factors, JES/JER, $b$-tagging, and unfolding uncertainties. The 'Others' category contains sub-dominant sources of uncertainties arising from missing transverse momentum reconstruction and the jet-to-vertex fraction uncertainties.

Differential distributions of the relative statistical and systematic uncertainties in the unfolded cross-section for $\Delta R_{\mathrm{min}}(\ell, \mathrm{jet}_i^{100})$ and $p_{\mathrm{T}}^{\ell\nu}$ in the inclusive region; $p_{\mathrm{T}}^{\ell\nu}/p_{\mathrm{T}}^{\text{closest jet}}$ and leading jet $p_{\mathrm{T}}$ in the collinear region are shown in Fig. 3. The total uncertainty is up to 10% in the inclusive region and up to 15% in the collinear region. The background modelling uncertainties are the dominant source of uncertainty and contribute at a similar level to the statistical uncertainty across most distributions. In the back-to-back region and highest energy bins of the leading jet $p_{\mathrm{T}}$ and the $W$-boson $p_{\mathrm{T}}$ the statistical uncertainties are one of the leading sources of uncertainty and are around 10–15%. All other sources of uncertainty contribute at the few percent level across all distributions.

**Table 4** Relative uncertainties (in %) in the measured integrated cross-sections. Statistical uncertainties from the data and sources of systematic uncertainties are shown separately. The 'Others' category contains sub-dominant uncertainties arising from missing transverse momentum reconstruction and the jet-to-vertex fraction uncertainties

| Uncertainty source | Regions | | | |
|---|---|---|---|---|
| | Inclusive | Inclusive 2-jet | Collinear | Back-to-back |
| Background modelling | 2.0 | 2.1 | 2.0 | 2.3 |
| JES/JER | 1.3 | 1.2 | 1.1 | 1.6 |
| *b*-tagging | 1.2 | 1.4 | 1.5 | 0.7 |
| Lepton | 0.8 | 0.8 | 0.7 | 1.2 |
| Unfolding | 0.34 | 0.4 | 0.6 | 0.05 |
| Luminosity | 0.8 | 0.8 | 0.8 | 0.8 |
| Pile-up | 0.19 | 0.15 | 0.22 | 0.18 |
| Others | 0.14 | 0.19 | 0.20 | 0.03 |
| Data statistical | 0.4 | 0.5 | 0.5 | 0.8 |
| Total uncertainty | 3.3 | 3.4 | 3.4 | 4 |

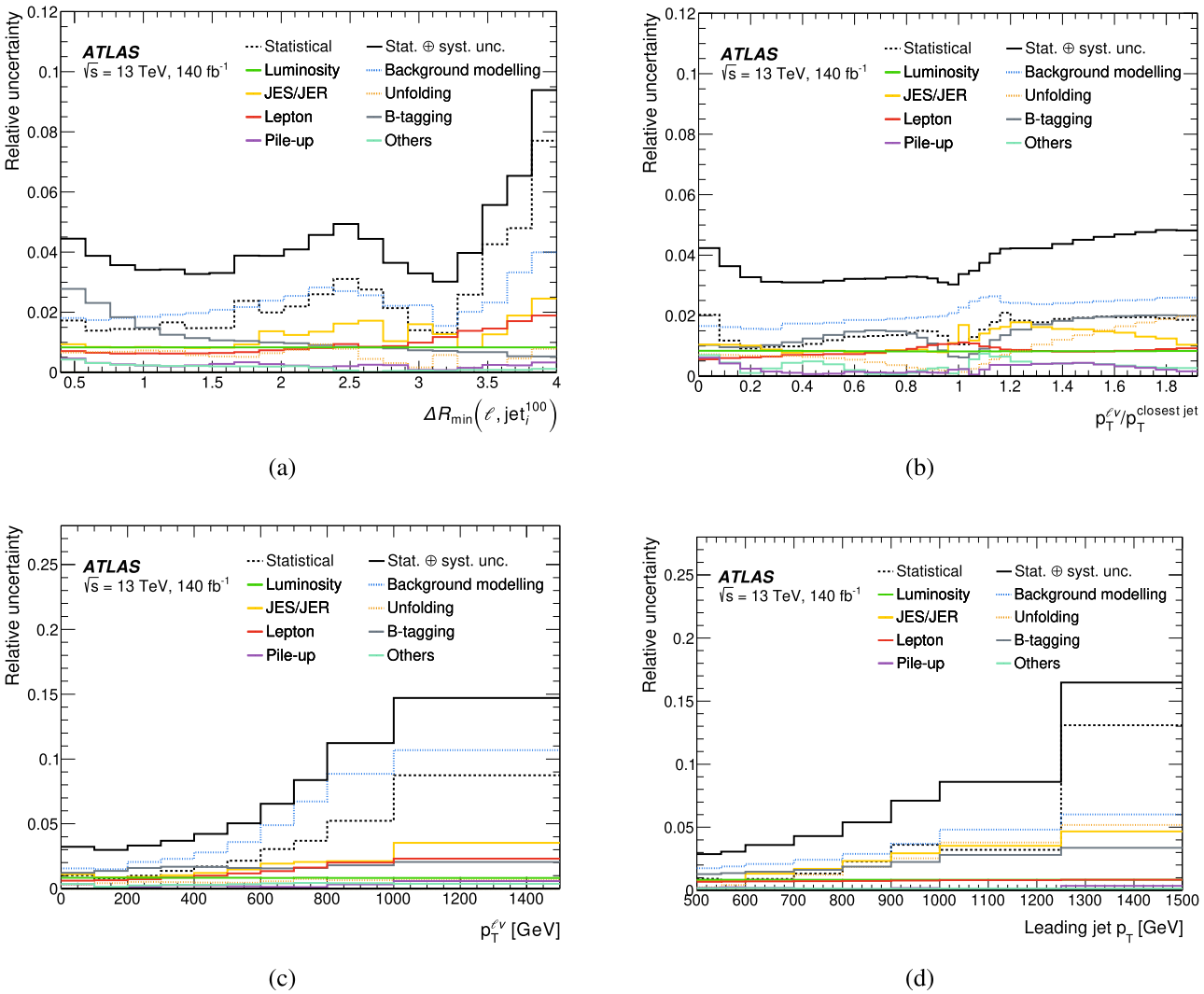


**Fig. 3** Relative systematic uncertainties in the averaged cross-section for various differential distributions in the **a**, **b** inclusive and **c**, **d** collinear phase spaces. The upper solid line shows the total uncertainty in the measured cross-section in data, and includes correlations between the systematic components. The 'Others' category contains sub-dominant uncertainties arising from missing transverse momentum reconstruction and the jet-to-vertex fraction uncertainties

## 9 Results

The cross-sections in the electron and muon channels are measured separately and an average cross-section is obtained using a $\chi^2$ likelihood fit with the COMBINER [97] package. In this method, all uncertainties are treated as correlated between the electron and muon channels, except for statistical uncertainties and lepton-specific systematic uncertainties such as unfolding uncertainties, lepton triggering, and the lepton energy and momentum resolution. Additionally, uncertainties in the multijet backgrounds are considered uncorrelated since the two channels are dominated by different fake-lepton processes. All systematic uncertainties are symmetrised before the combination. The combined cross-section is found to be consistent with the individual electron and muon channels for the full set of regions and observables.

The measured data is compared with several state-of-the-art theoretical predictions, including two NLO multi-jet merged generator predictions: the SHERPA 2.2.11 and MADGRAPH5_AMC@NLO+PYTHIA8 samples described in Sect. 3. The SHERPA 2.2.11 predictions are shown with and without NLO $\text{EW}_{\text{virt}}$ corrections to demonstrate their impact on the measured distributions. Additionally, a fixed-order prediction of $W+1$-jet was generated at NNLO in $\alpha_s$ using the MCFM program [23,98,99] and is compared with the data. The NNLO calculation relies on the $N$-jettiness subtraction formalism and the event shape variable $N$-jettiness $\tau$ [100]. For all results presented in this paper, a requirement of $\tau_{\text{cut}} = 10^{-4}$ is used and found to impact the final results at the sub-percent level for all differential distributions measured. A dynamic scale choice is used where $\mu = \sqrt{m_{\ell\nu}^2 + \sum_{\text{jets}} p_{\text{T}}^2}$, where $m_{\ell\nu}$ is the invariant mass of the lepton–neutrino system and the second term contains the scalar sum of the transverse momentum squared of all jets with $p_{\text{T}} > 30$ GeV. The NNPDF3.0NNLO set of PDFs was used. The PDF uncertainties from the MCFM calculation are expected to be similar in size to SHERPA 2.2.11 NLO calculations and shown in Table 5. The renormalisation and factorisation scales are varied coherently by a factor of two, avoiding asymmetric variations. Non-perturbative effects in the high-momentum phase space of this analysis were found to be negligible for all measured observables. The effects of higher-order EW corrections on the MCFM prediction are assessed by extrapolating from the SHERPA prediction. A bin-by-bin correction factor computed from the ratio of the SHERPA QCD with $\text{EW}_{\text{virt}}$ prediction to the QCD-only prediction is applied to the MCFM prediction and displayed separately throughout all results. This procedure was discussed with the MCFM authors and also done in the corresponding $Z$ + jets analysis [18].

The combined inclusive cross-sections in the inclusive, inclusive 2-jet, collinear, and back-to-back regions are shown in Fig. 4 and tabulated in Table 5. For results showing predictions accurate to QCD, uncertainties include scale and PDF uncertainties added in quadrature, while the results reported with EW virtual corrections display uncertainties arising from the different EW combination schemes only. The measurement uncertainties are significantly smaller than the uncertainties in the signal predictions from the SHERPA 2.2.11 and MADGRAPH5_AMC@NLO+PYTHIA8 event generators, which are dominated by variations in the renormalisation and factorisation scale uncertainties. In particular, SHERPA 2.2.11 uncertainties are larger than the MADGRAPH5_AMC@NLO uncertainties due to the 3-5j@LO calculations of the matrix element for SHERPA. The uncertainty shown in Fig. 4 is the total uncertainty in the prediction which is very large in comparison to the EW corrections and scale uncertainties in the QCD predictions. The fixed-order MCFM $W+1$-jet prediction computed at NNLO accuracy is found to be in good agreement with the data across all regions with a precision comparable to that of the measured cross-sections from data. The NLO $\text{EW}_{\text{virt}}$ corrections lead to an overall decrease in the inclusive cross-section by 10%–12%, in agreement with fixed-order calculations computed for $V$+2-jet in Ref. [101]. This improves the agreement of the SHERPA prediction with the data in the collinear region, but leads to an approximate 10% underestimate of the cross-sections for the MCFM prediction.

Measurements of the differential cross-section for all observables are shown in Figs. 5, 6 and 7. The measured differential distributions are compared with the same three signal predictions as described above. For all figures, the main panel shows the various theoretical predictions that do not include NLO EW corrections, while the two lower panels additionally show the effect of NLO $\text{EW}_{\text{virt}}$ as computed from SHERPA 2.2.11. The uncertainties in the QCD accurate predictions contain uncertainties due to scale and PDF uncertainties added in quadrature, while the predictions including NLO $\text{EW}_{\text{virt}}$ corrections display only the uncertainty due to different EW correction combination schemes. The measured cross-sections in data and their statistical uncertainty are shown by the solid dots and error bars, while the shaded band shows the systematic and statistical uncertainties added in quadrature.

Figure 5 shows the differential cross-sections as a function of $\Delta R_{\text{min}}(\ell, \text{jet}_i^{100})$ and $p_{\text{T}}^{\ell\nu}/p_{\text{T}}^{\text{closest jet}}$ in the inclusive phase space. These observables can be used to distinguish $W$-boson emission from a high-momentum jet, referred to as the collinear events, from events where the $W$-boson recoils against a single initial-state-radiation jet, referred to as back-to-back events. Due to the leading jet $p_{\text{T}} > 500$ GeV requirement, these back-to-back topologies

**Table 5** Measured fiducial cross-section ($\sigma_{\text{fid}}$) in each signal region with theoretical predictions from SHERPA 2.2.11, MADGRAPH5_AMC@NLO+PYTHIA8, and MCFM W+1-jet@NNLO. Systematic uncertainties in the measured cross-sections are separated into statistical and non-statistical sources, while theoretical predictions show uncertainties arising from scale and PDF variations separately. For results showing predictions accurate to QCD, uncertainties include scale and PDF uncertainties added in quadrature, while the results reported with EW virtual corrections display uncertainties arising from the different EW combination schemes only

| Inclusive | $\sigma_{\text{fid}}$ (fb) | | Total $\Delta\sigma_{\text{fid}}$ (fb) | |
|---|---|---|---|---|
| Data | 778 | $\pm 3$ (stat.) | | $\pm 25$ (syst.+stat.) |
| SHERPA 2.2.11 | 823 | $^{+8}_{-10}$ (PDF) | $^{+360}_{-210}$ (scale) | $^{+360}_{-210}$ |
| SHERPA 2.2.11 QCD+EW | 733 | | $^{+32}_{-32}$ (EW virt) | $^{+360}_{-210}$ |
| MADGRAPH5_AMC@NLO+PYTHIA8 | 851 | $^{+6}_{-6}$ (PDF) | $^{+90}_{-130}$ (scale) | $^{+90}_{-130}$ |
| MCFM | 765 | | $^{+26}_{-26}$ (scale) | |
| MCFM QCD+EW | 680 | | $^{+30}_{-30}$ (EW virt) | $^{+40}_{-40}$ |
| Inclusive 2-jet | $\sigma_{\text{fid}}$ (fb) | | Total $\Delta\sigma_{\text{fid}}$ (fb) | |
| Data | 684 | $\pm 3$ (stat.) | | $\pm 23$ (syst.+stat.) |
| SHERPA 2.2.11 | 728 | $^{+7}_{-10}$ (PDF) | $^{+340}_{-200}$ (scale) | $^{+350}_{-200}$ |
| SHERPA 2.2.11 QCD+EW | 649 | | $^{+28}_{-28}$ (EW virt) | $^{+350}_{-200}$ |
| MADGRAPH5_AMC@NLO+PYTHIA8 | 754 | $^{+5}_{-5}$ (PDF) | $^{+76}_{-110}$ (scale) | $^{+76}_{-110}$ |
| MCFM | 693 | | $^{+28}_{-28}$ (scale) | |
| MCFM QCD+EW | 620 | | $^{+30}_{-30}$ (EW virt) | $^{+40}_{-40}$ |
| Collinear | $\sigma_{\text{fid}}$ (fb) | | Total $\Delta\sigma_{\text{fid}}$ (fb) | |
| Data | 532 | $\pm 3$ (stat.) | | $\pm 18$ (syst.+stat.) |
| SHERPA 2.2.11 | 574 | $^{+6}_{-8}$ (PDF) | $^{+290}_{-170}$ (scale) | $^{+300}_{-170}$ |
| SHERPA 2.2.11 QCD+EW | 521 | | $^{+18}_{-18}$ (EW virt) | $^{+300}_{-170}$ |
| MADGRAPH5_AMC@NLO+PYTHIA8 | 578 | $^{+4}_{-4}$ (PDF) | $^{+50}_{-90}$ (scale) | $^{+50}_{-90}$ |
| MCFM | 530 | | $^{+31}_{-31}$ (scale) | |
| MCFM QCD+EW | 480 | | $^{+17}_{-17}$ (EW virt) | $^{+35}_{-35}$ |
| Back-to-back | $\sigma_{\text{fid}}$ (fb) | | Total $\Delta\sigma_{\text{fid}}$ (fb) | |
| Data | 247 | $\pm 2$ (stat.) | | $\pm 9$ (syst.+stat.) |
| SHERPA 2.2.11 | 249 | $^{+2}_{-3}$ (PDF) | $^{+60}_{-40}$ (scale) | $^{+60}_{-40}$ |
| SHERPA 2.2.11 QCD+EW | 210 | | $^{+10}_{-10}$ (EW virt) | $^{+60}_{-40}$ |
| MADGRAPH5_AMC@NLO+PYTHIA8 | 273 | $^{+2}_{-2}$ (PDF) | $^{+40}_{-40}$ (scale) | $^{+40}_{-40}$ |
| MCFM | 235 | | $^{+5}_{-5}$ (scale) | |
| MCFM QCD+EW | 200 | | $^{+13}_{-13}$ (EW virt) | $^{+14}_{-14}$ |

typically lead to high-momentum $W$-boson events containing a lepton whose angular separation with the leading jet is $\Delta R(\ell, \text{jet}^{\text{leading}}) \sim \pi$. Furthermore, these single-jet events contain a $W$-boson with momentum that balances the leading jet in the transverse plane, leading to $p_{\text{T}}^{\ell\nu}/p_{\text{T}}^{\text{closest jet}}$ close to one. In contrast, events where the $W$-boson is emitted from a high-momentum jet receive an overall collinear enhancement in the distribution of the angular distance between the $W$-boson and the closest jet. Moreover, the largest contribution occurs when the $W$-boson momentum is relatively soft and leads to $p_{\text{T}}^{\ell\nu}/p_{\text{T}}^{\text{closest jet}}$ close to zero. For larger $p_{\text{T}}^{\ell\nu}/p_{\text{T}}^{\text{closest jet}}$ where the $W$-boson is not quite as soft, this disagreement with the MCFM prediction is more noticeable in light of the smaller uncertainties. These features can be clearly seen in Fig. 5. The multijet merged SHERPA and MADGRAPH5_AMC@NLO+PYTHIA8 event generators provide an excellent description of the data across both variables. The inclusion of NLO EW corrections in the SHERPA prediction generally improve the agreement with the data in the collinear regions, but lead to an underestimate of the cross-sections in the back-to-back region while remaining consistent within uncertainties of the SHERPA prediction. The fixed-order MCFM $W$ + 1-jet NNLO prediction provides a good description of the data, except for back-to-back regions with $\Delta R_{\text{min}}(\ell, \text{jet}_i^{100}) > \pi$. In these regions, the MCFM prediction undershoots the data well beyond measurement and prediction uncertainties.

Figure 6 shows the differential cross-section as a function of the invariant mass of the leading two jets ($m_{\text{jj}}$) in the inclusive 2-jet region. As discussed above, the cross-section due to a relatively soft $W$-boson emitted from an outgoing quark

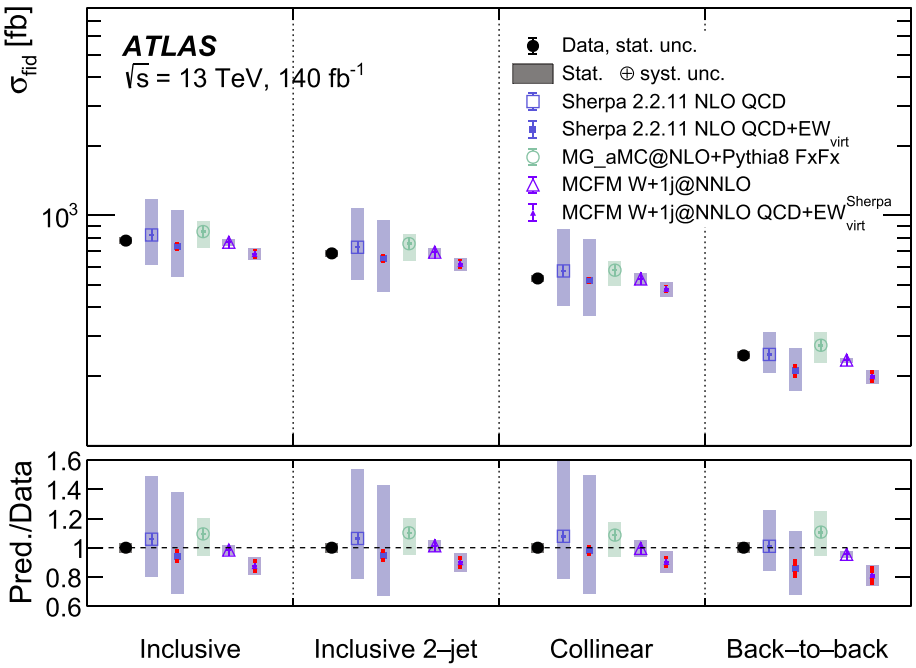


**Fig. 4** Measured fiducial cross-sections in each signal region. The measured cross-sections in data and their total uncertainty are shown by the solid dots and error band. Various theoretical predictions are overlaid and compared with the data in the lower panel. The small error bars inside the markers are the statistical uncertainties. The large shaded areas are the theoretical systematic uncertainties. Uncertainties in predictions accurate to NLO precision include QCD scale and PDF uncertainties, while predictions that add NLO $EW_{virt}$ (electroweak) corrections show uncertainties only due to different electroweak combination schemes. Uncertainties in predictions accurate at fixed-order NNLO precision are derived primarily from MCFM, do not include PDF variations, with an additional extrapolation from the SHERPA QCD with $EW_{virt}$ prediction to assess the effects of higher-order electroweak corrections. On predictions with $EW_{virt}$ corrections, the total uncertainty is shown as a shaded region, while the electroweak correction is overlaid with an error bar line

contributes significantly to the overall production rate in the inclusive phase space. Due to the leading jet $p_T > 500$ GeV requirement, this leads to an overall enhancement in the rate for $m_{jj}$ around 1 TeV since the $W$-boson carries only a small amount of the momentum. Events with large $m_{jj}$ are dominated by extremely high momentum jets with large opening angles. This variable is an important observable for a range of BSM searches and EW-induced measurements that have historically been difficult to model [19–22]. Since the MCFM prediction is computed at NNLO precision for the process $W + 1$-jet, it provides NLO precision for the $m_{jj}$ variable due to the two-jet requirement. All theoretical predictions overestimate the cross-section around $m_{jj} > 2$ TeV beyond their corresponding systematic uncertainties.

In the collinear selection, defined by the requirement of $\Delta R_{min}(\ell, \text{jet}_i^{100}) < 2.6$, the differential cross-section as a function of the leading-jet transverse momentum, the inclusive jet multiplicity, the scalar sum of jet momenta, and the $W$-boson candidate transverse momentum are measured. These measurements are shown in Fig. 7.

The leading jet $p_T$ distribution is shown in Fig. 7a and probes jet momenta up to the 1.5 TeV scale. The MADGRAPH5_AMC@NLO+PYTHIA8 and SHERPA predictions provide an excellent description of the data across the entire measured range. There remain large uncertainties associated with the SHERPA predictions even though the SHERPA NLO $EW_{virt}$ corrections improve the agreement of the central value with the data. The fixed-order MCFM provides an excellent description of the data with precision that matches or exceeds that of the measured data in the highest measured bins. The application of the NLO $EW_{virt}$ corrections to the MCFM reduces the cross-section in all bins and generally leads to a ∼10% underestimate of the cross-section.

Measurements of the differential cross-section as a function of the inclusive jet multiplicity and the scalar sum of all the jet momenta are shown in Fig. 7b, c. Similar to the leading jet $p_T$ measurement, the multijet merged predictions provide an excellent description of the data across all measured values. For the most extreme $S_T$ bins, the scale uncertainties in the SHERPA prediction exceed 50% due to large contributions from the leading-order matrix elements in this region of phase space. The fixed-order MCFM provides a good description of the data for $S_T < 1.4$ TeV but underestimates the cross-section for more extreme values. For such extreme regions, the dominant contribution comes from events with three or

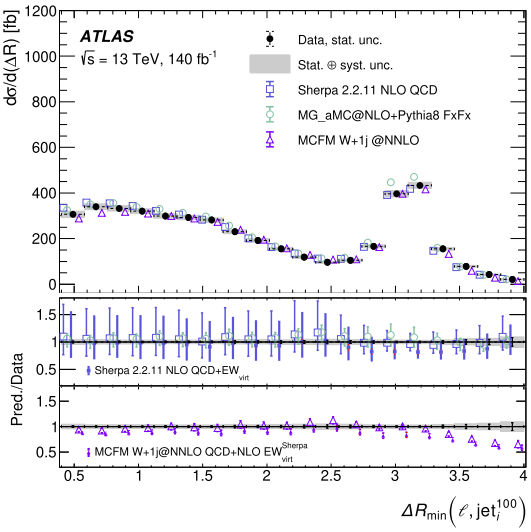


(a)

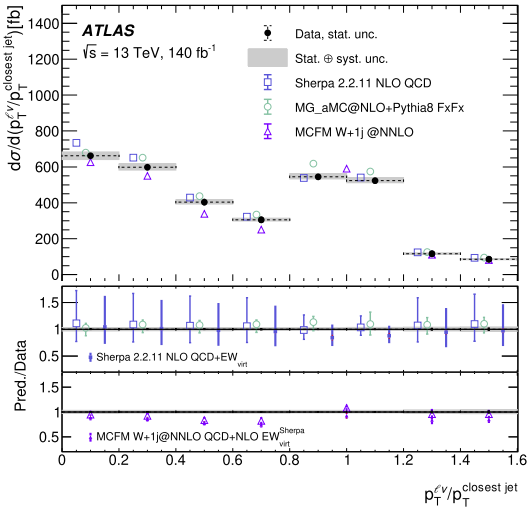


(b)

**Fig. 5** Differential cross-section measurement in the inclusive phase space as function of **a** the minimum angular separation between the lepton and any jet with transverse momentum greater than 100 GeV ($\Delta R_{\min}(\ell, \text{jet}_i^{100})$), and **b** the ratio of $W$-boson $p_{\mathrm{T}}$ to the closest-jet $p_{\mathrm{T}}$ ($p_{\mathrm{T}}^{\ell\nu}/p_{\mathrm{T}}^{\text{closest jet}}$). The measured cross-sections in data and their statistical uncertainty are shown by the solid dots and error bars, while the shaded band shows the systematic and statistical uncertainties added in quadrature. Errors bars on the theory prediction include theoretical uncertainties as discussed in the text. The bins around $p_{\mathrm{T}}^{\ell\nu}/p_{\mathrm{T}}^{\text{closest jet}}$ equal to 1 are merged to be insensitive to the singularity that exists in the fixed-order MCFM calculation. Additionally, in **b**, the central two bins from the MCFM prediction are merged due to a singularity in fixed-order calculations, which requires $p_{\mathrm{T}}$ resummation of the $W$+ jets system. The two lower panels show the effect of NLO $\mathrm{EW}_{\mathrm{virt}}$ as computed from SHERPA 2.2.11

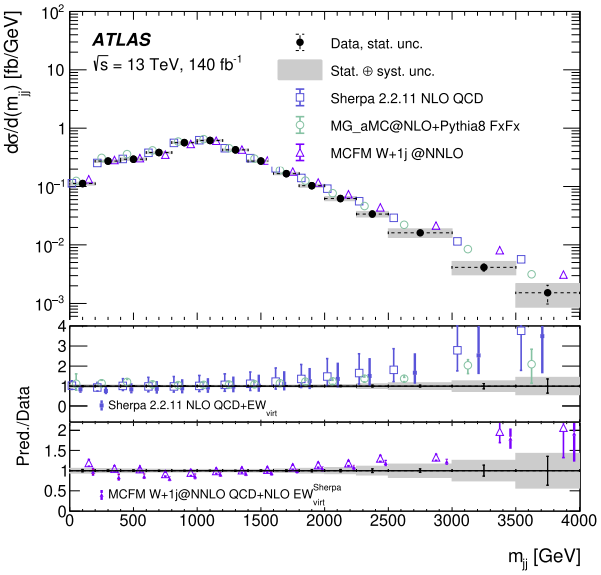


**Fig. 6** Differential cross-section as a function of the invariant mass of the leading two jets ($m_{\mathrm{jj}}$) in the inclusive, 2-jet phase space. The measured cross-sections in data and their statistical uncertainty are shown by the solid dots and error bars, while the shaded band shows the systematic and statistical uncertainties added in quadrature. Errors bars on the theory prediction include theoretical uncertainties as discussed in the text. The two lower panels show the effect of NLO $\mathrm{EW}_{\mathrm{virt}}$ as computed from SHERPA 2.2.11

more jets, beyond the formal accuracy of the MCFM calculation.

The differential distribution of the measured cross-section as a function of $p_{\mathrm{T}}^{\ell\nu}$ is shown in Fig. 7d. The QCD-only predictions agree well with the data at low $p_{\mathrm{T}}^{\ell\nu}$ values but lead to a small overestimate in the high $p_{\mathrm{T}}^{\ell\nu}$ regime that is improved with inclusion of NLO EW corrections. At high $p_{\mathrm{T}}^{\ell\nu}$, the NLO $\mathrm{EW}_{\mathrm{virt}}$ corrections show the standard Sudakov behaviour and lead to large negative corrections over the QCD-only cross-section at high transverse momentum. The size of these corrections can be as large as 30% and exceed uncertainties in the fixed-order MCFM NNLO prediction in the highest momentum jet bins. The application of the NLO $\mathrm{EW}_{\mathrm{virt}}$ corrections significantly improves the agreement of the MCFM prediction with data in the highest $p_{\mathrm{T}}^{\ell\nu}$ bins. Towards softer $W$-boson emissions, the SHERPA prediction is dominated by many jet events that are described by its LO accurate matrix elements and leads to large scale uncertainties for smaller $p_{\mathrm{T}}^{\ell\nu}$ values.

## 10 Conclusions

A measurement of cross-sections for a $W$-boson produced in association with at least one high-transverse-momentum

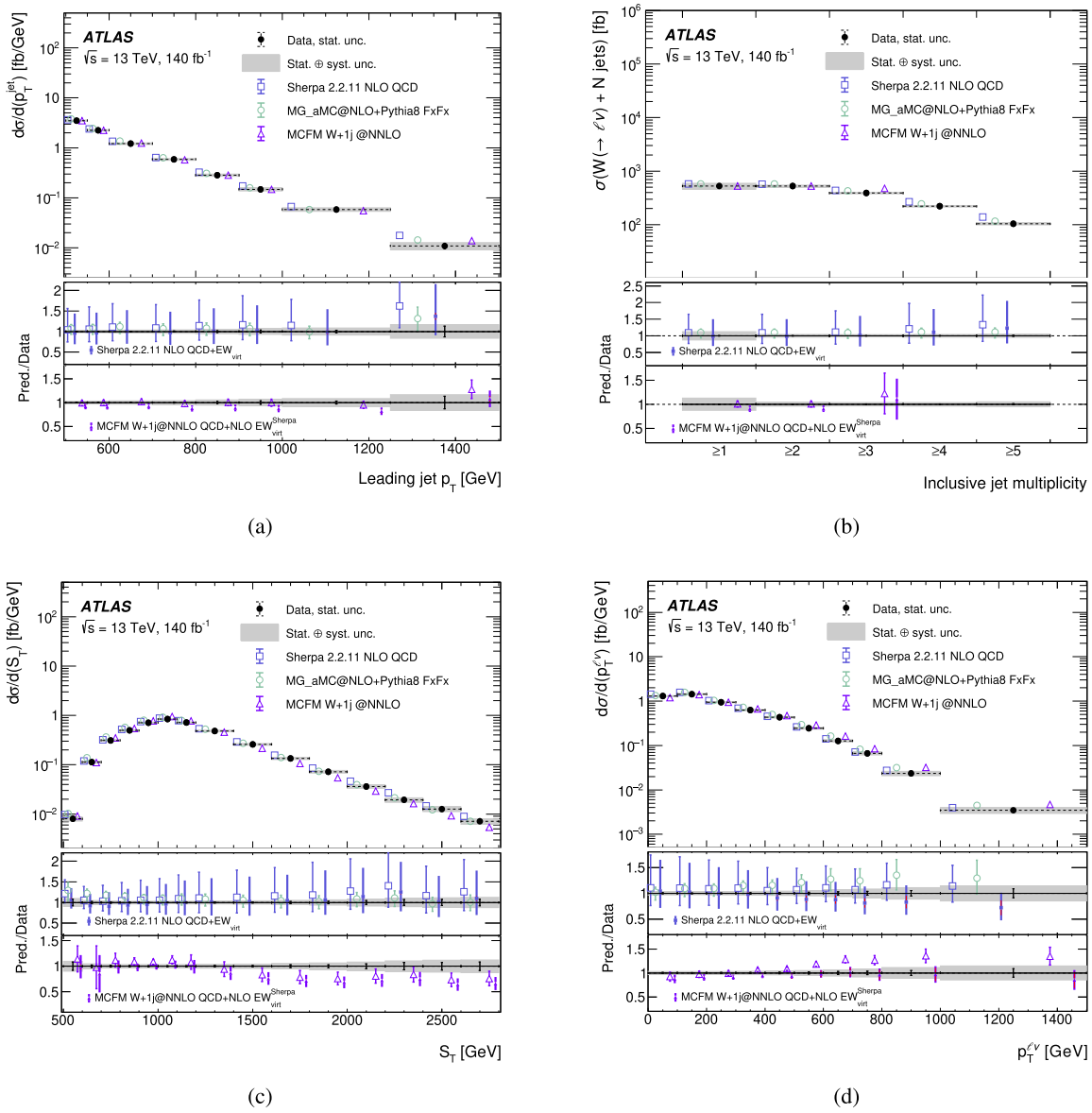


**Fig. 7** Differential cross-section as a function of **a** the leading $p_{\mathrm{T}}^{\mathrm{jet}}$, **b** the inclusive jet multiplicity, **c** $S_{\mathrm{T}}$, and **d** $p_{\mathrm{T}}^{\ell\nu}$ in the collinear phase-space. The measured cross-sections in data and their statistical uncertainty are shown by the solid dots and error bars, while the shaded band shows the systematic and statistical uncertainties added in quadrature. Errors bars on the theory prediction include theoretical uncertainties as discussed in the text. The two lower panels show the effect of NLO $\mathrm{EW}_{\mathrm{virt}}$ as computed from SHERPA 2.2.11

jet is presented. This measurement utilises 140 fb$^{-1}$ of proton–proton collision data collected at a centre-of-mass energy of $\sqrt{s}$ = 13 TeV by the ATLAS detector at the LHC. Measurements are performed on events containing a single electron or muon from the $W \to \ell\nu$ decay and at least one high-momentum jet with $p_{\mathrm{T}}$> 500 GeV. This paper focuses on events where the angular separation between the lepton and a high-momentum jet is small to define a collinear phase space. This region is populated either by dijet events radiating a $W$-boson or events with a $W$-boson produced in association with several jets and it serves as an excellent data sample to probe higher-order theoretical predictions. Measurements of the inclusive and differential cross-sections in the collinear phase space as a function of a variety of observables sensitive to the emission of $W$-bosons from high-momentum jets are presented. Measurements probe $W$-bosons produced in association with jets with transverse momentum above the TeV scale.

The background-subtracted data distributions are unfolded to the particle level and compared with several multijet

generator predictions and to a fixed-order calculation. The SHERPA and MADGRAPH5_AMC@NLO +PYTHIA8 multi-jet merged predictions, accurate to NLO in $\alpha_s$, provide an excellent description of the data across all measured distributions. The scale uncertainties in the SHERPA predictions are found to be significantly larger than those from MADGRAPH5_AMC@NLO, due to the extra leading-order matrix elements in the SHERPA sample used to describe the high-jet-multiplicity final states. The fixed-order calculation for $W$ + 1-jet from MCFM, computed to NNLO in $\alpha_s$, provides a good description of the data with a precision that is comparable to the measurement uncertainties. In regions of phase space with large angular separations between the lepton and leading jet, the MCFM prediction underestimates the cross-section. The impact of NLO EW virtual corrections is assessed using the SHERPA event generator, the size of the corrections is found to be larger than the scale uncertainties in the MCFM prediction. NLO EW corrections improve the agreement of the theory prediction with measured data in regions of phase space with highly-boosted $W$-bosons.

**Acknowledgements** We thank CERN for the very successful operation of the LHC and its injectors, as well as the support staff at CERN and at our institutions worldwide without whom ATLAS could not be operated efficiently. The crucial computing support from all WLCG partners is acknowledged gratefully, in particular from CERN, the ATLAS Tier-1 facilities at TRIUMF/SFU (Canada), NDGF (Denmark, Norway, Sweden), CC-IN2P3 (France), KIT/GridKA (Germany), INFN-CNAF (Italy), NL-T1 (Netherlands), PIC (Spain), RAL (UK) and BNL (USA), the Tier-2 facilities worldwide and large non-WLCG resource providers. Major contributors of computing resources are listed in Ref. [ATL-SOFT-PUB-2025-001]. We gratefully acknowledge the support of ANPCyT, Argentina; YerPhI, Armenia; ARC, Australia; BMWFW and FWF, Austria; ANAS, Azerbaijan; CNPq and FAPESP, Brazil; NSERC, NRC and CFI, Canada; CERN; ANID, Chile; CAS, MOST and NSFC, China; Minciencias, Colombia; MEYS CR, Czech Republic; DNRF and DNSRC, Denmark; IN2P3-CNRS and CEA-DRF/IRFU, France; SRNSFG, Georgia; BMBF, HGF and MPG, Germany; GSRI, Greece; RGC and Hong Kong SAR, China; ICHEP and Academy of Sciences and Humanities, Israel; INFN, Italy; MEXT and JSPS, Japan; CNRST, Morocco; NWO, Netherlands; RCN, Norway; MNiSW, Poland; FCT, Portugal; MNE/IFA, Romania; MSTDI, Serbia; MSSR, Slovakia; ARIS and MVZI, Slovenia; DSI/NRF, South Africa; MICIU/AEI, Spain; SRC and Wallenberg Foundation, Sweden; SERI, SNSF and Cantons of Bern and Geneva, Switzerland; NSTC, Taipei; TENMAK, Türkiye; STFC/UKRI, United Kingdom; DOE and NSF, United States of America. Individual groups and members have received support from BCKDF, CANARIE, CRC and DRAC, Canada; CERN-CZ, FORTE and PRIMUS, Czech Republic; COST, ERC, ERDF, Horizon 2020, ICSC-NextGenerationEU and Marie Skłodowska-Curie Actions, European Union; Investissements d'Avenir Labex, Investissements d'Avenir Idex and ANR, France; DFG and AvH Foundation, Germany; Herakleitos, Thales and Aristeia programmes co-financed by EU-ESF and the Greek NSRF, Greece; BSF-NSF and MINERVA, Israel; NCN and NAWA, Poland; La Caixa Banking Foundation, CERCA Programme Generalitat de Catalunya and PROMETEO and GenT Programmes Generalitat Valenciana, Spain; Göran Gustafssons Stiftelse, Sweden; The Royal Society and Leverhulme Trust, United Kingdom. In addition, individual members wish to acknowledge support from Armenia: Yerevan Physics Institute (FAPERJ); CERN: European Organization for Nuclear Research (CERN DOCT); Chile: Agencia Nacional de Investigación y Desarrollo (FONDECYT 1230812, FONDECYT 1230987, FONDECYT 1240864); China: Chinese Ministry of Science and Technology (MOST-2023YFA1605700, MOST-2023YFA1609300), National Natural Science Foundation of China (NSFC - 12175119, NSFC 12275265, NSFC-12075060); Czech Republic: Czech Science Foundation (GACR - 24-11373 S), Ministry of Education Youth and Sports (FORTE CZ.02.01.01/00/22_008/0004632), PRIMUS Research Programme (PRIMUS/21/SCI/017); EU: H2020 European Research Council (ERC - 101002463); European Union: European Research Council (ERC - 948254, ERC 101089007, ERC, BARD, 101116429), European Union, Future Artificial Intelligence Research (FAIR-NextGenerationEU PE00000013), Italian Center for High Performance Computing, Big Data and Quantum Computing (ICSC, NextGenerationEU); France: Agence Nationale de la Recherche (ANR-20-CE31-0013, ANR-21-CE31-0013, ANR-21-CE31-0022, ANR-22-EDIR-0002); Germany: Baden-Württemberg Stiftung (BW Stiftung-Postdoc Eliteprogramme), Deutsche Forschungsgemeinschaft (DFG - 469666862, DFG - CR 312/5-2); Italy: Istituto Nazionale di Fisica Nucleare (ICSC, NextGenerationEU), Ministero dell'Università e della Ricerca (PRIN - 20223N7F8K - PNRR M4.C2.1.1); Japan: Japan Society for the Promotion of Science (JSPS KAKENHI JP22H01227, JSPS KAKENHI JP22H04944, JSPS KAKENHI JP22KK0227, JSPS KAKENHI JP23KK0245); Netherlands: Netherlands Organisation for Scientific Research (NWO Veni 2020 - VI.Veni.202.179); Norway: Research Council of Norway (RCN-314472); Poland: Ministry of Science and Higher Education (IDUB AGH, POB8, D4 no 9722), Polish National Agency for Academic Exchange (PPN/PPO/2020/1/00002/U/00001), Polish National Science Centre (NCN 2021/42/E/ST2/00350, NCN OPUS 2023/51/B/ST2/02507, NCN OPUS nr 2022/47/B/ST2/03059, NCN UMO-2019/34/E/ST2/00393, NCN & H2020 MSCA 945339, UMO-2020/37/B/ST2/01043, UMO-2021/40/C/ST2/00187, UMO-2022/47/O/ST2/00148, UMO-2023/49/B/ST2/04085, UMO-2023/51/B/ST2/00920); Slovenia: Slovenian Research Agency (ARIS grant J1-3010); Spain: Generalitat Valenciana (Artemisa, FEDER, IDIFEDER/2018/048), Ministry of Science and Innovation (MCIN & NextGenEU PCI2022-135018-2, MICIN & FEDER PID2021-125273NB, RYC2019-028510-I, RYC2020-030254-I, RYC2021-031273-I, RYC2022-038164-I); Sweden: Carl Trygger Foundation (Carl Trygger Foundation CTS 22:2312), Swedish Research Council (Swedish Research Council 2023-04654, VR 2018-00482, VR 2021-03651, VR 2022-03845, VR 2022-04683, VR 2023-03403), Knut and Alice Wallenberg Foundation (KAW 2018.0458, KAW 2019.0447, KAW 2022.0358); Switzerland: Swiss National Science Foundation (SNSF - PCEFP2_194658); United Kingdom: Leverhulme Trust (Leverhulme Trust RPG-2020-004), Royal Society (NIF-R1-231091); United States of America: U.S. Department of Energy (ECA DE-AC02-76SF00515), Neubauer Family Foundation.

**Data Availability Statement** My manuscript has associated data in a data repository. [Authors' comment: All ATLAS scientific output is published in journals, and preliminary results are made available in Conference Notes. All are openly available, without restriction on use by external parties beyond copyright law and the standard conditions agreed by CERN. Data associated with journal publications are also made available: tables and data from plots (e.g. cross section values, likelihood profiles, selection efficiencies, cross section limits,...) are stored in appropriate repositories such as HEPDATA (http://hepdata.cedar.ac.uk/). ATLAS also strives to make additional material related to the paper available that allows a reinterpretation of the data in the context of new theoretical models. For example, an extended encapsulation of the analysis is often provided for measurements in the framework of RIVET (http://rivet.hepforge.org/). This information is taken from the ATLAS Data Access Policy, which is a public document that can be downloaded from http://opendata.cern.ch/record/413 [opendata.cern.ch].

**Code Availability Statement** My manuscript has associated code/software in a data repository. [Authors' comment: ATLAS collaboration software is open source, and all code necessary to recreate an analysis is publicly available. The Athena (http://gitlab.cern.ch/atlas/athena) software repository provides all code needed for calibration and uncertainty application, with configuration files that are also publicly available via Docker containers and cvmfs. The specific code and configurations written in support of this analysis are not public; however, these are internally preserved.]


Funded by SCOAP[3].

## References

1. ATLAS Collaboration, Measurement of the associated production of a Higgs boson decaying into $b$-quarks with a vector boson at high transverse momentum in $pp$ collisions at $\sqrt{s} = 13TeV$ with the ATLAS detector. Phys. Lett. B **816**, 136204 (2021). https://doi.org/10.1016/j.physletb.2021.136204. arXiv:2008.02508 [hep-ex]
2. ATLAS Collaboration, Measurement of the production cross section for a Higgs boson in association with a vector boson in the $H \to WW^*\ell\nu\ell\nu$ channel in $pp$ collisions at $\sqrt{s} = 13\,TeV$ with the ATLAS detector. Phys. Lett. B **798**, 134949 (2019). https://doi.org/10.1016/j.physletb.2019.134949. arXiv:1903.10052 [hep-ex]
3. CMS Collaboration, Search for Higgs boson pair production with one associated vector boson in proton–proton collisions at $\sqrt{s} = 13\,TeV$. (2024). arXiv:2404.08462 [hep-ex]
4. CMS Collaboration, Constraints on anomalous Higgs boson couplings from its production and decay using the $WW$ channel in proton–proton collisions at $\sqrt{s} = 13TeV$. (2024). arXiv:2403.00657 [hep-ex]
5. ATLAS Collaboration, Measurement of the $t\bar{t}$ production cross-section in the lepton+jets channel at $\sqrt{s} = 13TeV$ with the ATLAS experiment. Phys. Lett. B **810**, 135797 (2020). https://doi.org/10.1016/j.physletb.2020.135797. arXiv:2006.13076 [hep-ex]
6. ATLAS Collaboration, Measurements of top-quark pair spin correlations in the $e\mu$ channel at $\sqrt{s} = 13TeV$ using $pp$ collisions in the ATLAS detector. Eur. Phys. J. C **80**, 754 (2020). https://doi.org/10.1140/epjc/s10052-020-8181-6. arXiv:1903.07570 [hep-ex]
7. CMS Collaboration, Inclusive and differential cross section measurements of $t\bar{t}b\bar{b}$ production in the lepton+jets channel at $\sqrt{s} = 13TeV$. (2023). arXiv:2309.14442 [hep-ex]
8. CMS Collaboration, Measurement of the top quark polarization and $t\bar{t}$ spin correlations using dilepton final states in proton–proton collisions at $\sqrt{s} = 13TeV$. Phys. Rev. D **100**, 072002 (2019). https://doi.org/10.1103/PhysRevD.100.072002. arXiv:1907.03729 [hep-ex]
9. ATLAS Collaboration, Search for squarks and gluinos in final states with one isolated lepton, jets, and missing transverse momentum at $\sqrt{s} = 13$ with the ATLAS detector. Eur. Phys. J. C **81**, 600 (2021). https://doi.org/10.1140/epjc/s10052-021-09344-w. arXiv:2101.01629 [hep-ex]
10. ATLAS Collaboration, Searches for electroweak production of supersymmetric particles with compressed mass spectra in $\sqrt{s} = 13$ TeV $pp$ collisions with the ATLAS detector. Phys. Rev. D **101**, 052005 (2020). https://doi.org/10.1103/PhysRevD.101.052005. arXiv:1911.12606 [hep-ex]
11. ATLAS Collaboration, Search for new phenomena with top quark pairs in final states with one lepton, jets, and missing transverse momentum in $pp$ collisions at $\sqrt{s} = 13$ TeV with the ATLAS detector. JHEP **04**, 174 (2021). https://doi.org/10.1007/JHEP04(2021)174. arXiv:2012.03799 [hep-ex]
12. CMS Collaboration, Search for top squarks in the four-body decay mode with single lepton final states in proton–proton collisions at $\sqrt{s} = 13TeV$. JHEP **06**, 060 (2023). https://doi.org/10.1007/JHEP06(2023)060. arXiv:2301.08096 [hep-ex]
13. CMS Collaboration, Search for supersymmetry with a compressed mass spectrum in the vector boson fusion topology with 1-lepton and 0-lepton final states in proton–proton collisions at $\sqrt{s} = 13TeV$. JHEP **08**, 150 (2019). https://doi.org/10.1007/JHEP08(2019)150. arXiv:1905.13059 [hep-ex]
14. CMS Collaboration, Search for supersymmetry in final states with a single electron or muon using angular correlations and heavy-object identification in proton-proton collisions at $\sqrt{s} = 13TeV$. JHEP **09**, 149 (2023). https://doi.org/10.1007/JHEP09(2023)149. arXiv:2211.08476 [hep-ex]
15. ATLAS Collaboration, Measurement of $W$ boson angular distributions in events with high transverse momentum jets at $\sqrt{s} = 8$ TeV using the ATLAS detector. Phys. Lett. B **765**, 132 (2017). https://doi.org/10.1016/j.physletb.2016.12.005. arXiv:1609.07045 [hep-ex]
16. CMS Collaboration, Measurements of differential cross sections for associated production of a $W$ boson and jets in proton–proton collisions at $\sqrt{s} = 8TeV$. Phys. Rev. D **95**, 052002 (2017). https://doi.org/10.1103/PhysRevD.95.052002. arXiv:1610.04222 [hep-ex]
17. CMS Collaboration, Measurement of the differential cross sections for the associated production of a $W$ boson and jets in proton–proton collisions at $\sqrt{s} = 13TeV$. Phys. Rev. D **96**, 072005 (2017). https://doi.org/10.1103/PhysRevD.96.072005. arXiv:1707.05979 [hep-ex]
18. ATLAS Collaboration, Cross-section measurements for the production of a Z boson in association with high-transverse-momentum jets in pp collisions at $\sqrt{s} = 13$ TeV with the ATLAS detector. JHEP **06**, 080 (2023). https://doi.org/10.1007/JHEP06(2023)080. arXiv:2205.02597 [hep-ex]
19. ATLAS Collaboration, Differential cross-section measurements for the electroweak production of Dijets in association with a $Z$ boson in proton–proton collisions at ATLAS. Eur. Phys. J. C **81**, 163 (2021). https://doi.org/10.1140/epjc/s10052-020-08734-w. arXiv:2006.15458 [hep-ex]
20. ATLAS Collaboration, Search for invisible decays of a Higgs boson using vector-boson fusion in $pp$ collisions at $\sqrt{s} = 8$ TeV with the ATLAS detector. JHEP **01**, 172 (2016). https://doi.org/10.1007/JHEP01(2016)172. arXiv:1508.07869 [hep-ex]
21. ATLAS Collaboration, Search for the electroweak production of supersymmetric particles in $\sqrt{s}$=8 TeV $pp$ collisions with the ATLAS detector. Phys. Rev. D **93**, 052002 (2016). https://doi.org/10.1103/PhysRevD.93.052002. arXiv:1509.07152 [hep-ex]
22. ATLAS Collaboration, Search for invisible Higgs-boson decays in events with vector-boson fusion signatures using 139 fb$^{-1}$ of proton-proton data recorded by the ATLAS experiment. JHEP **08**, 104 (2022). https://doi.org/10.1007/JHEP08(2022)104. arXiv:2202.07953 [hep-ex]

23. J. Campbell, T. Neumann, Precision phenomenology with MCFM. JHEP **12**, 034 (2019). https://doi.org/10.1007/JHEP12(2019)034. arXiv:1909.09117 [hep-ph]
24. E. Maguire, L. Heinrich, G. Watt, HEPData: a repository for high energy physics data. J. Phys. Conf. Ser. **898**, 102006 (2017). https://doi.org/10.1088/1742-6596/898/10/102006. arXiv:1704.05473 [hep-ex]. (*ed. by R. Mount and C. Tull*)
25. C. Bierlich et al., Robust independent validation of experiment and theory: Rivet version 3. SciPost Phys. **8**, 026 (2020). https://doi.org/10.21468/SciPostPhys.8.2.026. arXiv:1912.05451 [hep-ph] https://doi.org/10.21468/SciPostPhys.8.2.026 https://doi.org/10.21468/SciPostPhys.8.2.026. arXiv:1912.05451 [hep-ph]
26. ATLAS Collaboration, The ATLAS Experiment at the CERN large hadron collider. JINST **3**, S08003 (2008). https://doi.org/10.1088/1748-0221/3/08/S08003
27. ATLAS Collaboration, ATLAS insertable B-layer: technical design report. ATLAS-TDR-19; CERN-LHCC-2010-013, 2010. https://cds.cern.ch/record/1291633. Addendum: ATLAS-TDR-19-ADD-1; CERN-LHCC-2012-009, 2012. https://cds.cern.ch/record/1451888
28. B. Abbott et al., Production and integration of the ATLAS insertable B-layer. JINST **13**, T05008 (2018). https://doi.org/10.1088/1748-0221/13/05/T05008. arXiv:1803.00844 [physics.ins-det]
29. G. Avoni et al., The new LUCID-2 detector for luminosity measurement and monitoring in ATLAS. JINST **13**, P07017 (2018). https://doi.org/10.1088/1748-0221/13/07/P07017
30. ATLAS Collaboration, Performance of the ATLAS trigger system in 2015. Eur. Phys. J. C **77**, 317 (2017). https://doi.org/10.1140/epjc/s10052-017-4852-3. arXiv:1611.09661 [hep-ex]
31. ATLAS Collaboration, Software and computing for Run 3 of the ATLAS experiment at the LHC. (2024). arXiv:2404.06335 [hep-ex]
32. ATLAS Collaboration, Luminosity determination in $pp$ collisions at $\sqrt{s} = 13$ TeV using the ATLAS detector at the LHC. (2022). https://doi.org/10.48550/ARXIV.2212.09379. arXiv:2212.09379 [hep-ex]
33. ATLAS Collaboration, The ATLAS simulation infrastructure. Eur. Phys. J. C **70**, 823 (2010). https://doi.org/10.1140/epjc/s10052-010-1429-9. arXiv:1005.4568 [physics.ins-det]
34. S. Agostinelli et al., GEANT4 – a simulation toolkit. Nucl. Instrum. Methods A **506**, 250 (2003). https://doi.org/10.1016/S0168-9002(03)01368-8
35. T. Sjöstrand, S. Mrenna, P. Skands, A brief introduction to PYTHIA 8.1. Comput. Phys. Commun. **178**, 852 (2008). https://doi.org/10.1016/j.cpc.2008.01.036. arXiv:0710.3820 [hep-ph]
36. ATLAS Collaboration, The Pythia 8 A3 tune description of ATLAS minimum bias and inelastic measurements incorporating the Donnachie–Landshoff diffractive model. ATL-PHYS-PUB-2016-017, 2016. https://cds.cern.ch/record/2206965
37. NNPDF Collaboration, R.D. Ball et al., Parton distributions with LHC data. Nucl. Phys. B **867**, 244 (2013). https://doi.org/10.1016/j.nuclphysb.2012.10.003. arXiv:1207.1303 [hep-ph]
38. S. Höche, F. Krauss, S. Schumann, F. Siegert, QCD matrix elements and truncated showers. JHEP **05**, 053 (2009). https://doi.org/10.1088/1126-6708/2009/05/053. arXiv:0903.1219 [hep-ph]
39. E. Bothmann et al., Event generation with Sherpa 2.2. SciPost Phys. **7**, 034 (2019). https://doi.org/10.21468/SciPostPhys.7.3.034. arXiv:1905.09127 [hep-ph] https://doi.org/10.21468/SciPostPhys.7.3.034 https://doi.org/10.21468/SciPostPhys.7.3.034. arXiv:1905.09127 [hep-ph] https://doi.org/10.21468/SciPostPhys.7.3.034 https://doi.org/10.21468/SciPostPhys.7.3.034 https://doi.org/10.21468/SciPostPhys.7.3.034. arXiv:1905.09127 [hep-ph]
40. ATLAS Collaboration, Modelling and computational improvements to the simulation of single vector-boson plus jet processes for the ATLAS experiment. JHEP **08**, 089 (2022). https://doi.org/10.1007/JHEP08(2022)089. arXiv:2112.09588 [hep-ex]
41. F. Cascioli, P. Maierhöfer, S. Pozzorini, Scattering amplitudes with open loops. Phys. Rev. Lett. **108**, 111601 (2012). https://doi.org/10.1103/PhysRevLett.108.111601. arXiv:1111.5206 [hep-ph]
42. A. Denner, S. Dittmaier, L. Hofer, COLLIER: a Fortran-based complex one-loop library in extended regularizations. Comput. Phys. Commun. **212**, 220 (2017). https://doi.org/10.1016/j.cpc.2016.10.013. arXiv:1604.06792 [hep-ph]
43. T. Gleisberg, S. Höche, Comix, a new matrix element generator. JHEP **12**, 039 (2008). https://doi.org/10.1088/1126-6708/2008/12/039. arXiv:0808.3674 [hep-ph]
44. S. Catani, F. Krauss, B.R. Webber, R. Kuhn, QCD matrix elements + parton showers. JHEP **11**, 063 (2001). https://doi.org/10.1088/1126-6708/2001/11/063. arXiv:hep-ph/0109231
45. NNPDF Collaboration, R.D. Ball et al., Parton distributions for the LHC run II. JHEP **04**, 040 (2015). https://doi.org/10.1007/JHEP04(2015)040. arXiv:1410.8849 [hep-ph]
46. S. Schumann, F. Krauss, A parton shower algorithm based on Catani–Seymour dipole factorisation. JHEP **03**, 038 (2008). https://doi.org/10.1088/1126-6708/2008/03/038. arXiv:0709.1027 [hep-ph]
47. J.-C. Winter, F. Krauss, G. Soff, A modified cluster-hadronisation model. Eur. Phys. J. C **36**, 381 (2004). https://doi.org/10.1140/epjc/s2004-01960-8. arXiv:hep-ph/0311085
48. E. Bothmann, M. Schönherr, S. Schumann, Reweighting QCD matrix-element and parton-shower calculations. Eur. Phys. J. C **76**, 590 (2016). https://doi.org/10.1140/epjc/s10052-016-4430-0. arXiv:1606.08753 [hep-ph]
49. J. Alwall et al., The automated computation of tree-level and next-to-leading order differential cross sections, and their matching to parton shower simulations. JHEP **07**, 079 (2014). https://doi.org/10.1007/JHEP07(2014)079. arXiv:1405.0301 [hep-ph]
50. T. Sjöstrand et al., An introduction to PYTHIA 8.2. Comput. Phys. Commun. **191**, 159 (2015). https://doi.org/10.1016/j.cpc.2015.01.024. arXiv:1410.3012 [hep-ph]
51. ATLAS Collaboration, ATLAS Pythia 8 tunes to 7 TeV data. ATL-PHYS-PUB-2014-021, 2014. https://cds.cern.ch/record/1966419
52. R. Frederix, S. Frixione, Merging meets matching in MC@NLO. JHEP **12**, 061 (2012). https://doi.org/10.1007/JHEP12(2012)061. arXiv:1209.6215 [hep-ph]
53. V. Bertone, S. Carrazza, N.P. Hartland, J. Rojo, Illuminating the photon content of the proton within a global PDF analysis. SciPost Phys. **5**, 008 (2018). https://doi.org/10.21468/SciPostPhys.5.1.008. arXiv:1712.07053 [hep-ph]
54. J. Andersen et al., Les Houches 2013: physics at TeV colliders: Standard Model working group report. (2014). arXiv:1405.1067 [hep-ph]
55. E. Re, Single-top $Wt$-channel production matched with parton showers using the POWHEG method. Eur. Phys. J. C **71**, 1547 (2011). https://doi.org/10.1140/epjc/s10052-011-1547-z. arXiv:1009.2450 [hep-ph]
56. P. Nason, A new method for combining NLO QCD with shower Monte Carlo algorithms. JHEP **11**, 040 (2004). https://doi.org/10.1088/1126-6708/2004/11/040. arXiv:hep-ph/0409146
57. S. Frixione, P. Nason, C. Oleari, Matching NLO QCD computations with parton shower simulations: the POWHEG method. JHEP **11**, 070 (2007). https://doi.org/10.1088/1126-6708/2007/11/070. arXiv:0709.2092 [hep-ph]
58. S. Alioli, P. Nason, C. Oleari, E. Re, A general framework for implementing NLO calculations in shower Monte Carlo programs: the POWHEG BOX. JHEP **06**, 043 (2010). https://doi.org/10.1007/JHEP06(2010)043. arXiv:1002.2581 [hep-ph]

59. N. Kidonakis, Next-to-next-to-leading-order collinear and soft gluon corrections for t-channel single top quark production. Phys. Rev. D **83**, 091503 (2011). https://doi.org/10.1103/PhysRevD.83.091503. arXiv:1103.2792 [hep-ph]
60. N. Kidonakis, Two-loop soft anomalous dimensions for single top quark associated production with a $W^-$ or $H^-$. Phys. Rev. D **82**, 054018 (2010). https://doi.org/10.1103/PhysRevD.82.054018. arXiv:1005.4451 [hep-ph]
61. N. Kidonakis, Next-to-next-to-leading logarithm resummation for $s$-channel single top quark production. Phys. Rev. D **81**, 054028 (2010). https://doi.org/10.1103/PhysRevD.81.054028. arXiv:1001.5034 [hep-ph]
62. N. Kidonakis, N. Yamanaka, Higher-order corrections for $tW$ production at high-energy hadron colliders. JHEP **05**, 278 (2021). https://doi.org/10.1007/JHEP05(2021)278. arXiv:2102.11300 [hep-ph]
63. P. Nason, G. Zanderighi, $W^+W^-$, $WZ$ and $ZZ$ production in the POWHEG-BOX-V2. Eur. Phys. J. C **74**, 2702 (2014). https://doi.org/10.1140/epjc/s10052-013-2702-5. arXiv:1311.1365 [hep-ph]
64. ATLAS Collaboration, Measurement of the $Z/\gamma^*$ boson transverse momentum distribution in $pp$ collisions at $\sqrt{s} = 7$ TeV with the ATLAS detector. JHEP **09**, 145 (2014). https://doi.org/10.1007/JHEP09(2014)145. arXiv:1406.3660 [hep-ex]
65. H.-L. Lai et al., New parton distributions for collider physics. Phys. Rev. D **82**, 074024 (2010). https://doi.org/10.1103/PhysRevD.82.074024. arXiv:1007.2241 [hep-ph]
66. J. Pumplin et al., New generation of parton distributions with uncertainties from global QCD analysis. JHEP **07**, 012 (2002). https://doi.org/10.1088/1126-6708/2002/07/012. arXiv:hep-ph/0201195
67. D.J. Lange, The EvtGen particle decay simulation package. Nucl. Instrum. Methods A **462**, 152 (2001). https://doi.org/10.1016/S0168-9002(01)00089-4
68. S. Mrenna, P. Skands, Automated parton-shower variations in PYTHIA 8. Phys. Rev. D **94**, 074005 (2016). https://doi.org/10.1103/PhysRevD.94.074005. arXiv:1605.08352 [hep-ph]
69. T. Gleisberg et al., Event generation with SHERPA 1.1. JHEP **02**, 007 (2009). https://doi.org/10.1088/1126-6708/2009/02/007. arXiv:0811.4622 [hep-ph]
70. S. Höche, F. Krauss, M. Schönherr, F. Siegert, QCD matrix elements + parton showers. The NLO case. JHEP **04**, 027 (2013). https://doi.org/10.1007/JHEP04(2013)027. arXiv:1207.5030 [hep-ph]
71. S. Alioli, P. Nason, C. Oleari, E. Re, NLO single-top production matched with shower in POWHEG: $s$- and $t$-channel contributions. JHEP **09**, 111 (2009). https://doi.org/10.1088/1126-6708/2009/09/111. arXiv:0907.4076 [hep-ph], Erratum: 10.1007/JHEP02(2010)011 JHEP 02 (2010)011
72. P.Z. Skands, Tuning Monte Carlo generators: the Perugia tunes. Phys. Rev. D **82**, 074018 (2010). https://doi.org/10.1103/PhysRevD.82.074018. arXiv:1005.3457 [hep-ph]
73. ATLAS Collaboration, ATLAS data quality operations and performance for 2015–2018 data-taking. JINST **15**, P04003 (2020). https://doi.org/10.1088/1748-0221/15/04/P04003. arXiv:1911.04632 [physics.ins-det]
74. ATLAS Collaboration, Vertex reconstruction performance of the ATLAS detector at $\sqrt{s} = 13$ TeV. ATL-PHYS-PUB-2015-026, 2015. https://cds.cern.ch/record/2037717
75. ATLAS Collaboration, Performance of electron and photon triggers in ATLAS during LHC Run 2. Eur. Phys. J. C **80**, 47 (2020). arXiv:1909.00761 [hep-ex]
76. ATLAS Collaboration, Performance of the ATLAS muon triggers in Run 2. JINST **15**, P09015 (2020). https://doi.org/10.1088/1748-0221/15/09/p09015. arXiv:2004.13447 [physics.ins-det]
77. ATLAS Collaboration, The ATLAS inner detector trigger performance in $PP$ collisions at 13 TeV during LHC Run 2. Eur. Phys. J. C **82**, 206 (2022). arXiv:2107.02485
78. ATLAS Collaboration, Electron and photon performance measurements with the ATLAS detector using the 2015–2017 LHC proton–proton collision data. JINST **14**, P12006 (2019). https://doi.org/10.1088/1748-0221/14/12/P12006. arXiv:1908.00005 [hep-ex]
79. ATLAS Collaboration, Electron and photon energy calibration with the ATLAS detector using LHC Run 2 data. JINST **19**, P02009 (2023). https://doi.org/10.1088/1748-0221/19/02/P02009. arXiv:2309.05471 [hep-ex]
80. ATLAS Collaboration, Muon reconstruction and identification efficiency in ATLAS using the full Run 2 $pp$ collision data set at $\sqrt{s} = 13$ TeV. Eur. Phys. J. C **81**, 578 (2021). https://doi.org/10.1140/epjc/s10052-021-09233-2. arXiv:2012.00578 [hep-ex]
81. ATLAS Collaboration, Studies of the muon momentum calibration and performance of the ATLAS detector with $pp$ collisions at $\sqrt{s} = 13$ TeV. Eur. Phys. J. C **83**, 686 (2023). https://doi.org/10.1140/epjc/s10052-023-11584-x. arXiv:2212.07338 [hep-ex]
82. M. Cacciari, G.P. Salam, G. Soyez, The anti-$k\_t$ jet clustering algorithm. JHEP **04**, 063 (2008). https://doi.org/10.1088/1126-6708/2008/04/063. arXiv:0802.1189 [hep-ph]
83. M. Cacciari, G.P. Salam, G. Soyez, FastJet user manual. Eur. Phys. J. C **72**, 1896 (2012). https://doi.org/10.1140/epjc/s10052-012-1896-2. arXiv:1111.6097 [hep-ph]
84. ATLAS Collaboration, Jet reconstruction and performance using particle flow with the ATLAS detector. Eur. Phys. J. C **77**, 466 (2017). https://doi.org/10.1140/epjc/s10052-017-5031-2. arXiv:1703.10485 [hep-ex]
85. ATLAS Collaboration, Jet energy scale and resolution measured in proton–proton collisions at $\sqrt{s} = 13$ TeV with the ATLAS detector. Eur. Phys. J. C **81**, 689 (2021). https://doi.org/10.1140/epjc/s10052-021-09402-3. arXiv:2007.02645 [hep-ex]
86. ATLAS Collaboration, Performance of pile-up mitigation techniques for jets in $pp$ collisions at $\sqrt{s} = 8\,TeV$ using the ATLAS detector. Eur. Phys. J. C **76**, 581 (2016). https://doi.org/10.1140/epjc/s10052-016-4395-z. arXiv:1510.03823 [hep-ex]
87. ATLAS Collaboration, ATLAS flavour-tagging algorithms for the LHC Run 2 $pp$ collision dataset. Eur. Phys. J. C **83**, 681 (2023). https://doi.org/10.1140/epjc/s10052-023-11699-1. arXiv:2211.16345 [physics.data-an]
88. ATLAS Collaboration, The performance of missing transverse momentum reconstruction and its significance with the ATLAS detector using 140 $fb^{-1}$ of $\sqrt{s} = 13$ TeV $pp$ collisions. (2024). arXiv:2402.05858 [hep-ex]
89. G. D'Agostini, A multidimensional unfolding method based on Bayes' theorem. Nucl. Instrum. Methods A **362**, 487 (1995). https://doi.org/10.1016/0168-9002(95)00274-X
90. T. Adye, Unfolding algorithms and tests using RooUnfold. Proceedings, 2011 Workshop on Statistical Issues Related to Discovery Claims in Search Experiments and Unfolding (PHYSTAT 2011) (CERN, Geneva, Switzerland, 17th–20th Jan. 2011), p. 313. arXiv:1105.1160 [physics.data-an]
91. ATLAS Collaboration, Electron and photon efficiencies in LHC Run 2 with the ATLAS experiment. JHEP **05**, 162 (2024). https://doi.org/10.1007/JHEP05(2024)162. arXiv:2308.13362 [hep-ex]
92. ATLAS Collaboration, Electron and photon energy calibration with the ATLAS detector using LHC Run2 data. JINST **19**, P02009 (2024). https://doi.org/10.1088/1748-0221/19/02/P02009. arXiv:2309.05471 [hep-ex]
93. ATLAS Collaboration, ATLAS $b$-jet identification performance and efficiency measurement with $t\bar{t}$ events in $pp$ collisions at $\sqrt{s} = 13$ TeV. Eur. Phys. J. C **79**, 970 (2019). https://doi.org/10.1140/epjc/s10052-019-7450-8. arXiv:1907.05120 [hep-ex]

**ATLAS Collaboration**[*]

G. Aad[104], E. Aakvaag[17], B. Abbott[123], S. Abdelhameed[119a], K. Abeling[56], N. J. Abicht[50], S. H. Abidi[30], M. Aboelela[46], A. Aboulhorma[36e], H. Abramowicz[155], Y. Abulaiti[120], B. S. Acharya[70a,70b,m], A. Ackermann[64a], C. Adam Bourdarios[4], L. Adamczyk[87a], S. V. Addepalli[147], M. J. Addison[103], J. Adelman[118], A. Adiguzel[22c], T. Adye[137], A. A. Affolder[139], Y. Afik[41], M. N. Agaras[13], A. Aggarwal[102], C. Agheorghiesei[28c], F. Ahmadov[40,ac], S. Ahuja[97], X. Ai[63e], G. Aielli[77a,77b], A. Aikot[167], M. Ait Tamlihat[36e], B. Aitbenchikh[36a], M. Akbiyik[102], T. P. A. Åkesson[100], A. V. Akimov[149], D. Akiyama[172], N. N. Akolkar[25], S. Aktas[22a], G. L. Alberghi[24b], J. Albert[169], P. Albicocco[54], G. L. Albouy[61], S. Alderweireldt[53], Z. L. Alegria[124], M. Aleksa[37], I. N. Aleksandrov[40], C. Alexa[28b], T. Alexopoulos[10], F. Alfonsi[24b], M. Algren[57], M. Alhroob[171], B. Ali[135], H. M. J. Ali[93,v], S. Ali[32], S. W. Alibocus[94], M. Aliev[34c], G. Alimonti[72a], W. Alkakhi[56], C. Allaire[67], B. M. M. Allbrooke[150], J. S. Allen[103], J. F. Allen[53], C. A. Allendes Flores[140f], P. P. Allport[21], A. Aloisio[73a,73b], F. Alonso[92], C. Alpigiani[142], Z. M. K. Alsolami[93], A. Alvarez Fernandez[102], M. Alves Cardoso[57], M. G. Alviggi[73a,73b], M. Aly[103], Y. Amaral Coutinho[84b], A. Ambler[106], C. Amelung[37], M. Amerl[103], C. G. Ames[111], D. Amidei[108], B. Amini[55], K. Amirie[158], S. P. Amor Dos Santos[133a], K. R. Amos[167], D. Amperiadou[156], S. An[85], V. Ananiev[128], C. Anastopoulos[143], T. Andeen[11], J. K. Anders[37], A. C. Anderson[60], A. Andreazza[72a,72b], S. Angelidakis[9], A. Angerami[43], A. V. Anisenkov[39], A. Annovi[75a], C. Antel[57], E. Antipov[149], M. Antonelli[54], F. Anulli[76a], M. Aoki[85], T. Aoki[157], M. A. Aparo[150], L. Aperio Bella[49], C. Appelt[155], A. Apyan[27], S. J. Arbiol Val[88], C. Arcangeletti[54], A. T. H. Arce[52], J.-F. Arguin[110], S. Argyropoulos[156], J.-H. Arling[49], O. Arnaez[4], H. Arnold[149], G. Artoni[76a,76b], H. Asada[113], K. Asai[121], S. Asai[157], N. A. Asbah[37], R. A. Ashby Pickering[171], K. Assamagan[30], R. Astalos[29a], K. S. V. Astrand[100], S. Atashi[162], R. J. Atkin[34a], H. Atmani[36f], P. A. Atmasiddha[131], K. Augsten[135], A. D. Auriol[42], V. A. Austrup[103], G. Avolio[37], K. Axiotis[57], G. Azuelos[110,ag], D. Babal[29b], H. Bachacou[138], K. Bachas[156,q], A. Bachiu[35], E. Bachmann[51], A. Badea[41], T. M. Baer[108], P. Bagnaia[76a,76b], M. Bahmani[19], D. Bahner[55], K. Bai[126], J. T. Baines[137], L. Baines[96], O. K. Baker[176], E. Bakos[16], D. Bakshi Gupta[8], L. E. Balabram Filho[84b], V. Balakrishnan[123], R. Balasubramanian[4], E. M. Baldin[39], P. Balek[87a], E. Ballabene[24a,24b], F. Balli[138], L. M. Baltes[64a], W. K. Balunas[33], J. Balz[102], I. Bamwidhi[119b], E. Banas[88], M. Bandieramonte[132], A. Bandyopadhyay[25], S. Bansal[25], L. Barak[155], M. Barakat[49], E. L. Barberio[107], D. Barberis[58a,58b], M. Barbero[104], M. Z. Barel[117], T. Barillari[112], M.-S. Barisits[37], T. Barklow[147], P. Baron[125], D. A. Baron Moreno[103], A. Baroncelli[63a], A. J. Barr[129], J. D. Barr[98], F. Barreiro[101], J. Barreiro Guimarães da Costa[14], M. G. Barros Teixeira[133a], S. Barsov[39], F. Bartels[64a], R. Bartoldus[147], A. E. Barton[93], P. Bartos[29a], A. Basan[102], M. Baselga[50], S. Bashiri[88], A. Bassalat[67,b], M. J. Basso[159a], S. Bataju[46], R. Bate[168], R. L. Bates[60], S. Batlamous[101], M. Battaglia[139], D. Battulga[19], M. Bauce[76a,76b], M. Bauer[80], P. Bauer[25], L. T. Bazzano Hurrell[31], J. B. Beacham[52], T. Beau[130], J. Y. Beaucamp[92], P. H. Beauchemin[161], P. Bechtle[25], H. P. Beck[20,p], K. Becker[171], A. J. Beddall[83], V. A. Bednyakov[40], C. P. Bee[149], L. J. Beemster[16], M. Begalli[84d], M. Begel[30], J. K. Behr[49], J. F. Beirer[37], F. Beisiegel[25], M. Belfkir[119b], G. Bella[155], L. Bellagamba[24b], A. Bellerive[35], P. Bellos[21], K. Beloborodov[39], D. Benchekroun[36a], F. Bendebba[36a], Y. Benhammou[155], K. C. Benkendorfer[62], L. Beresford[49], M. Beretta[54], E. Bergeaas Kuutmann[165], N. Berger[4], B. Bergmann[135], J. Beringer[18a], G. Bernardi[5], C. Bernius[147], F. U. Bernlochner[25], F. Bernon[37], A. Berrocal Guardia[13], T. Berry[97], P. Berta[136], A. Berthold[51], S. Bethke[112], A. Betti[76a,76b], A. J. Bevan[96], N. K. Bhalla[55], S. Bharthuar[112], S. Bhatta[149], D. S. Bhattacharya[170], P. Bhattarai[147], Z. M. Bhatti[120], K. D. Bhide[55], V. S. Bhopatkar[124], R. M. Bianchi[132], G. Bianco[24a,24b], O. Biebel[111], M. Biglietti[78a], C. S. Billingsley[46], Y. Bimgdi[36f], M. Bindi[56], A. Bingham[175], A. Bingul[22b], C. Bini[76a,76b], G. A. Bird[33], M. Birman[173], M. Biros[136], S. Biryukov[150], T. Bisanz[50], E. Bisceglie[45a,45b], J. P. Biswal[137], D. Biswas[145], I. Bloch[49], A. Blue[60], U. Blumenschein[96], J. Blumenthal[102], V. S. Bobrovnikov[39], M. Boehler[55], B. Boehm[170], D. Bogavac[37], A. G. Bogdanchikov[39], L. S. Boggia[130], V. Boisvert[97], P. Bokan[37], T. Bold[87a], M. Bomben[5], M. Bona[96], M. Boonekamp[138], A. G. Borbély[60], I. S. Bordulev[39], G. Borissov[93], D. Bortoletto[129], D. Boscherini[24b], M. Bosman[13], K. Bouaouda[36a], N. Bouchhar[167], L. Boudet[4], J. Boudreau[132], E. V. Bouhova-Thacker[93], D. Boumediene[42], R. Bouquet[58a,58b], A. Boveia[122], J. Boyd[37], D. Boye[30], I. R. Boyko[40], L. Bozianu[57], J. Bracinik[21], N. Brahimi[4], G. Brandt[175], O. Brandt[33], B. Brau[105], J. E. Brau[126], R. Brener[173], L. Brenner[117], R. Brenner[165], S. Bressler[173], G. Brianti[79a,79b], D. Britton[60],

D. Britzger[112], I. Brock[25], R. Brock[109], G. Brooijmans[43], A. J. Brooks[69], E. M. Brooks[159b], E. Brost[30], L. M. Brown[169], L. E. Bruce[62], T. L. Bruckler[129], P. A. Bruckman de Renstrom[88], B. Brüers[49], A. Bruni[24b], G. Bruni[24b], D. Brunner[48a,48b], M. Bruschi[24b], N. Bruscino[76a,76b], T. Buanes[17], Q. Buat[142], D. Buchin[112], A. G. Buckley[60], O. Bulekov[39], B. A. Bullard[147], S. Burdin[94], C. D. Burgard[50], A. M. Burger[37], B. Burghgrave[8], O. Burlayenko[55], J. Burleson[166], J. T. P. Burr[33], J. C. Burzynski[146], E. L. Busch[43], V. Büscher[102], P. J. Bussey[60], J. M. Butler[26], C. M. Buttar[60], J. M. Butterworth[98], W. Buttinger[137], C. J. Buxo Vazquez[109], A. R. Buzykaev[39], S. Cabrera Urbán[167], L. Cadamuro[67], D. Caforio[59], H. Cai[132], Y. Cai[14,114c], Y. Cai[114a], V. M. M. Cairo[37], O. Cakir[3a], N. Calace[37], P. Calafiura[18a], G. Calderini[130], P. Calfayan[35], G. Callea[60], L. P. Caloba[84b], D. Calvet[42], S. Calvet[42], R. Camacho Toro[130], S. Camarda[37], D. Camarero Munoz[27], P. Camarri[77a,77b], M. T. Camerlingo[73a,73b], D. Cameron[37], C. Camincher[169], M. Campanelli[98], A. Camplani[44], V. Canale[73a,73b], A. C. Canbay[3a], E. Canonero[97], J. Cantero[167], Y. Cao[166], F. Capocasa[27], M. Capua[45a,45b], A. Carbone[72a,72b], R. Cardarelli[77a], J. C. J. Cardenas[8], M. P. Cardiff[27], G. Carducci[45a,45b], T. Carli[37], G. Carlino[73a], J. I. Carlotto[13], B. T. Carlson[132,r], E. M. Carlson[169], J. Carmignani[94], L. Carminati[72a,72b], A. Carnelli[138], M. Carnesale[37], S. Caron[116], E. Carquin[140f], I. B. Carr[107], S. Carrá[72a], G. Carratta[24a,24b], A. M. Carroll[126], M. P. Casado[13,i], M. Caspar[49], F. L. Castillo[4], L. Castillo Garcia[13], V. Castillo Gimenez[167], N. F. Castro[133a,133e], A. Catinaccio[37], J. R. Catmore[128], T. Cavaliere[4], V. Cavaliere[30], L. J. Caviedes Betancourt[23b], Y. C. Cekmecelioglu[49], E. Celebi[83], S. Cella[37], V. Cepaitis[57], K. Cerny[125], A. S. Cerqueira[84a], A. Cerri[150], L. Cerrito[77a,77b], F. Cerutti[18a], B. Cervato[145], A. Cervelli[24b], G. Cesarini[54], S. A. Cetin[83], P. M. Chabrillat[130], J. Chan[18a], W. Y. Chan[157], J. D. Chapman[33], E. Chapon[138], B. Chargeishvili[153b], D. G. Charlton[21], C. Chauhan[136], Y. Che[114a], S. Chekanov[6], S. V. Chekulaev[159a], G. A. Chelkov[40,a], B. Chen[155], B. Chen[169], H. Chen[114a], H. Chen[30], J. Chen[63c], J. Chen[146], M. Chen[129], S. Chen[89], S. J. Chen[114a], X. Chen[63c], X. Chen[15,af], Y. Chen[63a], C. L. Cheng[174], H. C. Cheng[65a], S. Cheong[147], A. Cheplakov[40], E. Cheremushkina[49], E. Cherepanova[117], R. Cherkaoui El Moursli[36e], E. Cheu[7], K. Cheung[66], L. Chevalier[138], V. Chiarella[54], G. Chiarelli[75a], N. Chiedde[104], G. Chiodini[71a], A. S. Chisholm[21], A. Chitan[28b], M. Chitishvili[167], M. V. Chizhov[40,s], K. Choi[11], Y. Chou[142], E. Y. S. Chow[116], K. L. Chu[173], M. C. Chu[65a], X. Chu[14,114c], Z. Chubinidze[54], J. Chudoba[134], J. J. Chwastowski[88], D. Cieri[112], K. M. Ciesla[87a], V. Cindro[95], A. Ciocio[18a], F. Cirotto[73a,73b], Z. H. Citron[173], M. Citterio[72a], D. A. Ciubotaru[28b], A. Clark[57], P. J. Clark[53], N. Clarke Hall[98], C. Clarry[158], S. E. Clawson[49], C. Clement[48a,48b], Y. Coadou[104], M. Cobal[70a,70c], A. Coccaro[58b], R. F. Coelho Barrue[133a], R. Coelho Lopes De Sa[105], S. Coelli[72a], L. S. Colangeli[158], B. Cole[43], J. Collot[61], P. Conde Muiño[133a,133g], M. P. Connell[34c], S. H. Connell[34c], E. I. Conroy[129], F. Conventi[73a,ah], H. G. Cooke[21], A. M. Cooper-Sarkar[129], F. A. Corchia[24a,24b], A. Cordeiro Oudot Choi[130], L. D. Corpe[42], M. Corradi[76a,76b], F. Corriveau[106,aa], A. Cortes-Gonzalez[19], M. J. Costa[167], F. Costanza[4], D. Costanzo[143], B. M. Cote[122], J. Couthures[4], G. Cowan[97], K. Cranmer[174], L. Cremer[50], D. Cremonini[24a,24b], S. Crépé-Renaudin[61], F. Crescioli[130], M. Cristinziani[145], M. Cristoforetti[79a,79b], V. Croft[117], J. E. Crosby[124], G. Crosetti[45a,45b], A. Cueto[101], H. Cui[98], Z. Cui[7], W. R. Cunningham[60], F. Curcio[167], J. R. Curran[53], P. Czodrowski[37], M. J. Da Cunha Sargedas De Sousa[58a,58b], J. V. Da Fonseca Pinto[84b], C. Da Via[103], W. Dabrowski[87a], T. Dado[37], S. Dahbi[152], T. Dai[108], D. Dal Santo[20], C. Dallapiccola[105], M. Dam[44], G. D'amen[30], V. D'Amico[111], J. Damp[102], J. R. Dandoy[35], D. Dannheim[37], M. Danninger[146], V. Dao[149], G. Darbo[58b], S. J. Das[30], F. Dattola[49], S. D'Auria[72a,72b], A. D'Avanzo[73a,73b], T. Davidek[136], I. Dawson[96], H. A. Day-hall[135], K. De[8], C. De Almeida Rossi[158], R. De Asmundis[73a], N. De Biase[49], S. De Castro[24a,24b], N. De Groot[116], P. de Jong[117], H. De la Torre[118], A. De Maria[114a], A. De Salvo[76a], U. De Sanctis[77a,77b], F. De Santis[71a,71b], A. De Santo[150], J. B. De Vivie De Regie[61], J. Debevc[95], D. V. Dedovich[40], J. Degens[94], A. M. Deiana[46], J. Del Peso[101], L. Delagrange[130], F. Deliot[138], C. M. Delitzsch[50], M. Della Pietra[73a,73b], D. Della Volpe[57], A. Dell'Acqua[37], L. Dell'Asta[72a,72b], M. Delmastro[4], C. C. Delogu[102], P. A. Delsart[61], S. Demers[176], M. Demichev[40], S. P. Denisov[39], H. Denizli[22a], L. D'Eramo[42], D. Derendarz[88], F. Derue[130], P. Dervan[94], K. Desch[25], C. Deutsch[25], F. A. Di Bello[58a,58b], A. Di Ciaccio[77a,77b], L. Di Ciaccio[4], A. Di Domenico[76a,76b], C. Di Donato[73a,73b], A. Di Girolamo[37], G. Di Gregorio[37], A. Di Luca[79a,79b], B. Di Micco[78a,78b], R. Di Nardo[78a,78b], K. F. Di Petrillo[41], M. Diamantopoulou[35], F. A. Dias[117], T. Dias Do Vale[146], M. A. Diaz[140a,140b], A. R. Didenko[40], M. Didenko[167], E. B. Diehl[108], S. Díez Cornell[49], C. Diez Pardos[145], C. Dimitriadi[148], A. Dimitrievska[21], J. Dingfelder[25], T. Dingley[129], I.-M. Dinu[28b], S. J. Dittmeier[64b], F. Dittus[37], M. Divisek[136], B. Dixit[94], F. Djama[104], T. Djobava[153b], C. Doglioni[100,103], A. Dohnalova[29a], Z. Dolezal[136], K. Domijan[87a], K. M. Dona[41], M. Donadelli[84d], B. Dong[109], J. Donini[42],

A. D'Onofrio[73a,73b], M. D'Onofrio[94], J. Dopke[137], A. Doria[73a], N. Dos Santos Fernandes[133a], P. Dougan[103], M. T. Dova[92], A. T. Doyle[60], M. A. Draguet[129], M. P. Drescher[56], E. Dreyer[173], I. Drivas-koulouris[10], M. Drnevich[120], M. Drozdova[57], D. Du[63a], T. A. du Pree[117], F. Dubinin[39], M. Dubovsky[29a], E. Duchovni[173], G. Duckeck[111], O. A. Ducu[28b], D. Duda[53], A. Dudarev[37], E. R. Duden[27], M. D'uffizi[103], L. Duflot[67], M. Dührssen[37], I. Duminica[28g], A. E. Dumitriu[28b], M. Dunford[64a], S. Dungs[50], K. Dunne[48a,48b], A. Duperrin[104], H. Duran Yildiz[3a], M. Düren[59], A. Durglishvili[153b], D. Duvnjak[35], B. L. Dwyer[118], G. I. Dyckes[18a], M. Dyndal[87a], B. S. Dziedzic[37], Z. O. Earnshaw[150], G. H. Eberwein[129], B. Eckerova[29a], S. Eggebrecht[56], E. Egidio Purcino De Souza[84e], L. F. Ehrke[57], G. Eigen[17], K. Einsweiler[18a], T. Ekelof[165], P. A. Ekman[100], S. El Farkh[36b], Y. El Ghazali[63a], H. El Jarrari[37], A. El Moussaouy[36a], V. Ellajosyula[165], M. Ellert[165], F. Ellinghaus[175], N. Ellis[37], J. Elmsheuser[30], M. Elsawy[119a], M. Elsing[37], D. Emeliyanov[137], Y. Enari[85], I. Ene[18a], S. Epari[13], P. A. Erland[88], D. Ernani Martins Neto[88], M. Errenst[175], M. Escalier[67], C. Escobar[167], E. Etzion[155], G. Evans[133a,133b], H. Evans[69], L. S. Evans[97], A. Ezhilov[39], S. Ezzarqtouni[36a], F. Fabbri[24a,24b], L. Fabbri[24a,24b], G. Facini[98], V. Fadeyev[139], R. M. Fakhrutdinov[39], D. Fakoudis[102], S. Falciano[76a], L. F. Falda Ulhoa Coelho[133a], F. Fallavollita[112], G. Falsetti[45a,45b], J. Faltova[136], C. Fan[166], K. Y. Fan[65b], Y. Fan[14], Y. Fang[14,114c], M. Fanti[72a,72b], M. Faraj[70a,70b], Z. Farazpay[99], A. Farbin[8], A. Farilla[78a], T. Farooque[109], J. N. Farr[176], S. M. Farrington[53,137], F. Fassi[36e], D. Fassouliotis[9], M. Faucci Giannelli[77a,77b], W. J. Fawcett[33], L. Fayard[67], P. Federic[136], P. Federicova[134], O. L. Fedin[39,a], M. Feickert[174], L. Feligioni[104], D. E. Fellers[126], C. Feng[63b], Z. Feng[117], M. J. Fenton[162], L. Ferencz[49], R. A. M. Ferguson[93], P. Fernandez Martinez[68], M. J. V. Fernoux[104], J. Ferrando[93], A. Ferrari[165], P. Ferrari[116,117], R. Ferrari[74a], D. Ferrere[57], C. Ferretti[108], M. P. Fewell[1], D. Fiacco[76a,76b], F. Fiedler[102], P. Fiedler[135], S. Filimonov[39], A. Filipčič[95], E. K. Filmer[159a], F. Filthaut[116], M. C. N. Fiolhais[133a,133c,c], L. Fiorini[167], W. C. Fisher[109], T. Fitschen[103], P. M. Fitzhugh[138], I. Fleck[145], P. Fleischmann[108], T. Flick[175], M. Flores[34d,ad], L. R. Flores Castillo[65a], L. Flores Sanz De Acedo[37], F. M. Follega[79a,79b], N. Fomin[33], J. H. Foo[158], A. Formica[138], A. C. Forti[103], E. Fortin[37], A. W. Fortman[18a], L. Fountas[9,j], D. Fournier[67], H. Fox[93], P. Francavilla[75a,75b], S. Francescato[62], S. Franchellucci[57], M. Franchini[24a,24b], S. Franchino[64a], D. Francis[37], L. Franco[116], V. Franco Lima[37], L. Franconi[49], M. Franklin[62], G. Frattari[27], Y. Y. Frid[155], J. Friend[60], N. Fritzsche[37], A. Froch[57], D. Froidevaux[37], J. A. Frost[129], Y. Fu[109], S. Fuenzalida Garrido[140f], M. Fujimoto[104], K. Y. Fung[65a], E. Furtado De Simas Filho[84e], M. Furukawa[157], J. Fuster[167], A. Gaa[56], A. Gabrielli[24a,24b], A. Gabrielli[158], P. Gadow[37], G. Gagliardi[58a,58b], L. G. Gagnon[18a], S. Gaid[164], S. Galantzan[155], J. Gallagher[1], E. J. Gallas[129], A. L. Gallen[165], B. J. Gallop[137], K. K. Gan[122], S. Ganguly[157], Y. Gao[53], A. Garabaglu[142], F. M. Garay Walls[140a,140b], B. Garcia[30], C. García[167], A. Garcia Alonso[117], A. G. Garcia Caffaro[176], J. E. García Navarro[167], M. Garcia-Sciveres[18a], G. L. Gardner[131], R. W. Gardner[41], N. Garelli[161], R. B. Garg[147], J. M. Gargan[53], C. A. Garner[158], C. M. Garvey[34a], V. K. Gassmann[161], G. Gaudio[74a], V. Gautam[13], P. Gauzzi[76a,76b], J. Gavranovic[95], I. L. Gavrilenko[39], A. Gavrilyuk[39], C. Gay[168], G. Gaycken[126], E. N. Gazis[10], A. Gekow[122], C. Gemme[58b], M. H. Genest[61], A. D. Gentry[115], S. George[97], W. F. George[21], T. Geralis[47], A. A. Gerwin[123], P. Gessinger-Befurt[37], M. E. Geyik[175], M. Ghani[171], K. Ghorbanian[96], A. Ghosal[145], A. Ghosh[162], A. Ghosh[7], B. Giacobbe[24b], S. Giagu[76a,76b], T. Giani[117], A. Giannini[63a], S. M. Gibson[97], M. Gignac[139], D. T. Gil[87b], A. K. Gilbert[87a], B. J. Gilbert[43], D. Gillberg[35], G. Gilles[117], L. Ginabat[130], D. M. Gingrich[2,ag], M. P. Giordani[70a,70c], P. F. Giraud[138], G. Giugliarelli[70a,70c], D. Giugni[72a], F. Giuli[77a,77b], I. Gkialas[9,j], L. K. Gladilin[39], C. Glasman[101], G. Glemža[49], M. Glisic[126], I. Gnesi[45b], Y. Go[30], M. Goblirsch-Kolb[37], B. Gocke[50], D. Godin[110], B. Gokturk[22a], S. Goldfarb[107], T. Golling[57], M. G. D. Gololo[34c], D. Golubkov[39], J. P. Gombas[109], A. Gomes[133a,133b], G. Gomes Da Silva[145], A. J. Gomez Delegido[167], R. Gonçalo[133a], L. Gonella[21], A. Gongadze[153c], F. Gonnella[21], J. L. Gonski[147], R. Y. González Andana[53], S. González de la Hoz[167], R. Gonzalez Lopez[94], C. Gonzalez Renteria[18a], M. V. Gonzalez Rodrigues[49], R. Gonzalez Suarez[165], S. Gonzalez-Sevilla[57], L. Goossens[37], B. Gorini[37], E. Gorini[71a,71b], A. Gorišek[95], T. C. Gosart[131], A. T. Goshaw[52], M. I. Gostkin[40], S. Goswami[124], C. A. Gottardo[37], S. A. Gotz[111], M. Gouighri[36b], A. G. Goussiou[142], N. Govender[34c], R. P. Grabarczyk[129], I. Grabowska-Bold[87a], K. Graham[35], E. Gramstad[128], S. Grancagnolo[71a,71b], C. M. Grant[1,138], P. M. Gravila[28f], F. G. Gravili[71a,71b], H. M. Gray[18a], M. Greco[112], M. J. Green[1], C. Grefe[25], A. S. Grefsrud[17], I. M. Gregor[49], K. T. Greif[162], P. Grenier[147], S. G. Grewe[112], A. A. Grillo[139], K. Grimm[32], S. Grinstein[13,w], J.-F. Grivaz[67], E. Gross[173], J. Grosse-Knetter[56], L. Guan[108], J. G. R. Guerrero Rojas[167], G. Guerrieri[37], R. Gugel[102], J. A. M. Guhit[108], A. Guida[19], E. Guilloton[171], S. Guindon[37], F. Guo[14,114c], J. Guo[63c], L. Guo[49], L. Guo[14,u], Y. Guo[108], A. Gupta[50],

R. Gupta[132], S. Gurbuz[25], S. S. Gurdasani[49], G. Gustavino[76a,76b], P. Gutierrez[123], L. F. Gutierrez Zagazeta[131], M. Gutsche[51], C. Gutschow[98], C. Gwenlan[129], C. B. Gwilliam[94], E. S. Haaland[128], A. Haas[120], M. Habedank[60], C. Haber[18a], H. K. Hadavand[8], A. Hadef[51], A. I. Hagan[93], J. J. Hahn[145], E. H. Haines[98], M. Haleem[170], J. Haley[124], G. D. Hallewell[104], L. Halser[20], K. Hamano[169], M. Hamer[25], E. J. Hampshire[97], J. Han[63b], L. Han[114a], L. Han[63a], S. Han[18a], K. Hanagaki[85], M. Hance[139], D. A. Hangal[43], H. Hanif[146], M. D. Hank[131], J. B. Hansen[44], P. H. Hansen[44], D. Harada[57], T. Harenberg[175], S. Harkusha[177], M. L. Harris[105], Y. T. Harris[25], J. Harrison[13], N. M. Harrison[122], P. F. Harrison[171], N. M. Hartman[112], N. M. Hartmann[111], R. Z. Hasan[97,137], Y. Hasegawa[144], F. Haslbeck[129], S. Hassan[17], R. Hauser[109], C. M. Hawkes[21], R. J. Hawkings[37], Y. Hayashi[157], D. Hayden[109], C. Hayes[108], R. L. Hayes[117], C. P. Hays[129], J. M. Hays[96], H. S. Hayward[94], F. He[63a], M. He[14,114c], Y. He[49], Y. He[98], N. B. Heatley[96], V. Hedberg[100], A. L. Heggelund[128], C. Heidegger[55], K. K. Heidegger[55], J. Heilman[35], S. Heim[49], T. Heim[18a], J. G. Heinlein[131], J. J. Heinrich[126], L. Heinrich[112,ae], J. Hejbal[134], A. Held[174], S. Hellesund[17], C. M. Helling[168], S. Hellman[48a,48b], R. C. W. Henderson[93], L. Henkelmann[33], A. M. Henriques Correia[37], H. Herde[100], Y. Hernández Jiménez[149], L. M. Herrmann[25], T. Herrmann[51], G. Herten[55], R. Hertenberger[111], L. Hervas[37], M. E. Hesping[102], N. P. Hessey[159a], J. Hessler[112], M. Hidaoui[36b], N. Hidic[136], E. Hill[158], S. J. Hillier[21], J. R. Hinds[109], F. Hinterkeuser[25], M. Hirose[127], S. Hirose[160], D. Hirschbuehl[175], T. G. Hitchings[103], B. Hiti[95], J. Hobbs[149], R. Hobincu[28e], N. Hod[173], M. C. Hodgkinson[143], B. H. Hodkinson[129], A. Hoecker[37], D. D. Hofer[108], J. Hofer[167], M. Holzbock[37], L. B. A. H. Hommels[33], B. P. Honan[103], J. J. Hong[69], J. Hong[63c], T. M. Hong[132], B. H. Hooberman[166], W. H. Hopkins[6], M. C. Hoppesch[166], Y. Horii[113], M. E. Horstmann[112], S. Hou[152], M. R. Housenga[166], A. S. Howard[95], J. Howarth[60], J. Hoya[6], M. Hrabovsky[125], T. Hryn'ova[4], P. J. Hsu[66], S.-C. Hsu[142], T. Hsu[67], M. Hu[18a], Q. Hu[63a], S. Huang[33], X. Huang[14,114c], Y. Huang[143], Y. Huang[102], Y. Huang[14], Z. Huang[103], Z. Hubacek[135], M. Huebner[25], F. Huegging[25], T. B. Huffman[129], M. Hufnagel Maranha De Faria[84a], C. A. Hugli[49], M. Huhtinen[37], S. K. Huiberts[17], R. Hulsken[106], N. Huseynov[12,g], J. Huston[109], J. Huth[62], R. Hyneman[7], G. Iacobucci[57], G. Iakovidis[30], L. Iconomidou-Fayard[67], J. P. Iddon[37], P. Iengo[73a,73b], R. Iguchi[157], Y. Iiyama[157], T. Iizawa[129], Y. Ikegami[85], D. Iliadis[156], N. Ilic[158], H. Imam[84c], G. Inacio Goncalves[84d], S. A. Infante Cabanas[140c], T. Ingebretsen Carlson[48a,48b], J. M. Inglis[96], G. Introzzi[74a,74b], M. Iodice[78a], V. Ippolito[76a,76b], R. K. Irwin[94], M. Ishino[157], W. Islam[174], C. Issever[19], S. Istin[22a,al], H. Ito[172], R. Iuppa[79a,79b], A. Ivina[173], V. Izzo[73a], P. Jacka[134], P. Jackson[1], C. S. Jagfeld[111], G. Jain[159a], P. Jain[49], K. Jakobs[55], T. Jakoubek[173], J. Jamieson[60], W. Jang[157], M. Javurkova[105], P. Jawahar[103], L. Jeanty[126], J. Jejelava[153a], P. Jenni[55,f], C. E. Jessiman[35], C. Jia[63b], H. Jia[168], J. Jia[149], X. Jia[14,114c], Z. Jia[114a], C. Jiang[53], Q. Jiang[65b], S. Jiggins[49], J. Jimenez Pena[13], S. Jin[114a], A. Jinaru[28b], O. Jinnouchi[141], P. Johansson[143], K. A. Johns[7], J. W. Johnson[139], F. A. Jolly[49], D. M. Jones[150], E. Jones[49], K. S. Jones[8], P. Jones[33], R. W. L. Jones[93], T. J. Jones[94], H. L. Joos[37,56], R. Joshi[122], J. Jovicevic[16], X. Ju[18a], J. J. Junggeburth[37], T. Junkermann[64a], A. Juste Rozas[13,w], M. K. Juzek[88], S. Kabana[140e], A. Kaczmarska[88], M. Kado[112], H. Kagan[122], M. Kagan[147], A. Kahn[131], C. Kahra[102], T. Kaji[157], E. Kajomovitz[154], N. Kakati[173], I. Kalaitzidou[55], N. J. Kang[139], D. Kar[34g], K. Karava[129], E. Karentzos[25], O. Karkout[117], S. N. Karpov[40], Z. M. Karpova[40], V. Kartvelishvili[93], A. N. Karyukhin[39], E. Kasimi[156], J. Katzy[49], S. Kaur[35], K. Kawade[144], M. P. Kawale[123], C. Kawamoto[89], T. Kawamoto[63a], E. F. Kay[37], F. I. Kaya[161], S. Kazakos[109], V. F. Kazanin[39], Y. Ke[149], J. M. Keaveney[34a], R. Keeler[169], G. V. Kehris[62], J. S. Keller[35], J. J. Kempster[150], O. Kepka[134], J. Kerr[159b], B. P. Kerridge[137], B. P. Kerševan[95], L. Keszeghova[29a], R. A. Khan[132], A. Khanov[124], A. G. Kharlamov[39], T. Kharlamova[39], E. E. Khoda[142], M. Kholodenko[133a], T. J. Khoo[19], G. Khoriauli[170], J. Khubua[153b,*], Y. A. R. Khwaira[130], B. Kibirige[34g], D. Kim[6], D. W. Kim[48a,48b], Y. K. Kim[41], N. Kimura[98], M. K. Kingston[56], A. Kirchhoff[56], C. Kirfel[25], F. Kirfel[25], J. Kirk[137], A. E. Kiryunin[112], S. Kita[160], C. Kitsaki[10], O. Kivernyk[25], M. Klassen[161], C. Klein[35], L. Klein[170], M. H. Klein[46], S. B. Klein[57], U. Klein[94], A. Klimentov[30], T. Klioutchnikova[37], P. Kluit[117], S. Kluth[112], E. Kneringer[80], T. M. Knight[158], A. Knue[50], M. Kobel[51], D. Kobylianskii[173], S. F. Koch[129], M. Kocian[147], P. Kodyš[136], D. M. Koeck[126], P. T. Koenig[25], T. Koffas[35], O. Kolay[51], I. Koletsou[4], T. Komarek[88], K. Köneke[56], A. X. Y. Kong[1], T. Kono[121], N. Konstantinidis[98], P. Kontaxakis[57], B. Konya[100], R. Kopeliansky[43], S. Koperny[87a], K. Korcyl[88], K. Kordas[156,e], A. Korn[98], S. Korn[56], I. Korolkov[13], N. Korotkova[39], B. Kortman[117], O. Kortner[112], S. Kortner[112], W. H. Kostecka[118], V. V. Kostyukhin[145], A. Kotsokechagia[37], A. Kotwal[52], A. Koulouris[37], A. Kourkoumeli-Charalampidi[74a,74b], C. Kourkoumelis[9], E. Kourlitis[112], O. Kovanda[126], R. Kowalewski[169], W. Kozanecki[126], A. S. Kozhin[39],

V. A. Kramarenko[39], G. Kramberger[95], P. Kramer[25], M. W. Krasny[130], A. Krasznahorkay[105], A. C. Kraus[118], J. W. Kraus[175], J. A. Kremer[49], T. Kresse[51], L. Kretschmann[175], J. Kretzschmar[94], K. Kreul[19], P. Krieger[158], K. Krizka[21], K. Kroeninger[50], H. Kroha[112], J. Kroll[134], J. Kroll[131], K. S. Krowpman[109], U. Kruchonak[40], H. Krüger[25], N. Krumnack[82], M. C. Kruse[52], O. Kuchinskaia[39], S. Kuday[3a], S. Kuehn[37], R. Kuesters[55], T. Kuhl[49], V. Kukhtin[40], Y. Kulchitsky[40], S. Kuleshov[140b,140d], M. Kumar[34g], N. Kumari[49], P. Kumari[159b], A. Kupco[134], T. Kupfer[50], A. Kupich[39], O. Kuprash[55], H. Kurashige[86], L. L. Kurchaninov[159a], O. Kurdysh[67], Y. A. Kurochkin[38], A. Kurova[39], M. Kuze[141], A. K. Kvam[105], J. Kvita[125], N. G. Kyriacou[108], L. A. O. Laatu[104], C. Lacasta[167], F. Lacava[76a,76b], H. Lacker[19], D. Lacour[130], N. N. Lad[98], E. Ladygin[40], A. Lafarge[42], B. Laforge[130], T. Lagouri[176], F. Z. Lahbabi[36a], S. Lai[56], J. E. Lambert[169], S. Lammers[69], W. Lampl[7], C. Lampoudis[156,e], G. Lamprinoudis[102], A. N. Lancaster[118], E. Lançon[30], U. Landgraf[55], M. P. J. Landon[96], V. S. Lang[55], O. K. B. Langrekken[128], A. J. Lankford[162], F. Lanni[37], K. Lantzsch[25], A. Lanza[74a], M. Lanzac Berrocal[167], J. F. Laporte[138], T. Lari[72a], F. Lasagni Manghi[24b], M. Lassnig[37], V. Latonova[134], S. D. Lawlor[143], Z. Lawrence[103], R. Lazaridou[171], M. Lazzaroni[72a,72b], H. D. M. Le[109], E. M. Le Boulicaut[176], L. T. Le Pottier[18a], B. Leban[24a,24b], M. LeBlanc[103], F. Ledroit-Guillon[61], S. C. Lee[152], S. Lee[48a,48b], T. F. Lee[94], L. L. Leeuw[34c,aj], M. Lefebvre[169], C. Leggett[18a], G. Lehmann Miotto[37], M. Leigh[57], W. A. Leight[105], W. Leinonen[116], A. Leisos[156,t], M. A. L. Leite[84c], C. E. Leitgeb[19], R. Leitner[136], K. J. C. Leney[46], T. Lenz[25], S. Leone[75a], C. Leonidopoulos[53], A. Leopold[148], R. Les[109], C. G. Lester[33], M. Levchenko[39], J. Levêque[4], L. J. Levinson[173], G. Levrini[24a,24b], M. P. Lewicki[88], C. Lewis[142], D. J. Lewis[4], L. Lewitt[143], A. Li[30], B. Li[63b], C. Li[108], C.-Q. Li[112], H. Li[63a], H. Li[63b], H. Li[114a], H. Li[15], H. Li[63b], J. Li[63c], K. Li[14], L. Li[63c], R. Li[176], S. Li[14,114c], S. Li[63c,63d,d], T. Li[5], X. Li[106], Z. Li[157], Z. Li[14,114c], Z. Li[63a], S. Liang[14,114c], Z. Liang[14], M. Liberatore[138], B. Liberti[77a], K. Lie[65c], J. Lieber Marin[84e], H. Lien[69], H. Lin[108], L. Linden[111], R. E. Lindley[7], J. H. Lindon[2], J. Ling[62], E. Lipeles[131], A. Lipniacka[17], A. Lister[168], J. D. Little[69], B. Liu[14], B. X. Liu[114b], D. Liu[63c,63d], E. H. L. Liu[21], J. K. K. Liu[33], K. Liu[63d], K. Liu[63c,63d], M. Liu[63a], M. Y. Liu[63a], P. Liu[14], Q. Liu[63c,63d,142], X. Liu[63a], X. Liu[63b], Y. Liu[114b,114c], Y. L. Liu[63b], Y. W. Liu[63a], S. L. Lloyd[96], E. M. Lobodzinska[49], P. Loch[7], E. Lodhi[158], T. Lohse[19], K. Lohwasser[143], E. Loiacono[49], J. D. Lomas[21], J. D. Long[43], I. Longarini[162], R. Longo[166], A. Lopez Solis[49], N. A. Lopez-canelas[7], N. Lorenzo Martinez[4], A. M. Lory[111], M. Losada[119a], G. Löschcke Centeno[150], O. Loseva[39], X. Lou[48a,48b], X. Lou[14,114c], A. Lounis[67], P. A. Love[93], G. Lu[14,114c], M. Lu[67], S. Lu[131], Y. J. Lu[152], H. J. Lubatti[142], C. Luci[76a,76b], F. L. Lucio Alves[114a], F. Luehring[69], O. Lukianchuk[67], B. S. Lunday[131], O. Lundberg[148], B. Lund-Jensen[148,*], N. A. Luongo[6], M. S. Lutz[37], A. B. Lux[26], D. Lynn[30], R. Lysak[134], E. Lytken[100], V. Lyubushkin[40], T. Lyubushkina[40], M. M. Lyukova[149], M.Firdaus M. Soberi[53], H. Ma[30], K. Ma[63a], L. L. Ma[63b], W. Ma[63a], Y. Ma[124], J. C. MacDonald[102], P. C. Machado De Abreu Farias[84e], R. Madar[42], T. Madula[98], J. Maeda[86], T. Maeno[30], P. T. Mafa[34c,k], H. Maguire[143], V. Maiboroda[138], A. Maio[133a,133b,133d], K. Maj[87a], O. Majersky[49], S. Majewski[126], N. Makovec[67], V. Maksimovic[16], B. Malaescu[130], Pa. Malecki[88], V. P. Maleev[39], F. Malek[61,o], M. Mali[95], D. Malito[97], U. Mallik[81,*], S. Maltezos[10], S. Malyukov[40], J. Mamuzic[13], G. Mancini[54], M. N. Mancini[27], G. Manco[74a,74b], J. P. Mandalia[96], S. S. Mandarry[150], I. Mandić[95], L. Manhaes de Andrade Filho[84a], I. M. Maniatis[173], J. Manjarres Ramos[91], D. C. Mankad[173], A. Mann[111], S. Manzoni[37], L. Mao[63c], X. Mapekula[34c], A. Marantis[156,t], G. Marchiori[5], M. Marcisovsky[134], C. Marcon[72a], M. Marinescu[21], S. Marium[49], M. Marjanovic[123], A. Markhoos[55], M. Markovitch[67], M. K. Maroun[105], E. J. Marshall[93], Z. Marshall[18a], S. Marti-Garcia[167], J. Martin[98], T. A. Martin[137], V. J. Martin[53], B. Martin dit Latour[17], L. Martinelli[76a,76b], M. Martinez[13,w], P. Martinez Agullo[167], V. I. Martinez Outschoorn[105], P. Martinez Suarez[13], S. Martin-Haugh[137], G. Martinovicova[136], V. S. Martoiu[28b], A. C. Martyniuk[98], A. Marzin[37], D. Mascione[79a,79b], L. Masetti[102], J. Masik[103], A. L. Maslennikov[39], S. L. Mason[43], P. Massarotti[73a,73b], P. Mastrandrea[75a,75b], A. Mastroberardino[45a,45b], T. Masubuchi[127], T. T. Mathew[126], J. Matousek[136], D. M. Mattern[50], J. Maurer[28b], T. Maurin[60], A. J. Maury[67], B. Maček[95], D. A. Maximov[39], A. E. May[103], R. Mazini[34g], I. Maznas[118], M. Mazza[109], S. M. Mazza[139], E. Mazzeo[72a,72b], J. P. Mc Gowan[169], S. P. Mc Kee[108], C. A. Mc Lean[6], C. C. McCracken[168], E. F. McDonald[107], A. E. McDougall[117], L. F. Mcelhinney[93], J. A. Mcfayden[150], R. P. McGovern[131], R. P. Mckenzie[34g], T. C. Mclachlan[49], D. J. Mclaughlin[98], S. J. McMahon[137], C. M. Mcpartland[94], R. A. McPherson[169,aa], S. Mehlhase[111], A. Mehta[94], D. Melini[167], B. R. Mellado Garcia[34g], A. H. Melo[56], F. Meloni[49], A. M. Mendes Jacques Da Costa[103], H. Y. Meng[158], L. Meng[93], S. Menke[112], M. Mentink[37], E. Meoni[45a,45b], G. Mercado[118], S. Merianos[156], C. Merlassino[70a,70c], C. Meroni[72a,72b], J. Metcalfe[6],

A. S. Mete[6], E. Meuser[102], C. Meyer[69], J.-P. Meyer[138], R. P. Middleton[137], L. Mijović[53], G. Mikenberg[173], M. Mikestikova[134], M. Mikuž[95], H. Mildner[102], A. Milic[37], D. W. Miller[41], E. H. Miller[147], L. S. Miller[35], A. Milov[173], D. A. Milstead[48a,48b], T. Min[114a], A. A. Minaenko[39], I. A. Minashvili[153b], A. I. Mincer[120], B. Mindur[87a], M. Mineev[40], Y. Mino[89], L. M. Mir[13], M. Miralles Lopez[60], M. Mironova[18a], M. C. Missio[116], A. Mitra[171], V. A. Mitsou[167], Y. Mitsumori[113], O. Miu[158], P. S. Miyagawa[96], T. Mkrtchyan[64a], M. Mlinarevic[98], T. Mlinarevic[98], M. Mlynarikova[37], S. Mobius[20], P. Mogg[111], M. H. Mohamed Farook[115], A. F. Mohammed[14,114c], S. Mohapatra[43], G. Mokgatitswane[34g], L. Moleri[173], B. Mondal[145], S. Mondal[135], K. Mönig[49], E. Monnier[104], L. Monsonis Romero[167], J. Montejo Berlingen[13], A. Montella[48a,48b], M. Montella[122], F. Montereali[78a,78b], F. Monticelli[92], S. Monzani[70a,70c], A. Morancho Tarda[44], N. Morange[67], A. L. Moreira De Carvalho[49], M. Moreno Llácer[167], C. Moreno Martinez[57], J. M. Moreno Perez[23b], P. Morettini[58b], S. Morgenstern[37], M. Morii[62], M. Morinaga[157], M. Moritsu[90], F. Morodei[76a,76b], P. Moschovakos[37], B. Moser[129], M. Mosidze[153b], T. Moskalets[46], P. Moskvitina[116], J. Moss[32,l], P. Moszkowicz[87a], A. Moussa[36d], Y. Moyal[173], E. J. W. Moyse[105], O. Mtintsilana[34g], S. Muanza[104], J. Mueller[132], D. Muenstermann[93], R. Müller[37], G. A. Mullier[165], A. J. Mullin[33], J. J. Mullin[131], A. E. Mulski[62], D. P. Mungo[158], D. Munoz Perez[167], F. J. Munoz Sanchez[103], M. Murin[103], W. J. Murray[137,171], M. Muškinja[95], C. Mwewa[30], A. G. Myagkov[39,a], A. J. Myers[8], G. Myers[108], M. Myska[135], B. P. Nachman[18a], K. Nagai[129], K. Nagano[85], R. Nagasaka[157], J. L. Nagle[30,ai], E. Nagy[104], A. M. Nairz[37], Y. Nakahama[85], K. Nakamura[85], K. Nakkalil[5], H. Nanjo[127], E. A. Narayanan[46], Y. Narukawa[157], I. Naryshkin[39], L. Nasella[72a,72b], S. Nasri[119b], C. Nass[25], G. Navarro[23a], J. Navarro-Gonzalez[167], A. Nayaz[19], P. Y. Nechaeva[39], S. Nechaeva[24a,24b], F. Nechansky[134], L. Nedic[129], T. J. Neep[21], A. Negri[74a,74b], M. Negrini[24b], C. Nellist[117], C. Nelson[106], K. Nelson[108], S. Nemecek[134], M. Nessi[37,h], M. S. Neubauer[166], F. Neuhaus[102], J. Newell[94], P. R. Newman[21], Y. W. Y. Ng[166], B. Ngair[119a], H. D. N. Nguyen[110], R. B. Nickerson[129], R. Nicolaidou[138], J. Nielsen[139], M. Niemeyer[56], J. Niermann[37], N. Nikiforou[37], V. Nikolaenko[39,a], I. Nikolic-Audit[130], P. Nilsson[30], I. Ninca[49], G. Ninio[155], A. Nisati[76a], N. Nishu[2], R. Nisius[112], N. Nitika[70a,70c], J.-E. Nitschke[51], E. K. Nkadimeng[34g], T. Nobe[157], T. Nommensen[151], M. B. Norfolk[143], B. J. Norman[35], M. Noury[36a], J. Novak[95], T. Novak[95], R. Novotny[115], L. Nozka[125], K. Ntekas[162], N. M. J. Nunes De Moura Junior[84b], J. Ocariz[130], A. Ochi[86], I. Ochoa[133a], S. Oerdek[49,x], J. T. Offermann[41], A. Ogrodnik[136], A. Oh[103], C. C. Ohm[148], H. Oide[85], R. Oishi[157], M. L. Ojeda[37], Y. Okumura[157], L. F. Oleiro Seabra[133a], I. Oleksiyuk[57], S. A. Olivares Pino[140d], G. Oliveira Correa[13], D. Oliveira Damazio[30], J. L. Oliver[162], Ö. O. Öncel[55], A. P. O'Neill[20], A. Onofre[133a,133e], P. U. E. Onyisi[11], M. J. Oreglia[41], D. Orestano[78a,78b], R. S. Orr[158], L. M. Osojnak[131], Y. Osumi[113], G. Otero y Garzon[31], H. Otono[90], P. S. Ott[64a], G. J. Ottino[18a], M. Ouchrif[36d], F. Ould-Saada[128], T. Ovsiannikova[142], M. Owen[60], R. E. Owen[137], V. E. Ozcan[22a], F. Ozturk[88], N. Ozturk[8], S. Ozturk[83], H. A. Pacey[129], A. Pacheco Pages[13], C. Padilla Aranda[13], G. Padovano[76a,76b], S. Pagan Griso[18a], G. Palacino[69], A. Palazzo[71a,71b], J. Pampel[25], J. Pan[176], T. Pan[65a], D. K. Panchal[11], C. E. Pandini[117], J. G. Panduro Vazquez[137], H. D. Pandya[1], H. Pang[138], P. Pani[49], G. Panizzo[70a,70c], L. Panwar[130], L. Paolozzi[57], S. Parajuli[166], A. Paramonov[6], C. Paraskevopoulos[54], D. Paredes Hernandez[65b], A. Pareti[74a,74b], K. R. Park[43], T. H. Park[112], F. Parodi[58a,58b], J. A. Parsons[43], U. Parzefall[55], B. Pascual Dias[110], L. Pascual Dominguez[101], E. Pasqualucci[76a], S. Passaggio[58b], F. Pastore[97], P. Patel[88], U. M. Patel[52], J. R. Pater[103], T. Pauly[37], F. Pauwels[136], C. I. Pazos[161], M. Pedersen[128], R. Pedro[133a], S. V. Peleganchuk[39], O. Penc[37], E. A. Pender[53], S. Peng[15], G. D. Penn[176], K. E. Penski[111], M. Penzin[39], B. S. Peralva[84d], A. P. Pereira Peixoto[142], L. Pereira Sanchez[147], D. V. Perepelitsa[30,ai], G. Perera[105], E. Perez Codina[159a], M. Perganti[10], H. Pernegger[37], S. Perrella[76a,76b], O. Perrin[42], K. Peters[49], R. F. Y. Peters[103], B. A. Petersen[37], T. C. Petersen[44], E. Petit[104], V. Petousis[135], C. Petridou[156,e], T. Petru[136], A. Petrukhin[145], M. Pettee[18a], A. Petukhov[83], K. Petukhova[37], R. Pezoa[140f], L. Pezzotti[37], G. Pezzullo[176], A. J. Pfleger[37], T. M. Pham[174], T. Pham[107], P. W. Phillips[137], G. Piacquadio[149], E. Pianori[18a], F. Piazza[126], R. Piegaia[31], D. Pietreanu[28b], A. D. Pilkington[103], M. Pinamonti[70a,70c], J. L. Pinfold[2], B. C. Pinheiro Pereira[133a], J. Pinol Bel[13], A. E. Pinto Pinoargote[138], L. Pintucci[70a,70c], K. M. Piper[150], A. Pirttikoski[57], D. A. Pizzi[35], L. Pizzimento[65b], M.-A. Pleier[30], V. Pleskot[136], E. Plotnikova[40], G. Poddar[96], R. Poettgen[100], L. Poggioli[130], S. Polacek[136], G. Polesello[74a], A. Poley[146,159a], A. Polini[24b], C. S. Pollard[171], Z. B. Pollock[122], E. Pompa Pacchi[123], N. I. Pond[98], D. Ponomarenko[69], L. Pontecorvo[37], S. Popa[28a], G. A. Popeneciu[28d], A. Poreba[37], D. M. Portillo Quintero[159a], S. Pospisil[135], M. A. Postill[143], P. Postolache[28c], K. Potamianos[171], P. A. Potepa[87a], I. N. Potrap[40], C. J. Potter[33], H. Potti[151],

J. Poveda[167], M. E. Pozo Astigarraga[37], A. Prades Ibanez[77a,77b], J. Pretel[169], D. Price[103], M. Primavera[71a], L. Primomo[70a,70c], M. A. Principe Martin[101], R. Privara[125], T. Procter[60], M. L. Proffitt[142], N. Proklova[131], K. Prokofiev[65c], G. Proto[112], J. Proudfoot[6], M. Przybycien[87a], W. W. Przygoda[87b], A. Psallidas[47], J. E. Puddefoot[143], D. Pudzha[55], D. Pyatiizbyantseva[39], J. Qian[108], R. Qian[109], D. Qichen[103], Y. Qin[13], T. Qiu[53], A. Quadt[56], M. Queitsch-Maitland[103], G. Quetant[57], R. P. Quinn[168], G. Rabanal Bolanos[62], D. Rafanoharana[55], F. Raffaeli[77a,77b], F. Ragusa[72a,72b], J. L. Rainbolt[41], J. A. Raine[57], S. Rajagopalan[30], E. Ramakoti[39], L. Rambelli[58a,58b], I. A. Ramirez-Berend[35], K. Ran[49,114c], D. S. Rankin[131], N. P. Rapheeha[34g], H. Rasheed[28b], V. Raskina[130], D. F. Rassloff[64a], A. Rastogi[18a], S. Rave[102], S. Ravera[58a,58b], B. Ravina[37], I. Ravinovich[173], M. Raymond[37], A. L. Read[128], N. P. Readioff[143], D. M. Rebuzzi[74a,74b], A. S. Reed[112], K. Reeves[27], J. A. Reidelsturz[175], D. Reikher[126], A. Rej[50], C. Rembser[37], H. Ren[63a], M. Renda[28b], F. Renner[49], A. G. Rennie[162], A. L. Rescia[49], S. Resconi[72a], M. Ressegotti[58a,58b], S. Rettie[37], W. F. Rettie[35], J. G. Reyes Rivera[109], E. Reynolds[18a], O. L. Rezanova[39], P. Reznicek[136], H. Riani[36d], N. Ribaric[52], E. Ricci[79a,79b], R. Richter[112], S. Richter[48a,48b], E. Richter-Was[87b], M. Ridel[130], S. Ridouani[36d], P. Rieck[120], P. Riedler[37], E. M. Riefel[48a,48b], J. O. Rieger[117], M. Rijssenbeek[149], M. Rimoldi[37], L. Rinaldi[24a,24b], P. Rincke[56], M. P. Rinnagel[111], G. Ripellino[165], I. Riu[13], J. C. Rivera Vergara[169], F. Rizatdinova[124], E. Rizvi[96], B. R. Roberts[18a], S. S. Roberts[139], D. Robinson[33], M. Robles Manzano[102], A. Robson[60], A. Rocchi[77a,77b], C. Roda[75a,75b], S. Rodriguez Bosca[37], Y. Rodriguez Garcia[23a], A. M. Rodríguez Vera[118], S. Roe[37], J. T. Roemer[37], O. Røhne[128], R. A. Rojas[37], C. P. A. Roland[130], J. Roloff[30], A. Romaniouk[80], E. Romano[74a,74b], M. Romano[24b], A. C. Romero Hernandez[166], N. Rompotis[94], L. Roos[130], S. Rosati[76a], B. J. Rosser[41], E. Rossi[129], E. Rossi[73a,73b], L. P. Rossi[62], L. Rossini[55], R. Rosten[122], M. Rotaru[28b], B. Rottler[55], C. Rougier[91], D. Rousseau[67], D. Rousso[49], S. Roy-Garand[158], A. Rozanov[104], Z. M. A. Rozario[60], Y. Rozen[154], A. Rubio Jimenez[167], V. H. Ruelas Rivera[19], T. A. Ruggeri[1], A. Ruggiero[129], A. Ruiz-Martinez[167], A. Rummler[37], Z. Rurikova[55], N. A. Rusakovich[40], H. L. Russell[169], G. Russo[76a,76b], J. P. Rutherfoord[7], S. Rutherford Colmenares[33], M. Rybar[136], E. B. Rye[128], A. Ryzhov[46], J. A. Sabater Iglesias[57], H.F.-W. Sadrozinski[139], F. Safai Tehrani[76a], S. Saha[1], M. Sahinsoy[83], A. Saibel[167], M. Saimpert[138], M. Saito[157], T. Saito[157], A. Sala[72a,72b], D. Salamani[37], A. Salnikov[147], J. Salt[167], A. Salvador Salas[155], D. Salvatore[45a,45b], F. Salvatore[150], A. Salzburger[37], D. Sammel[55], E. Sampson[93], D. Sampsonidis[156,e], D. Sampsonidou[126], J. Sánchez[167], V. Sanchez Sebastian[167], H. Sandaker[128], C. O. Sander[49], J. A. Sandesara[105], M. Sandhoff[175], C. Sandoval[23b], L. Sanfilippo[64a], D. P. C. Sankey[137], T. Sano[89], A. Sansoni[54], L. Santi[37,76b], C. Santoni[42], H. Santos[133a,133b], A. Santra[173], E. Sanzani[24a,24b], K. A. Saoucha[164], J. G. Saraiva[133a,133d], J. Sardain[7], O. Sasaki[85], K. Sato[160], C. Sauer[37], E. Sauvan[4], P. Savard[158,ag], R. Sawada[157], C. Sawyer[137], L. Sawyer[99], C. Sbarra[24b], A. Sbrizzi[24a,24b], T. Scanlon[98], J. Schaarschmidt[142], U. Schäfer[102], A. C. Schaffer[46,67], D. Schaile[111], R. D. Schamberger[149], C. Scharf[19], M. M. Schefer[20], V. A. Schegelsky[39], D. Scheirich[136], M. Schernau[140e], C. Scheulen[57], C. Schiavi[58a,58b], M. Schioppa[45a,45b], B. Schlag[147], S. Schlenker[37], J. Schmeing[175], M. A. Schmidt[175], K. Schmieden[102], C. Schmitt[102], N. Schmitt[102], S. Schmitt[49], L. Schoeffel[138], A. Schoening[64b], P. G. Scholer[35], E. Schopf[129], M. Schott[25], J. Schovancova[37], S. Schramm[57], T. Schroer[57], H.-C. Schultz-Coulon[64a], M. Schumacher[55], B. A. Schumm[139], Ph. Schune[138], H. R. Schwartz[139], A. Schwartzman[147], T. A. Schwarz[108], Ph. Schwemling[138], R. Schwienhorst[109], F. G. Sciacca[20], A. Sciandra[30], G. Sciolla[27], F. Scuri[75a], C. D. Sebastiani[94], K. Sedlaczek[118], S. C. Seidel[115], A. Seiden[139], B. D. Seidlitz[43], C. Seitz[49], J. M. Seixas[84b], G. Sekhniaidze[73a], L. Selem[61], N. Semprini-Cesari[24a,24b], A. Semushin[39,177], D. Sengupta[57], V. Senthilkumar[167], L. Serin[67], M. Sessa[77a,77b], H. Severini[123], F. Sforza[58a,58b], A. Sfyrla[57], Q. Sha[14], E. Shabalina[56], H. Shaddix[118], A. H. Shah[33], R. Shaheen[148], J. D. Shahinian[131], D. Shaked Renous[173], L. Y. Shan[14], M. Shapiro[18a], A. Sharma[37], A. S. Sharma[168], P. Sharma[30], P. B. Shatalov[39], K. Shaw[150], S. M. Shaw[103], Q. Shen[63c], D. J. Sheppard[146], P. Sherwood[98], L. Shi[98], X. Shi[14], S. Shimizu[85], C. O. Shimmin[176], I. P. J. Shipsey[129,*], S. Shirabe[90], M. Shiyakova[40,y], M. J. Shochet[41], D. R. Shope[128], B. Shrestha[123], S. Shrestha[122,ak], I. Shreyber[39], M. J. Shroff[169], P. Sicho[134], A. M. Sickles[166], E. Sideras Haddad[34g,163], A. C. Sidley[117], A. Sidoti[24b], F. Siegert[51], Dj. Sijacki[16], F. Sili[92], J. M. Silva[53], I. Silva Ferreira[84b], M. V. Silva Oliveira[30], S. B. Silverstein[48a], S. Simion[67], R. Simoniello[37], E. L. Simpson[103], H. Simpson[150], L. R. Simpson[108], S. Simsek[83], S. Sindhu[56], P. Sinervo[158], S. N. Singh[27], S. Singh[30], S. Sinha[49], S. Sinha[103], M. Sioli[24a,24b], I. Siral[37], E. Sitnikova[49], J. Sjölin[48a,48b], A. Skaf[56], E. Skorda[21], P. Skubic[123], M. Slawinska[88], I. Slazyk[17], V. Smakhtin[173], B. H. Smart[137], S.Yu. Smirnov[39], Y. Smirnov[39], L. N. Smirnova[39,a], O. Smirnova[100], A. C. Smith[43],

D. R. Smith[162], E. A. Smith[41], J. L. Smith[103], R. Smith[147], H. Smitmanns[102], M. Smizanska[93], K. Smolek[135], A. A. Snesarev[39], H. L. Snoek[117], S. Snyder[30], R. Sobie[169,aa], A. Soffer[155], C. A. Solans Sanchez[37], E.Yu. Soldatov[39], U. Soldevila[167], A. A. Solodkov[39], S. Solomon[27], A. Soloshenko[40], K. Solovieva[55], O. V. Solovyanov[42], P. Sommer[51], A. Sonay[13], W. Y. Song[159b], A. Sopczak[135], A. L. Sopio[53], F. Sopkova[29b], J. D. Sorenson[115], I. R. Sotarriva Alvarez[141], V. Sothilingam[64a], O. J. Soto Sandoval[140b,140c], S. Sottocornola[69], R. Soualah[164], Z. Soumaimi[36e], D. South[49], N. Soybelman[173], S. Spagnolo[71a,71b], M. Spalla[112], D. Sperlich[55], B. Spisso[73a,73b], D. P. Spiteri[60], M. Spousta[136], E. J. Staats[35], R. Stamen[64a], A. Stampekis[21], E. Stanecka[88], W. Stanek-Maslouska[49], M. V. Stange[51], B. Stanislaus[18a], M. M. Stanitzki[49], B. Stapf[49], E. A. Starchenko[39], G. H. Stark[139], J. Stark[91], P. Staroba[134], P. Starovoitov[164], R. Staszewski[88], G. Stavropoulos[47], A. Stefl[37], P. Steinberg[30], B. Stelzer[146,159a], H. J. Stelzer[132], O. Stelzer-Chilton[159a], H. Stenzel[59], T. J. Stevenson[150], G. A. Stewart[37], J. R. Stewart[124], M. C. Stockton[37], G. Stoicea[28b], M. Stolarski[133a], S. Stonjek[112], A. Straessner[51], J. Strandberg[148], S. Strandberg[48a,48b], M. Stratmann[175], M. Strauss[123], T. Strebler[104], P. Strizenec[29b], R. Ströhmer[170], D. M. Strom[126], R. Stroynowski[46], A. Strubig[48a,48b], S. A. Stucci[30], B. Stugu[17], J. Stupak[123], N. A. Styles[49], D. Su[147], S. Su[63a], W. Su[63d], X. Su[63a], D. Suchy[29a], K. Sugizaki[157], V. V. Sulin[39], M. J. Sullivan[94], D. M. S. Sultan[129], L. Sultanaliyeva[39], S. Sultansoy[3b], S. Sun[174], W. Sun[14], O. Sunneborn Gudnadottir[165], N. Sur[104], M. R. Sutton[150], H. Suzuki[160], M. Svatos[134], M. Swiatlowski[159a], T. Swirski[170], I. Sykora[29a], M. Sykora[136], T. Sykora[136], D. Ta[102], K. Tackmann[49,x], A. Taffard[162], R. Tafirout[159a], J. S. Tafoya Vargas[67], Y. Takubo[85], M. Talby[104], A. A. Talyshev[39], K. C. Tam[65b], N. M. Tamir[155], A. Tanaka[157], J. Tanaka[157], R. Tanaka[67], M. Tanasini[149], Z. Tao[168], S. Tapia Araya[140f], S. Tapprogge[102], A. Tarek Abouelfadl Mohamed[109], S. Tarem[154], K. Tariq[14], G. Tarna[28b], G. F. Tartarelli[72a], M. J. Tartarin[91], P. Tas[136], M. Tasevsky[134], E. Tassi[45a,45b], A. C. Tate[166], G. Tateno[157], Y. Tayalati[36e,z], G. N. Taylor[107], W. Taylor[159b], P. Teixeira-Dias[97], J. J. Teoh[158], K. Terashi[157], J. Terron[101], S. Terzo[13], M. Testa[54], R. J. Teuscher[158,aa], A. Thaler[80], O. Theiner[57], T. Theveneaux-Pelzer[104], O. Thielmann[175], D. W. Thomas[97], J. P. Thomas[21], E. A. Thompson[18a], P. D. Thompson[21], E. Thomson[131], R. E. Thornberry[46], C. Tian[63a], Y. Tian[57], V. Tikhomirov[39,a], Yu.A. Tikhonov[39], S. Timoshenko[39], D. Timoshyn[136], E. X. L. Ting[1], P. Tipton[176], A. Tishelman-Charny[30], S. H. Tlou[34g], K. Todome[141], S. Todorova-Nova[136], S. Todt[51], L. Toffolin[70a,70c], M. Togawa[85], J. Tojo[90], S. Tokár[29a], O. Toldaiev[69], G. Tolkachev[104], M. Tomoto[85,113], L. Tompkins[147,n], E. Torrence[126], H. Torres[91], E. Torró Pastor[167], M. Toscani[31], C. Tosciri[41], M. Tost[11], D. R. Tovey[143], T. Trefzger[170], A. Tricoli[30], I. M. Trigger[159a], S. Trincaz-Duvoid[130], D. A. Trischuk[27], A. Tropina[40], L. Truong[34c], M. Trzebinski[88], A. Trzupek[88], F. Tsai[149], M. Tsai[108], A. Tsiamis[156], P. V. Tsiareshka[40], S. Tsigaridas[159a], A. Tsirigotis[156,t], V. Tsiskaridze[158], E. G. Tskhadadze[153a], M. Tsopoulou[156], Y. Tsujikawa[89], I. I. Tsukerman[39], V. Tsulaia[18a], S. Tsuno[85], K. Tsuri[121], D. Tsybychev[149], Y. Tu[65b], A. Tudorache[28b], V. Tudorache[28b], S. Turchikhin[58a,58b], I. Turk Cakir[3a], R. Turra[72a], T. Turtuvshin[40,ab], P. M. Tuts[43], S. Tzamarias[156,e], E. Tzovara[102], F. Ukegawa[160], P. A. Ulloa Poblete[140b,140c], E. N. Umaka[30], G. Unal[37], A. Undrus[30], G. Unel[162], J. Urban[29b], P. Urrejola[140a], G. Usai[8], R. Ushioda[141], M. Usman[110], F. Ustuner[53], Z. Uysal[83], V. Vacek[135], B. Vachon[106], T. Vafeiadis[37], A. Vaitkus[98], C. Valderanis[111], E. Valdes Santurio[48a,48b], M. Valente[159a], S. Valentinetti[24a,24b], A. Valero[167], E. Valiente Moreno[167], A. Vallier[91], J. A. Valls Ferrer[167], D. R. Van Arneman[117], T. R. Van Daalen[142], A. Van Der Graaf[50], P. Van Gemmeren[6], M. Van Rijnbach[37], S. Van Stroud[98], I. Van Vulpen[117], P. Vana[136], M. Vanadia[77a,77b], U. M. Vande Voorde[148], W. Vandelli[37], E. R. Vandewall[124], D. Vannicola[155], L. Vannoli[54], R. Vari[76a], E. W. Varnes[7], C. Varni[18b], D. Varouchas[67], L. Varriale[167], K. E. Varvell[151], M. E. Vasile[28b], L. Vaslin[85], A. Vasyukov[40], L. M. Vaughan[124], R. Vavricka[102], T. Vazquez Schroeder[13], J. Veatch[32], V. Vecchio[103], M. J. Veen[105], I. Veliscek[30], L. M. Veloce[158], F. Veloso[133a,133c], S. Veneziano[76a], A. Ventura[71a,71b], S. Ventura Gonzalez[138], A. Verbytskyi[112], M. Verducci[75a,75b], C. Vergis[96], M. Verissimo De Araujo[84b], W. Verkerke[117], J. C. Vermeulen[117], C. Vernieri[147], M. Vessella[162], M. C. Vetterli[146,ag], A. Vgenopoulos[102], N. Viaux Maira[140f], T. Vickey[143], O. E. Vickey Boeriu[143], G. H. A. Viehhauser[129], L. Vigani[64b], M. Vigl[112], M. Villa[24a,24b], M. Villaplana Perez[167], E. M. Villhauer[53], E. Vilucchi[54], M. G. Vincter[35], A. Visibile[117], C. Vittori[37], I. Vivarelli[24a,24b], E. Voevodina[112], F. Vogel[111], J. C. Voigt[51], P. Vokac[135], Yu. Volkotrub[87b], E. Von Toerne[25], B. Vormwald[37], K. Vorobev[39], M. Vos[167], K. Voss[145], M. Vozak[117], L. Vozdecky[123], N. Vranjes[16], M. Vranjes Milosavljevic[16], M. Vreeswijk[117], N. K. Vu[63c,63d], R. Vuillermet[37], O. Vujinovic[102], I. Vukotic[41], I. K. Vyas[35], S. Wada[160], C. Wagner[147], J. M. Wagner[18a], W. Wagner[175], S. Wahdan[175], H. Wahlberg[92], C. H. Waits[123], J. Walder[137], R. Walker[111], W. Walkowiak[145], A. Wall[131], E. J. Wallin[100],

T. Wamorkar[18a], A. Z. Wang[139], C. Wang[102], C. Wang[11], H. Wang[18a], J. Wang[65c], P. Wang[103], P. Wang[98], R. Wang[62], R. Wang[6], S. M. Wang[152], S. Wang[14], T. Wang[63a], W. T. Wang[81], W. Wang[14], X. Wang[166], X. Wang[63c], Y. Wang[114a], Y. Wang[63a], Z. Wang[108], Z. Wang[52,63c,63d], Z. Wang[108], A. Warburton[106], R. J. Ward[21], A. L. Warnerbring[145], N. Warrack[60], S. Waterhouse[97], A. T. Watson[21], H. Watson[53], M. F. Watson[21], E. Watton[60,137], G. Watts[142], B. M. Waugh[98], J. M. Webb[55], C. Weber[30], H. A. Weber[19], M. S. Weber[20], S. M. Weber[64a], C. Wei[63a], Y. Wei[55], A. R. Weidberg[129], E. J. Weik[120], J. Weingarten[50], C. Weiser[55], C. J. Wells[49], T. Wenaus[30], B. Wendland[50], T. Wengler[37], N. S. Wenke[112], N. Wermes[25], M. Wessels[64a], A. M. Wharton[93], A. S. White[62], A. White[8], M. J. White[1], D. Whiteson[162], L. Wickremasinghe[127], W. Wiedenmann[174], M. Wielers[137], C. Wiglesworth[44], D. J. Wilbern[123], H. G. Wilkens[37], J. J. H. Wilkinson[33], D. M. Williams[43], H. H. Williams[131], S. Williams[33], S. Willocq[105], B. J. Wilson[103], D. J. Wilson[103], P. J. Windischhofer[41], F. I. Winkel[31], F. Winklmeier[126], B. T. Winter[55], M. Wittgen[147], M. Wobisch[99], T. Wojtkowski[61], Z. Wolffs[117], J. Wollrath[37], M. W. Wolter[88], H. Wolters[133a,133c], M. C. Wong[139], E. L. Woodward[43], S. D. Worm[49], B. K. Wosiek[88], K. W. Woźniak[88], S. Wozniewski[56], K. Wraight[60], C. Wu[21], M. Wu[114b], M. Wu[116], S. L. Wu[174], X. Wu[57], X. Wu[63a], Y. Wu[63a], Z. Wu[4], J. Wuerzinger[112,ae], T. R. Wyatt[103], B. M. Wynne[53], S. Xella[44], L. Xia[114a], M. Xia[15], M. Xie[63a], A. Xiong[126], J. Xiong[18a], D. Xu[14], H. Xu[63a], L. Xu[63a], R. Xu[131], T. Xu[108], Y. Xu[142], Z. Xu[53], Z. Xu[114a], B. Yabsley[151], S. Yacoob[34a], Y. Yamaguchi[85], E. Yamashita[157], H. Yamauchi[160], T. Yamazaki[18a], Y. Yamazaki[86], S. Yan[60], Z. Yan[105], H. J. Yang[63c,63d], H. T. Yang[63a], S. Yang[63a], T. Yang[65c], X. Yang[37], X. Yang[14], Y. Yang[46], Y. Yang[63a], W.-M. Yao[18a], H. Ye[56], J. Ye[14], S. Ye[30], X. Ye[63a], Y. Yeh[98], I. Yeletskikh[40], B. Yeo[18b], M. R. Yexley[98], T. P. Yildirim[129], P. Yin[43], K. Yorita[172], S. Younas[28b], C. J. S. Young[37], C. Young[147], C. Yu[14,114c], Y. Yu[63a], J. Yuan[14,114c], M. Yuan[108], R. Yuan[63c,63d], L. Yue[98], M. Zaazoua[63a], B. Zabinski[88], I. Zahir[36a], Z. K. Zak[88], T. Zakareishvili[167], S. Zambito[57], J. A. Zamora Saa[140b,140d], J. Zang[157], D. Zanzi[55], R. Zanzottera[72a,72b], O. Zaplatilek[135], C. Zeitnitz[175], H. Zeng[14], J. C. Zeng[166], D. T. Zenger Jr[27], O. Zenin[39], T. Ženiš[29a], S. Zenz[96], S. Zerradi[36a], D. Zerwas[67], M. Zhai[14,114c], D. F. Zhang[143], J. Zhang[63b], J. Zhang[6], K. Zhang[14,114c], L. Zhang[63a], L. Zhang[114a], P. Zhang[14,114c], R. Zhang[174], S. Zhang[91], T. Zhang[157], X. Zhang[63c], Y. Zhang[142], Y. Zhang[98], Y. Zhang[114a], Z. Zhang[18a], Z. Zhang[63b], Z. Zhang[67], H. Zhao[142], T. Zhao[63b], Y. Zhao[35], Z. Zhao[63a], Z. Zhao[63a], A. Zhemchugov[40], J. Zheng[114a], K. Zheng[166], X. Zheng[63a], Z. Zheng[147], D. Zhong[166], B. Zhou[108], H. Zhou[7], N. Zhou[63c], Y. Zhou[15], Y. Zhou[114a], Y. Zhou[7], C. G. Zhu[63b], J. Zhu[108], X. Zhu[63d], Y. Zhu[63c], Y. Zhu[63a], X. Zhuang[14], K. Zhukov[69], N. I. Zimine[40], J. Zinsser[64b], M. Ziolkowski[145], L. Živković[16], A. Zoccoli[24a,24b], K. Zoch[62], T. G. Zorbas[143], O. Zormpa[47], W. Zou[43], L. Zwalinski[37]

[1] Department of Physics, University of Adelaide, Adelaide, Australia
[2] Department of Physics, University of Alberta, Edmonton, AB, Canada
[3] [(a)]Department of Physics, Ankara University, Ankara, Turkey; [(b)]Division of Physics, TOBB University of Economics and Technology, Ankara, Turkey
[4] LAPP, Université Savoie Mont Blanc, CNRS/IN2P3, Annecy, France
[5] APC, Université Paris Cité, CNRS/IN2P3, Paris, France
[6] High Energy Physics Division, Argonne National Laboratory, Argonne, IL, USA
[7] Department of Physics, University of Arizona, Tucson, AZ, USA
[8] Department of Physics, University of Texas at Arlington, Arlington, TX, USA
[9] Physics Department, National and Kapodistrian University of Athens, Athens, Greece
[10] Physics Department, National Technical University of Athens, Zografou, Greece
[11] Department of Physics, University of Texas at Austin, Austin, TX, USA
[12] Institute of Physics, Azerbaijan Academy of Sciences, Baku, Azerbaijan
[13] Institut de Física d'Altes Energies (IFAE), Barcelona Institute of Science and Technology, Barcelona, Spain
[14] Institute of High Energy Physics, Chinese Academy of Sciences, Beijing, China
[15] Physics Department, Tsinghua University, Beijing, China
[16] Institute of Physics, University of Belgrade, Belgrade, Serbia
[17] Department for Physics and Technology, University of Bergen, Bergen, Norway
[18] [(a)]Physics Division, Lawrence Berkeley National Laboratory, Berkeley, CA, USA; [(b)]University of California, Berkeley, CA, USA
[19] Institut für Physik, Humboldt Universität zu Berlin, Berlin, Germany

[20] Albert Einstein Center for Fundamental Physics and Laboratory for High Energy Physics, University of Bern, Bern, Switzerland
[21] School of Physics and Astronomy, University of Birmingham, Birmingham, UK
[22] [(a)]Department of Physics, Bogazici University, Istanbul, Turkey; [(b)]Department of Physics Engineering, Gaziantep University, Gaziantep, Turkey; [(c)]Department of Physics, Istanbul University, Istanbul, Turkey
[23] [(a)]Facultad de Ciencias y Centro de Investigaciónes, Universidad Antonio Nariño, Bogotá, Colombia; [(b)]Departamento de Física, Universidad Nacional de Colombia, Bogotá, Colombia
[24] [(a)]Dipartimento di Fisica e Astronomia A. Righi, Università di Bologna, Bologna, Italy; [(b)]INFN Sezione di Bologna, Bologna, Italy
[25] Physikalisches Institut, Universität Bonn, Bonn, Germany
[26] Department of Physics, Boston University, Boston, MA, USA
[27] Department of Physics, Brandeis University, Waltham, MA, USA
[28] [(a)]Transilvania University of Brasov, Brasov, Romania; [(b)]Horia Hulubei National Institute of Physics and Nuclear Engineering, Bucharest, Romania; [(c)]Department of Physics, Alexandru Ioan Cuza University of Iasi, Iasi, Romania ; [(d)]National Institute for Research and Development of Isotopic and Molecular Technologies, Physics Department, Cluj-Napoca, Romania; [(e)]National University of Science and Technology Politechnica, Bucharest, Romania; [(f)]West University in Timisoara, Timisoara, Romania; [(g)]Faculty of Physics, University of Bucharest, Bucharest, Romania
[29] [(a)]Faculty of Mathematics, Physics and Informatics, Comenius University, Bratislava, Slovakia; [(b)]Department of Subnuclear Physics, Institute of Experimental Physics of the Slovak Academy of Sciences, Kosice, Slovak Republic
[30] Physics Department, Brookhaven National Laboratory, Upton, NY, USA
[31] Universidad de Buenos Aires, Facultad de Ciencias Exactas y Naturales, Departamento de Física, y CONICET, Instituto de Física de Buenos Aires (IFIBA), Buenos Aires, Argentina
[32] California State University, Long Beach, CA, USA
[33] Cavendish Laboratory, University of Cambridge, Cambridge, UK
[34] [(a)]Department of Physics, University of Cape Town, Cape Town, South Africa; [(b)]iThemba Labs, Cape Town, Western Cape, South Africa; [(c)]Department of Mechanical Engineering Science, University of Johannesburg, Johannesburg, South Africa; [(d)]National Institute of Physics, University of the Philippines Diliman (Philippines), Quezon City, Philippines; [(e)]University of South Africa, Department of Physics, Pretoria, South Africa; [(f)]University of Zululand, KwaDlangezwa, South Africa; [(g)]School of Physics, University of the Witwatersrand, Johannesburg, South Africa
[35] Department of Physics, Carleton University, Ottawa, ON, Canada
[36] [(a)]Faculté des Sciences Ain Chock, Université Hassan II de Casablanca, Casablanca, Morocco; [(b)]Faculté des Sciences, Université Ibn-Tofail, Kenitra, Morocco; [(c)]Faculté des Sciences Semlalia, Université Cadi Ayyad, LPHEA-Marrakech, Marrakech, Morocco; [(d)]LPMR, Faculté des Sciences, Université Mohamed Premier, Oujda, Morocco; [(e)]Faculté des sciences, Université Mohammed V, Rabat, Morocco; [(f)]Institute of Applied Physics, Mohammed VI Polytechnic University, Ben Guerir, Morocco
[37] CERN, Geneva, Switzerland
[38] Affiliated with an Institute Formerly Covered by a Cooperation Agreement with CERN, Geneva, Switzerland
[39] Affiliated with an Institute Covered by a Cooperation Agreement with CERN, Geneva, Switzerland
[40] Affiliated with an International Laboratory Covered by a Cooperation Agreement with CERN, Geneva, Switzerland
[41] Enrico Fermi Institute, University of Chicago, Chicago, IL, USA
[42] LPC, Université Clermont Auvergne, CNRS/IN2P3, Clermont-Ferrand, France
[43] Nevis Laboratory, Columbia University, Irvington, NY, USA
[44] Niels Bohr Institute, University of Copenhagen, Copenhagen, Denmark
[45] [(a)]Dipartimento di Fisica, Università della Calabria, Rende, Italy; [(b)]INFN Gruppo Collegato di Cosenza, Laboratori Nazionali di Frascati, Frascati, Italy
[46] Physics Department, Southern Methodist University, Dallas, TX, USA
[47] National Centre for Scientific Research “Demokritos”, Agia Paraskevi, Greece
[48] [(a)]Department of Physics, Stockholm University, Stockholm, Sweden; [(b)]Oskar Klein Centre, Stockholm, Sweden
[49] Deutsches Elektronen-Synchrotron DESY, Hamburg and Zeuthen, Germany
[50] Fakultät Physik , Technische Universität Dortmund, Dortmund, Germany
[51] Institut für Kern- und Teilchenphysik, Technische Universität Dresden, Dresden, Germany
[52] Department of Physics, Duke University, Durham, NC, USA
[53] SUPA-School of Physics and Astronomy, University of Edinburgh, Edinburgh, UK

[54] INFN e Laboratori Nazionali di Frascati, Frascati, Italy
[55] Physikalisches Institut, Albert-Ludwigs-Universität Freiburg, Freiburg, Germany
[56] II. Physikalisches Institut, Georg-August-Universität Göttingen, Göttingen, Germany
[57] Département de Physique Nucléaire et Corpusculaire, Université de Genève, Geneva, Switzerland
[58] [(a)]Dipartimento di Fisica, Università di Genova, Genoa, Italy; [(b)]INFN Sezione di Genova, Genoa, Italy
[59] II. Physikalisches Institut, Justus-Liebig-Universität Giessen, Giessen, Germany
[60] SUPA-School of Physics and Astronomy, University of Glasgow, Glasgow, UK
[61] LPSC, Université Grenoble Alpes, CNRS/IN2P3, Grenoble INP, Grenoble, France
[62] Laboratory for Particle Physics and Cosmology, Harvard University, Cambridge, MA, USA
[63] [(a)]Department of Modern Physics and State Key Laboratory of Particle Detection and Electronics, University of Science and Technology of China, Hefei, China; [(b)]Institute of Frontier and Interdisciplinary Science and Key Laboratory of Particle Physics and Particle Irradiation (MOE), Shandong University, Qingdao, China; [(c)]School of Physics and Astronomy, Shanghai Jiao Tong University, Key Laboratory for Particle Astrophysics and Cosmology (MOE), SKLPPC, Shanghai, China; [(d)]Tsung-Dao Lee Institute, Shanghai, China; [(e)]School of Physics, Zhengzhou University, Zhengzhou, China
[64] [(a)]Kirchhoff-Institut für Physik, Ruprecht-Karls-Universität Heidelberg, Heidelberg, Germany; [(b)]Physikalisches Institut, Ruprecht-Karls-Universität Heidelberg, Heidelberg, Germany
[65] [(a)]Department of Physics, Chinese University of Hong Kong, Shatin, N.T., Hong Kong; [(b)]Department of Physics, University of Hong Kong, Pok Fu Lam, Hong Kong; [(c)]Department of Physics and Institute for Advanced Study, Hong Kong University of Science and Technology, Clear Water Bay, Kowloon, Hong Kong, China
[66] Department of Physics, National Tsing Hua University, Hsinchu, Taiwan
[67] IJCLab, Université Paris-Saclay, CNRS/IN2P3, 91405 Orsay, France
[68] Centro Nacional de Microelectrónica (IMB-CNM-CSIC), Barcelona, Spain
[69] Department of Physics, Indiana University, Bloomington, IN, USA
[70] [(a)]INFN Gruppo Collegato di Udine, Sezione di Trieste, Udine, Italy; [(b)]ICTP, Trieste, Italy; [(c)]Dipartimento Politecnico di Ingegneria e Architettura, Università di Udine, Udine, Italy
[71] [(a)]INFN Sezione di Lecce, Lecce, Italy; [(b)]Dipartimento di Matematica e Fisica, Università del Salento, Lecce, Italy
[72] [(a)]INFN Sezione di Milano, Milan, Italy; [(b)]Dipartimento di Fisica, Università di Milano, Milan, Italy
[73] [(a)]INFN Sezione di Napoli, Naples, Italy; [(b)]Dipartimento di Fisica, Università di Napoli, Naples, Italy
[74] [(a)]INFN Sezione di Pavia, Pavia, Italy; [(b)]Dipartimento di Fisica, Università di Pavia, Pavia, Italy
[75] [(a)]INFN Sezione di Pisa, Pisa, Italy; [(b)]Dipartimento di Fisica E. Fermi, Università di Pisa, Pisa, Italy
[76] [(a)]INFN Sezione di Roma, Rome, Italy; [(b)]Dipartimento di Fisica, Sapienza Università di Roma, Rome, Italy
[77] [(a)]INFN Sezione di Roma Tor Vergata, Rome, Italy; [(b)]Dipartimento di Fisica, Università di Roma Tor Vergata, Rome, Italy
[78] [(a)]INFN Sezione di Roma Tre, Rome, Italy; [(b)]Dipartimento di Matematica e Fisica, Università Roma Tre, Rome, Italy
[79] [(a)]INFN-TIFPA, Povo, Italy; [(b)]Università degli Studi di Trento, Trento, Italy
[80] Universität Innsbruck, Department of Astro and Particle Physics, Innsbruck, Austria
[81] University of Iowa, Iowa City, IA, USA
[82] Department of Physics and Astronomy, Iowa State University, Ames, IA, USA
[83] Istinye University, Sariyer, Istanbul, Turkey
[84] [(a)]Departamento de Engenharia Elétrica, Universidade Federal de Juiz de Fora (UFJF), Juiz de Fora, Brazil ; [(b)]Universidade Federal do Rio De Janeiro COPPE/EE/IF, Rio de Janeiro, Brazil; [(c)]Instituto de Física, Universidade de São Paulo, São Paulo, Brazil; [(d)]Rio de Janeiro State University, Rio de Janeiro, Brazil; [(e)]Federal University of Bahia, Bahia, Brazil
[85] KEK, High Energy Accelerator Research Organization, Tsukuba, Japan
[86] Graduate School of Science, Kobe University, Kobe, Japan
[87] [(a)]AGH University of Krakow, Faculty of Physics and Applied Computer Science, Krakow, Poland; [(b)]Marian Smoluchowski Institute of Physics, Jagiellonian University, Krakow, Poland
[88] Institute of Nuclear Physics Polish Academy of Sciences, Krakow, Poland
[89] Faculty of Science, Kyoto University, Kyoto, Japan
[90] Research Center for Advanced Particle Physics and Department of Physics, Kyushu University, Fukuoka, Japan
[91] L2IT, Université de Toulouse, CNRS/IN2P3, UPS, Toulouse, France
[92] Instituto de Física La Plata, Universidad Nacional de La Plata and CONICET, La Plata, Argentina

[93] Physics Department, Lancaster University, Lancaster, UK
[94] Oliver Lodge Laboratory, University of Liverpool, Liverpool, UK
[95] Department of Experimental Particle Physics, Jožef Stefan Institute and Department of Physics, University of Ljubljana, Ljubljana, Slovenia
[96] School of Physics and Astronomy, Queen Mary University of London, London, UK
[97] Department of Physics, Royal Holloway University of London, Egham, UK
[98] Department of Physics and Astronomy, University College London, London, UK
[99] Louisiana Tech University, Ruston, LA, USA
[100] Fysiska institutionen, Lunds universitet, Lund, Sweden
[101] Departamento de Física Teorica C-15 and CIAFF, Universidad Autónoma de Madrid, Madrid, Spain
[102] Institut für Physik, Universität Mainz, Mainz, Germany
[103] School of Physics and Astronomy, University of Manchester, Manchester, UK
[104] CPPM, Aix-Marseille Université, CNRS/IN2P3, Marseille, France
[105] Department of Physics, University of Massachusetts, Amherst, MA, USA
[106] Department of Physics, McGill University, Montreal, QC, Canada
[107] School of Physics, University of Melbourne, Melbourne, VIC, Australia
[108] Department of Physics, University of Michigan, Ann Arbor, MI, USA
[109] Department of Physics and Astronomy, Michigan State University, East Lansing, MI, USA
[110] Group of Particle Physics, University of Montreal, Montreal, QC, Canada
[111] Fakultät für Physik, Ludwig-Maximilians-Universität München, Munich, Germany
[112] Max-Planck-Institut für Physik (Werner-Heisenberg-Institut), Munich, Germany
[113] Graduate School of Science and Kobayashi-Maskawa Institute, Nagoya University, Nagoya, Japan
[114] [(a)]Department of Physics, Nanjing University, Nanjing, China; [(b)]School of Science, Shenzhen Campus of Sun Yat-sen University, Shenzhen, China; [(c)]University of Chinese Academy of Science (UCAS), Beijing, China
[115] Department of Physics and Astronomy, University of New Mexico, Albuquerque, NM, USA
[116] Institute for Mathematics, Astrophysics and Particle Physics, Radboud University/Nikhef, Nijmegen, The Netherlands
[117] Nikhef National Institute for Subatomic Physics and University of Amsterdam, Amsterdam, The Netherlands
[118] Department of Physics, Northern Illinois University, DeKalb, IL, USA
[119] [(a)]New York University Abu Dhabi, Abu Dhabi, United Arab Emirates; [(b)]United Arab Emirates University, Al Ain, United Arab Emirates
[120] Department of Physics, New York University, New York, NY, USA
[121] Ochanomizu University, Otsuka, Bunkyo-ku, Tokyo, Japan
[122] Ohio State University, Columbus, OH, USA
[123] Homer L. Dodge Department of Physics and Astronomy, University of Oklahoma, Norman, OK, USA
[124] Department of Physics, Oklahoma State University, Stillwater, OK, USA
[125] Palacký University, Joint Laboratory of Optics, Olomouc, Czech Republic
[126] Institute for Fundamental Science, University of Oregon, Eugene, OR, USA
[127] Graduate School of Science, Osaka University, Osaka, Japan
[128] Department of Physics, University of Oslo, Oslo, Norway
[129] Department of Physics, Oxford University, Oxford, UK
[130] LPNHE, Sorbonne Université, Université Paris Cité, CNRS/IN2P3, Paris, France
[131] Department of Physics, University of Pennsylvania, Philadelphia, PA, USA
[132] Department of Physics and Astronomy, University of Pittsburgh, Pittsburgh, PA, USA
[133] [(a)]Laboratório de Instrumentação e Física Experimental de Partículas-LIP, Lisbon, Portugal; [(b)]Departamento de Física, Faculdade de Ciências, Universidade de Lisboa, Lisbon, Portugal; [(c)]Departamento de Física, Universidade de Coimbra, Coimbra, Portugal; [(d)]Centro de Física Nuclear da Universidade de Lisboa, Lisbon, Portugal; [(e)]Departamento de Física, Escola de Ciências, Universidade do Minho, Braga, Portugal; [(f)]Departamento de Física Teórica y del Cosmos, Universidad de Granada, Granada, Spain; [(g)]Departamento de Física, Instituto Superior Técnico, Universidade de Lisboa, Lisbon, Portugal
[134] Institute of Physics of the Czech Academy of Sciences, Prague, Czech Republic
[135] Czech Technical University in Prague, Prague, Czech Republic
[136] Faculty of Mathematics and Physics, Charles University, Prague, Czech Republic
[137] Particle Physics Department, Rutherford Appleton Laboratory, Didcot, UK

[138] IRFU, CEA, Université Paris-Saclay, Gif-sur-Yvette, France
[139] Santa Cruz Institute for Particle Physics, University of California Santa Cruz, Santa Cruz, CA, USA
[140] [(a)]Departamento de Física, Pontificia Universidad Católica de Chile, Santiago, Chile; [(b)]Millennium Institute for Subatomic physics at high energy frontier (SAPHIR), Santiago, Chile; [(c)]Instituto de Investigación Multidisciplinario en Ciencia y Tecnología y Departamento de Física, Universidad de La Serena, La Serena, Chile; [(d)]Department of Physics, Universidad Andres Bello, Santiago, Chile; [(e)]Instituto de Alta Investigación, Universidad de Tarapacá, Arica, Chile ; [(f)]Departamento de Física, Universidad Técnica Federico Santa María, Valparaiso, Chile
[141] Department of Physics, Institute of Science, Tokyo, Japan
[142] Department of Physics, University of Washington, Seattle, WA, USA
[143] Department of Physics and Astronomy, University of Sheffield, Sheffield, UK
[144] Department of Physics, Shinshu University, Nagano, Japan
[145] Department Physik, Universität Siegen, Siegen, Germany
[146] Department of Physics, Simon Fraser University, Burnaby, BC, Canada
[147] SLAC National Accelerator Laboratory, Stanford, CA, USA
[148] Department of Physics, Royal Institute of Technology, Stockholm, Sweden
[149] Departments of Physics and Astronomy, Stony Brook University, Stony Brook, NY, USA
[150] Department of Physics and Astronomy, University of Sussex, Brighton, UK
[151] School of Physics, University of Sydney, Sydney, Australia
[152] Institute of Physics, Academia Sinica, Taipei, Taiwan
[153] [(a)]E. Andronikashvili Institute of Physics, Iv. Javakhishvili Tbilisi State University, Tbilisi, Georgia; [(b)]High Energy Physics Institute, Tbilisi State University, Tbilisi, Georgia; [(c)]University of Georgia, Tbilisi, Georgia
[154] Department of Physics, Technion, Israel Institute of Technology, Haifa, Israel
[155] Raymond and Beverly Sackler School of Physics and Astronomy, Tel Aviv University, Tel Aviv, Israel
[156] Department of Physics, Aristotle University of Thessaloniki, Thessaloniki, Greece
[157] International Center for Elementary Particle Physics and Department of Physics, University of Tokyo, Tokyo, Japan
[158] Department of Physics, University of Toronto, Toronto, ON, Canada
[159] [(a)]TRIUMF, Vancouver, BC, Canada; [(b)]Department of Physics and Astronomy, York University, Toronto, ON, Canada
[160] Division of Physics and Tomonaga Center for the History of the Universe, Faculty of Pure and Applied Sciences, University of Tsukuba, Tsukuba, Japan
[161] Department of Physics and Astronomy, Tufts University, Medford, MA, USA
[162] Department of Physics and Astronomy, University of California Irvine, Irvine, CA, USA
[163] University of West Attica, Athens, Greece
[164] University of Sharjah, Sharjah, United Arab Emirates
[165] Department of Physics and Astronomy, University of Uppsala, Uppsala, Sweden
[166] Department of Physics, University of Illinois, Urbana, IL, USA
[167] Instituto de Física Corpuscular (IFIC), Centro Mixto Universidad de Valencia-CSIC, Valencia, Spain
[168] Department of Physics, University of British Columbia, Vancouver, BC, Canada
[169] Department of Physics and Astronomy, University of Victoria, Victoria, BC, Canada
[170] Fakultät für Physik und Astronomie, Julius-Maximilians-Universität Würzburg, Würzburg, Germany
[171] Department of Physics, University of Warwick, Coventry, UK
[172] Waseda University, Tokyo, Japan
[173] Department of Particle Physics and Astrophysics, Weizmann Institute of Science, Rehovot, Israel
[174] Department of Physics, University of Wisconsin, Madison, WI, USA
[175] Fakultät für Mathematik und Naturwissenschaften, Fachgruppe Physik, Bergische Universität Wuppertal, Wuppertal, Germany
[176] Department of Physics, Yale University, New Haven, CT, USA
[177] Yerevan Physics Institute, Yerevan, Armenia

[a] Also Affiliated with an Institute Covered by a Cooperation Agreement with CERN, Geneva, Switzerland
[b] Also at An-Najah National University, Nablus, Palestine
[c] Also at Borough of Manhattan Community College, City University of New York, New York, NY, USA
[d] Also at Center for High Energy Physics, Peking University, Beijing, China
[e] Also at Center for Interdisciplinary Research and Innovation (CIRI-AUTH), Thessaloniki, Greece

[f] Also at CERN, Geneva, Switzerland
[g] Also at CMD-AC UNEC Research Center, Azerbaijan State University of Economics (UNEC), Baku, Azerbaijan
[h] Also at Département de Physique Nucléaire et Corpusculaire, Université de Genève, Geneva, Switzerland
[i] Also at Departament de Fisica de la Universitat Autonoma de Barcelona, Barcelona, Spain
[j] Also at Department of Financial and Management Engineering, University of the Aegean, Chios, Greece
[k] Also at Department of Mathematical Sciences, University of South Africa, Johannesburg, South Africa
[l] Also at Department of Physics, California State University, Sacramento, USA
[m] Also at Department of Physics, King's College London, London, UK
[n] Also at Department of Physics, Stanford University, Stanford, CA, USA
[o] Also at Department of Physics, Stellenbosch University, Stellenbosch, South Africa
[p] Also at Department of Physics, University of Fribourg, Fribourg, Switzerland
[q] Also at Department of Physics, University of Thessaly, Volos, Greece
[r] Also at Department of Physics, Westmont College, Santa Barbara, USA
[s] Also at Faculty of Physics, Sofia University, 'St. Kliment Ohridski', Sofia, Bulgaria
[t] Also at Hellenic Open University, Patras, Greece
[u] Also at Henan University, Kaifeng, China
[v] Also at Imam Mohammad Ibn Saud Islamic University, Riyadh, Saudi Arabia
[w] Also at Institucio Catalana de Recerca i Estudis Avancats, ICREA, Barcelona, Spain
[x] Also at Institut für Experimentalphysik, Universität Hamburg, Hamburg, Germany
[y] Also at Institute for Nuclear Research and Nuclear Energy (INRNE) of the Bulgarian Academy of Sciences, Sofia, Bulgaria
[z] Also at Institute of Applied Physics, Mohammed VI Polytechnic University, Ben Guerir, Morocco
[aa] Also at Institute of Particle Physics (IPP), Toronto, Canada
[ab] Also at Institute of Physics and Technology, Mongolian Academy of Sciences, Ulaanbaatar, Mongolia
[ac] Also at Institute of Physics, Azerbaijan Academy of Sciences, Baku, Azerbaijan
[ad] Also at National Institute of Physics, University of the Philippines Diliman (Philippines), Quezon City, Philippines
[ae] Also at Technical University of Munich, Munich, Germany
[af] Also at The Collaborative Innovation Center of Quantum Matter (CICQM), Beijing, China
[ag] Also at TRIUMF, Vancouver, BC, Canada
[ah] Also at Università di Napoli Parthenope, Naples, Italy
[ai] Also at University of Colorado Boulder, Department of Physics, Colorado, USA
[aj] Also at University of the Western Cape, Cape Town, South Africa
[ak] Also at Washington College, Chestertown, MD, USA
[al] Also at Yeditepe University, Physics Department, Istanbul, Turkey
* Deceased